THE EIGENSOLUTIONS OF THE BALANCE EQUATIONS OVER A SPHERE

BY

ANTONIO DIVINO MOURA

E.E., Universidade Federal de Minas Gerais (Brazil)

1969

SUBMITTED IN PARTIAL FULFILLMENT OF THE

REQUIREMENTS FOR THE DEGREE OF DOCTOR OF PHILOSOPHY

at the

MASSACHUSETTS INSTITUTE OF TECHNOLOGY

December 1974
ie February 1975

Signature of Author . . . . . .
Department of Meteorology, December 1974

Certified by . . . . . .
Thesis Supervisor

Accepted by . . . . . .
Chairman, Departmental Committee on Graduate Students

Archives

MASS. INST. TECH.
JAN 8 1975

THE EIGENSOLUTIONS OF THE BALANCE EQUATIONS OVER A SPHERE

by

Antonio Divino Moura

Submitted to the Department of Meteorology on
23 December 1974, in partial fulfillment of the
requirements for the degree of Doctor of Philosophy

ABSTRACT

Eigenvalues and eigenfunctions for the linearized (resting state) balance equations over a sphere are obtained and compared with the solutions of Laplace's tidal equations obtained by Longuet-Higgins. The results show a good agreement between the two sets of equations for the Hough's second class waves (small values of the parameter $\varepsilon = 4\Omega^2 a^2 / c^2$). But at large values of the parameter ε there are some apparent discrepancies. For negative values of ε there are high frequency solutions, which are unrealistic in the light of the balance approximation. The equatorial Rossby symmetric (v=0 at the equator) modes differ from the limiting type 2 solutions described by Longuet-Higgins. However, for the antisymmetric modes the agreement is good. The linearized version of the motions analyzed by Burger is a solution of the balance equations and it agrees with Longuet-Higgins' type 6 motions.

An integral theorem is derived and shows that the equatorial Kelvin wave solution of the Laplace's tidal equations is not a solution of the balance equations. It also shows that only westward propagating waves are solutions for positive values of ε. The westward propagating part of the mixed Rossby-gravity mode is a solution of the balance equations, but with slightly higher frequency when compared to Longuet-Higgins' results. This mode has the divergent part of the meridional velocity greater than its rotational part.

All the equatorial Rossby modes are shown to be well described by the "modified balance" equations derived by Charney. These equations also describe the equatorial Kelvin wave at large values of ε. But, unfortunately, they also allow for high frequency eastward propagating waves as free mode solutions. A brief discussion of their use for practical purposes in numerical prediction is presented and a possible method for their numerical integration is suggested.

A baroclinic stability study is performed for a simple family of zonal shear profiles over a sphere, by means of a two-layer model. It is shown that curvature effects play a major role in locating some important features of the baroclinic stability problem, such as the maximum meridional heat transport, maximum flux convergence of angular momentum. The locations of these quantities are shown to be very well correlated with the location of maximum excess of shear over the local criterion for instability. It is also shown that curvature affects the local and mean meridional scales of the most unstable baroclinic waves.

Thesis Supervisors: Norman A. Phillips, Peter H. Stone
Titles: Professors of Meteorology

DEDICATION

To Lilia

and

to our son Alexandre

whose happy presence has
helped keep this theoretical
work in proper perspective

ACKNOWLEDGEMENTS

The author wishes to express his gratitude to his chief thesis advisor, Professor Norman A. Phillips for his never failing guidance throughout this investigation. He kindly suggested the problem and has been a constant source of inspiration. The author is also grateful to Professor Peter H. Stone, who continued to supervise this thesis and who added new perspectives to the investigation carried out in chapter six.

Thanks are also due to Professors Jule G. Charney, John A. Young, and Richard S. Lindzen, and Drs. Fernando de Mendonça and Luiz G. Meira for contributing much to the author's meteorological education. Several discussions with Dr. Edward Sarachick, Dr. Dennis Moore, and many fellow students are acknowledged with sincere thanks. Professor Henry G. Houghton will always be remembered for his help during the author's early days at M.I.T.

Financial support was provided by the Instituto de Pesquisas Espaciais (Brazil). Additional financial support during the author's first two years of graduate study was provided by a NASA International Fellowship. Subsequent additional support under NSF GA 28724 is also acknowledged with thanks. FAPESP (Brazil) provided air transportation when the author first came to this country.

The author's wife, Lilia Moura, patiently typed the first draft, and Mrs. Eve Sullivan has efficiently typed this manuscript.

TABLE OF CONTENTS

Abstract 2

Dedication 3

Acknowledgements 4

Table of Contents 5

List of Figures 7

List of Symbols 12

1. Introduction 14

2. Forced Linear Problem 17

2.1 The Balance System of Equations 18

2.2 Forced Linear Problem 19

2.3 Horizontal and Vertical Structures 21

3. Tidal Theory: A Summary 24

3.1 The Tidal Equations 24

3.2 The Eigenvalues of Laplace's Tidal Equations 26

3.3 Asymptotic Solutions 29

3.3.1 Asymptotic Solutions as $\varepsilon \to 0$ 29

3.3.2 Asymptotic Solutions as $\varepsilon \to +\infty$ 33

3.3.3 Asymptotic Solutions as $\varepsilon \to -\infty$ 35

3.3.4 Asymptotic Solutions for $s = 0$ and $\lambda \to 0$ 37

3.4 Relevance of the Solutions 37

4. Balance Equations: Eigenvalues and Asymptotic Relations . . . 39

4.1 Integral Theorem for the Balance Equations 39

4.2 The Eigenvalues of the Balance Equations 41

4.2.1 Method of Solution 41

4.2.2 Discussion of the Computed Eigenvalues 44

4.2.3 Asymptotic Solutions as $\varepsilon \to 0$ 50

4.2.4 Asymptotic Solutions as $\varepsilon \to -\infty$ 50

4.2.5 Asymptotic Solutions as $\varepsilon \to +\infty$ 52

4.2.6 Behavior of the Solutions for $s = 0$ 55

4.2.7 Asymptotic Behavior as $\lambda \to \infty$ 56

5. Eigenfunctions 59

6. Stability Study of a Basic Zonal Velocity Profile 74

6.1 The Model Equations 75

6.2 Two-layer Model 77

6.3 Comparison of the Two Systems of Equations with $\gamma = 0$ and $\gamma = 1$ 81

6.4 Study of Curvature Effects on Baroclinic Instability 84

6.4.1 The Geopotential Eigenfunctions ϕ_1' and ϕ_3' 97

6.4.2 Angular Momentum Flux 98

6.4.3 Horizontal and Vertical Heat Transports 110

6.4.4 Meridional Scale of Baroclinic Waves 111

7. Modified Balance Equations 119

7.1 Discussion of the Results 119

7.2 Kelvin Wave Solution 123

7.3 Asymptotic Solutions as $\varepsilon \to \pm 0$ 126

Appendices

Appendix A. Expansion in Surface Spherical Harmonics 131

Appendix B. Integral Theorem for Truncated Matrix 137

Appendix C. Asymptotic Solutions as $\varepsilon \to -\infty$ 139

Appendix D. Asymptotic Solutions as $\varepsilon \to +\infty$ 146

Appendix E. Asymptotic Solutions as $\varepsilon \to 0$ 149

Appendix F.1 Numerical Solution of the Matrix Equation $\underset{\sim}{A}\dot{\underset{\sim}{Y}} = \underset{\sim}{B}\underset{\sim}{Y}$ for $\delta = 0$ 152

Appendix F.2 Energetics of the Model with $\delta = 0$ 159

Appendix G.1 Numerical Solution of the Matrix Equation $\underset{\sim}{A}\dot{\underset{\sim}{Y}} = \underset{\sim}{B}\underset{\sim}{Y}$ for $\gamma = 0$ 161

Appendix G.2 Energetics of the Model with $\gamma = 0$ 166

References 168

Biographical Note 171

LIST OF FIGURES

Figure		Page
1	Eigenvalues of Laplace's tidal equations	27
2	Eigenvalues of Laplace's tidal equations for ϵ=100	28
3	Eigenvalues of Laplace's tidal equations for s=0	30
4	Eigenvalues of Laplace's tidal equations for s=1	31
5	Eigenvalues of Laplace's tidal equations for s=-1	32
6	Eigenvalues of the balance equations	45
7	Eigenvalues of the balance equations for s=0	47
8	Eigenvalues of the balance equations for s=1	48
9	Eigenvalues of the balance equations for s=-1	49
10	Eigenvalues of the balance equations for λ =10	58
11	Eigenfunctions $\lvert\epsilon\rvert^{1/2}R$, U_{ROT}, V_{ROT} for the "mixed Rossby-gravity" mode for s=-1 ($\epsilon > 0$)	61
12	Eigenfunctions $\lvert\epsilon\rvert^{1/2}R$, U_{ROT}, V_{ROT} for the continuation ($\epsilon < 0$) of the first second class mode for s=-1	62
13	Eigenfunctions $\lvert\epsilon\rvert^{1/2}R$, U_{ROT}, V_{ROT} for the (n-s)=1 Rossby mode ($\epsilon > 0$) for s=-1	63
14	Eigenfunctions $\lvert\epsilon\rvert^{1/2}R$, U_{ROT}, V_{ROT} for the continuation ($\epsilon < 0$) of the (n-s)=1 Rossby mode for s=-1	64
15	Eigenfunctions $\lvert\epsilon\rvert^{1/2}R$, U_{ROT}, V_{ROT} for the (n-s)=2 Rossby mode ($\epsilon > 0$) for s=-1	65

Figure		Page
16	Eigenfunctions $\|\varepsilon\|^{1/2}R$, U_{ROT}, V_{ROT} for the continuation ($\varepsilon > 0$) of the (n-s)=2 Rossby mode for s=-1	66
17	Eigenfunctions $\|\varepsilon\|^{1/2}R$, U_{ROT}, V_{ROT} for the (n-s)=3 Rossby mode ($\varepsilon < 0$) for s=-1	67
18	Eigenfunctions $\|\varepsilon\|^{1/2}R$, U_{ROT}, V_{ROT} for the continuation ($\varepsilon < 0$) of the (n-s)=3 Rossby mode for s=-1	68
19	Eigenfunctions $\|\varepsilon\|^{1/2}R$, U_{ROT}, V_{ROT} for the "Burger 0" mode ($\varepsilon < 0$) for s=1	69
20	Eigenfunctions $\|\varepsilon\|^{1/2}R$, U_{ROT}, V_{ROT} for the "Burger 1" mode ($\varepsilon < 0$) for s=1	70
21	Eigenfunctions $\|\varepsilon\|^{1/2}R$, U_{ROT}, V_{ROT} for the "Burger 2" mode ($\varepsilon < 0$) for s=1	71
22	Eigenfunctions $\|\varepsilon\|^{1/2}R$, U_{ROT}, V_{ROT} for the "Burger 3" ($\varepsilon < 0$) for s=1	72
23	Comparison of the eigenfunctions of the first two ($\varepsilon > 0$) modes as described by the balance equations with the respective tidal asymptotes for $\varepsilon = 10^4$	73
24	Schematic drawing of a two-layer model	77
25.a	Growth rates for modes with Ψ symmetric	85
25.b	Growth rates for modes with Ψ antisymmetric	86
26.a	Eigenfunctions ϕ_1' , ϕ_3' for the most unstable mode for the cos(lat) zonal profile; Υ =1, S=0.005, $\omega = \Lambda = 0.01$	87

Figure		Page
26.b	Momentum and heat transports corresponding to figure 26.a	88
27.a	Eigenfunctions ϕ_1' , ϕ_3' for the most unstable mode for the cos(lat) zonal profile; $\gamma = 0$, $S = 0.005$, $\omega = \Lambda = 0.01$	89
27.b	Momentum and heat transports corresponding to figure 27.a	90
28.a	Eigenfunctions ϕ_1' , ϕ_3' for the most unstable mode (near neutral stability) for the cos(lat) zonal profile; $\gamma = 0$, $S = 0.005$, $\omega = \Lambda = 0.006$	93
28.b	Momentum and heat transports corresponding to figure 28.a	94
29	Zonal profiles used for the solutions far from neutral stability	95
30	Zonal profiles used for the solutions near neutral stability	96
Table I	Location of important features of the most unstable solutions	99
31.a	Eigenfunctions ϕ_1' , ϕ_3' for the most unstable mode (far from neutral stability) for the cos (lat)(1 + $\delta\sin^2$(lat)) profile; $S = 0.005$, $\omega = \Lambda = 0.007$; $\delta = 2$	100
31.b	Momentum and heat transports corresponding to figure 31.a	101
32.a	Eigenfunctions ϕ_1' , ϕ_3' for the most unstable mode (near neutral stability) for the cos(lat)(1+$\delta\sin^2$(lat)) profile; $S = 0.005$, $\omega = \Lambda = 0.002$; $\delta = 2$	102

Figure		Page
32.b	Momentum and heat transports corresponding to fig. 32.a	103
33.a	Eigenfunctions ϕ_1' , ϕ_3' for the most unstable mode (far from neutral stability) for the $\cos^3(\text{lat})$ profile; $S = 0.005$, $\omega = \Lambda = 0.025$	104
33.b	Momentum and heat transports corresponding to fig. 33.a	105
34.a	Eigenfunctions ϕ_1' , ϕ_3' for the most unstable mode (near neutral stability) for the $\cos^3(\text{lat})$ profile; $S = 0.005$, $\omega = \Lambda = 0.02$	106
34.b	Momentum and heat transports corresponding to fig. 34.a	107
35.a	Eigenfunctions ϕ_1' , ϕ_3' for the most unstable mode (far from neutral stability) for the $\cos(\text{lat})(1+\delta\sin^2(\text{lat}))$ profile; $S=0.005$, $\omega = \Lambda = -0.001$; $\delta = -28$	108
35.b	Momentum and heat transports corresponding to fig. 35.a	109
36.a	Eigenfunctions ϕ_1' , ϕ_3' for the most unstable mode (far from neutral stability) for the $\cos(\text{lat})(1+\delta\sin^2(\text{lat}))$ profile; $S = 0.00125$, $\omega = \Lambda = -0.00025$; $\delta = -28$	113
36.b	Momentum and heat transports corresponding to fig. 36.a	114
37.a	Eigenfunctions ϕ_1' , ϕ_3' for the most unstable mode (near neutral stability) for the $\cos(\text{lat})(1+\delta\sin^{+2}(\text{lat}))$ profile; $S = 0.00125$, $\omega = \Lambda = 0.0005$; $\delta = 2$	115
37.b	Momentum and heat transports corresponding to fig. 37.a	116
38	Eigenvalues for the "modified balance equations" for $s = -1$	120
39	Eigenvalues for the "modified balance equations" for $s = 1$	122

Figure		Page
40	Comparison of the eigenfunctions of the first two Rossby modes for s = −1 as described by the "modified balance equations" with the respective tidal asymptotes for $\varepsilon = 10^4$	124
41	"Kelvin wave" solution of the "modified balance equations" for s = 1 and $\varepsilon = 10^4$	125

LIST OF SYMBOLS

a Earth's mean radius

Ω Earth's rate of rotation

g acceleration due to gravity

$\mathcal{R}$ gas constant for dry air

z height

p pressure (p_o = reference pressure)

T temperature

ρ density

Θ potential temperature

Θ_s potential temperature for a standard atmosphere

$Z = -\ln(p/p_o)$ vertical coordinate

t time

θ colatitude

$\mu = \cos\theta$

$f = 2\Omega\mu$ Coriolis parameter

β derivative of the Coriolis parameter evaluated at a fixed latitude

φ longitude

$\phi = gz$ geopotential

$\overline{S}$ static stability

N^2 (Brunt-Väisälä frequency)^2

s longitudinal wave number

n modal number

σ frequency

$\lambda = \frac{\sigma}{2\Omega}$ non-dimensional frequency

ν growth rate (also a modal index)

Ψ streamfunction

χ velocity potential

ζ vertical component of the relative vorticity

$\mathcal{D}$ divergence of the horizontal motion

$\tilde{\omega} = \frac{Dp}{Dt}$ "vertical p-velocity"

$\dot{Z} = \frac{DZ}{Dt} = -\frac{\tilde{\omega}}{p}$ "vertical Z-velocity"

q rate of heating

$\vec{F}$ horizontal component of frictional force

$\hat{i}$, $\hat{j}$, $\hat{k}$ unity vectors toward the east, north, vertical

c^2 separation constant

$\varepsilon = \frac{4\Omega^2 a^2}{c^2}$ Lamb's parameter ($c^2 = gh$ for a homogeneous ocean)

h "equivalent depth"

P, Q, R latitudinal dependence of Ψ, χ, ϕ

$\mathcal{L} = \left(\frac{d}{d\mu}(1-\mu^2)\frac{d}{d\mu} - \frac{s^2}{1-\mu^2}\right)$

$L = \left(\sin\theta \frac{d^2}{d\theta^2} + \sin\theta \cos\theta \frac{d}{d\theta} - s^2\right)$

$P_n^s(\mu)$ Associated Legendre "polynomial" of degree n and order s

$H_\nu(\eta)$ Hermite polynomial of degree ν

$L_\nu^{(k)}(\omega)$ generalized Laguerre polynomial of degree ν and order k

A_n^s, B_n^s expansion coefficients for Q, P (also $\mathbb{A}_n^s$, $\mathbb{B}_n^s$)

$u = \frac{1}{a}\left\{-(1-\mu^2)^{1/2}\frac{\partial\Psi}{\partial\mu} + (1-\mu^2)^{-1/2}\frac{\partial\chi}{\partial\varphi}\right\}$ zonal velocity

$v = \frac{1}{a}\left\{(1-\mu^2)^{1/2}\frac{\partial\chi}{\partial\mu} + (1-\mu^2)^{-1/2}\frac{\partial\Psi}{\partial\varphi}\right\}$ meridional velocity

$U = -\left\{(1-\mu^2)^{1/2}\frac{dP}{d\mu} + (1-\mu^2)^{-1/2} s Q\right\}$ "zonal velocity"

$V = \left\{(1-\mu^2)^{1/2}\frac{dQ}{d\mu} + (1-\mu^2)^{-1/2} s P\right\}$ "meridional velocity"

$U_o = -\frac{dP_o}{d\eta}$ "zeroth order zonal velocity"

$V_o = \frac{dQ_o}{d\eta} + sP$ "zeroth order meridional velocity"

$U_{ROT} = -(1-\mu^2)^{1/2}\frac{dP}{d\mu}$ rotational part of the zonal velocity

$V_{ROT} = sP$ rotational part of the meridional velocity

$\eta = \varepsilon^{1/4}\mu$ and $\omega = (-\varepsilon)^{1/4}\theta$ are stretched coordinates

δ_{mn} Kronecker delta

$\mathcal{E}$ energy

α, α' indices (0 or 1) used to indicate the balance approximation

R_o Rossby number

R_i Richardson number

δ, Λ, ω parameters used in a two-layer model

γ parameter (0 or 1)

$a_n, b_n \ldots$ coefficients used in a spherical harmonics expansion

1. INTRODUCTION

The balance equations are a simplified set of meteorological equations in which the divergence equation is replaced by a diagnostic relationship between the horizontal non-divergent velocity and the horizontal variations in the pressure field. This is on the assumption that, for large scale motions, the horizontal divergence is much smaller than the vertical component of the vorticity. They are suitable for treating motions without gravity waves, but are able to treat more general type of motions than the quasi-geostrophic relation.

These equations appear in the works of Charney (1955) and Bolin (1955) and have been used in global models of the atmosphere where the mid-latitude β-plane gives unacceptable results (Brian, 1959; Peng, 1965; Clark, 1970; Cunnold et al, 1974). They are obtained as a second order approximation in the expansion of the primitive equations in terms of the Rossby number (Charney, 1962, 1973; Monin, 1952, 1958). Charney's (1962, 1973) derivation is a more rigorous one, and shows that the expansion holds even for $R_o = 0$ (1) if the Richardson number (R_i) is large enough that $(R_i R_o)^{-1}$ remains small.

Lorenz (1960) has shown that the equations form an energetically consistent set in a very enlightening manner. He is able to derive the balance equations by means of a systematic and consistent omission of certain terms in the primitive equations. The equation of balance has been used in the context of obtaining the initial set of data required to solve a well posed initial-boundary

value problem for the equations describing the large scale motions in dynamic meteorology (Charney, 1955; Phillips, 1960).

Because the equations do not treat gravity waves, they may be integrated through a numerical scheme with larger time steps, which is a highly desirable feature when lengthy integrations have to be performed (e.g., in a general circulation model).

The equations, however, form a highly implicit set, which makes their study difficult. Charney (1962) has numerically integrated them through an iterative process, the convergence of which requires the potential vorticity to be positive throughout the region of integration. He argues that this criterion for convergence holds even when the ellipticity condition for the Monge-Ampère equation (Bolin, 1955; Miyakoda, 1960; Houghton, 1968) is not satisfied.

We want to consider the following question: <u>how accurate is the balance system for describing slow, large scale motions in the atmosphere</u>?

To partly answer this question, we look at linear solutions of the balance system, on a sphere, and compare them with the more fundamental linear solutions for the Laplace tidal equation (referred to henceforth as LTE) obtained by Longuet-Higgins (1968). In general we will make use of numerical methods for the solution of this problem, accompanied with analytical solutions to some asymptotic cases.

The balance system is briefly described in chapter 2, where we also treat the linearization of the equations, with respect to a resting basic state. The latter allows for the separation of horizontal and vertical structures of the equations. A summary of the

solutions to the LTE is presented in chapter 3, with special attention to the asymptotic solutions. Here we have attempted to illustrate compactly the eigenvalues of the LTE in one figure (fig. 1).

In chapter 4, the eigenvalue-eigenfunction problem is formulated for the balance equations and an integral theorem is derived. The latter shows that the equatorial Kelvin wave of the LTE is not a solution of the balance equations. Numerical solutions and some asymptotic studies of the eigenvalue problem are compared with the LTE results. Eigenfunctions for some selected modes are shown in chapter 5 to describe their variation with latitude and the parameters involved.

In chapter 6 we present a study of baroclinic stability using a simple family of zonal wind profiles ($\overline{U} = a\alpha(p)\cos(\text{lat.})(1+\delta\sin^2(\text{lat.}))$) in a two-layer model. Here our main concern is to study the effects of curvature on some important aspects of the baroclinic problem, such as the latitudinal structure of the eigenfunctions, the transports by baroclinic eddies, and the meridional scale of the most unstable disturbance.

In an attempt to find a better description for the equatorial Rossby modes as described by the balance equations, we consider in chapter 7 the inclusion of the "$\beta \frac{\partial \chi}{\partial x}$" term in the equation of balance. The resulting set of equations is denominated "modified balance equations" and also forms an energetically consistent set. These equations are found in the work of Charney (1962) but are even more difficult to solve numerically than the balance equations.

2. FORCED LINEAR PROBLEM

Since we intend to verify how well the slow motions are described by the balance system, a comparative parallel study of the primitive and balance equations seems to be the appropriate approach to the problem.

We now formulate the equations using indices (α, α') and brackets ($\{\ \}$) to identify simplifications to be made in order to get the balance system.

The hydrostatic forms of the vorticity, divergence, thermodynamic, and continuity equations using $Z = -\ln(\frac{p}{p_o})$ are (Phillips, 1973):

$$\nabla^2\frac{\partial\psi}{\partial t} = -\hat{k}\times\nabla\psi\cdot\nabla(\zeta+f) - \nabla\cdot(\zeta+f)\nabla\chi - \nabla\cdot\left(\dot{Z}\,\nabla\frac{\partial\psi}{\partial Z}\right) + \left\{\nabla\cdot\left(\dot{Z}\,\hat{k}\times\nabla\frac{\partial\chi}{\partial Z}\right)\right\} - \nabla\cdot(\hat{k}\times\vec{F}) \tag{2.1}$$

$$\alpha'\left[\nabla^2\frac{\partial\chi}{\partial t}\right] = -\nabla^2\left(\phi + \tfrac{1}{2}\nabla\psi\cdot\nabla\psi\right) + \nabla\cdot(\zeta+f)\nabla\psi - \alpha\left[\hat{k}\times\nabla\chi\cdot\nabla f\right] - \left\{\nabla^2\left(\tfrac{1}{2}\nabla\chi\cdot\nabla\chi + \nabla\psi\cdot\nabla\chi\right) + \nabla\cdot\left(\dot{Z}\,\nabla\frac{\partial\chi}{\partial Z}\right) + \hat{k}\times\nabla\chi\cdot\nabla\zeta - \hat{k}\cdot\nabla\dot{Z}\times\nabla\frac{\partial\psi}{\partial Z} - \nabla\cdot\vec{F}\right\} \tag{2.2}$$

$$\frac{\partial}{\partial t}\left(\frac{\partial\phi}{\partial Z}\right) = -\left(\hat{k}\times\nabla\psi + \nabla\chi\right)\cdot\nabla\left(\frac{\partial\phi}{\partial Z}\right) - S\,\dot{Z} + \frac{R}{C_p}Q_f \tag{2.3}$$

$$\nabla^2\chi = -\left(\frac{\partial}{\partial Z} - 1\right)\dot{Z} \tag{2.4}$$

$$S = -\frac{p^2}{\rho}\frac{\partial \ln\Theta}{\partial p} = RT\frac{\partial \ln\Theta}{\partial z} = \left(\frac{RTN}{g}\right)^2 \tag{2.5}$$

is the static stability and ∇ is the horizontal "del operator" in spherical coordinates.

The lower boundary condition is obtained by applying

$$\dot{Z} = -\frac{1}{RT}\left[\frac{\partial \phi}{\partial t} + \left(\hat{k}\times\nabla\Psi + \nabla\chi\right)\cdot\nabla\phi - g w\right] \tag{2.6}$$

at the ground. $\dot{Z}$ is $-\frac{1}{\rho}\frac{dp}{dt} = -\frac{\tilde{\omega}}{\rho}$ and the equations without simplification have the indices (α, α') all equal to one.

2.1 The Balance System of Equations

The simplification which leads to the so-called balance equations is obtained by omitting the bracketed ({ }) terms and letting $\alpha' = 0$ with $\alpha = 0$ or 1 in (2.1) and (2.2). This forms an energy preserving system (Lorenz, 1960; Charney, 1962) if $\vec{F}=q=0$ and $\tilde{\omega}= 0$ at $p=0$ and $p=p_o$, and is correct up to two orders in the Rossby number expansion of the quasi-geostrophic system on a mid-latitude β-plane (Monin, 1958; Charney, 1962). [Charney retains the $\alpha=1$ term. This is energetically consistent but it is a small term in the quasi-geostrophic expansion.]

For future reference let us specialize now to the balance equations:

$$\nabla^2\frac{\partial \Psi}{\partial t} = -\hat{k}\times\nabla\Psi\cdot\nabla(\zeta+f) - \nabla\cdot(\underline{\zeta}+f)\nabla\chi - \underline{\nabla\cdot\left(\dot{Z}\nabla\frac{\partial \Psi}{\partial Z}\right)} - \nabla\cdot(\hat{k}\times\vec{F}) \tag{2.7}$$

$$\nabla^2\phi = \nabla\cdot f\nabla\psi + \underline{\nabla\cdot(\zeta\nabla\psi - \tfrac{1}{2}\nabla(\nabla\psi\cdot\nabla\psi))} - \\ -\alpha\left[\nabla\cdot(f\hat{k}\times\nabla\chi)\right] \tag{2.8}$$

$$\frac{\partial}{\partial t}\left(\frac{\partial\phi}{\partial z}\right) = -\left(\hat{k}\times\nabla\psi+\nabla\chi\right)\cdot\nabla\left(\frac{\partial\phi}{\partial z}\right) - S\dot{Z} + \frac{R}{c_p}q_T \tag{2.9}$$

$$\nabla^2\chi = -\left(\frac{\partial}{\partial z}-1\right)\dot{Z} \tag{2.10}$$

$$\dot{Z} = -\frac{1}{RT}\left[\frac{\partial\phi}{\partial t} + \left(\hat{k}\times\nabla\psi+\nabla\chi\right)\cdot\nabla\phi - gw\right] \tag{2.11}$$

at the ground. The cases α=0 or 1 will be referred to respectively as the "balance" or "modified balance" system. The non-linear underlined terms in (2.7) and (2.8) can be omitted without violating conservation of energy. This option is examined in chapter 6.

2.2 Forced Linear Problem

Before one attempts to solve the full non-linear equations, it is highly desirable first to become familiar with the physical processes that can be described by the linearized forms of the equations. The particular choice of basic state depends on the physical phenomena under consideration, and should lead to a mathematical formulation of the perturbation equations with accessible solutions. A method of solving the linear forced problem is to first solve the homogeneous equations (with $\vec{F}$=0 and q=0) and then to expand the forcings in the eigensolutions of the homogeneous problem. Under

special choices of the basic state it is possible to separate out the vertical and horizontal dependence of the equations.

Later (chapter 6) we shall consider a somewhat realistic basic state bearing some resemblance to the atmosphere, but now we will analyze the equations describing hydrostatic perturbations in a resting, stratified atmosphere without heating and friction over a spherical rotating earth. What we have in mind is to compare, whenever possible, the eigensolutions of the balance system with those of the hydrostatic equations resulting from the thorough study by Longuet-Higgins (1968). In this linearized homogeneous problem, equations (2.1) - (2.6) become

$$\nabla^2 \frac{\partial \psi'}{\partial t} = -\frac{2\Omega}{a^2}\frac{\partial \psi'}{\partial \varphi} - 2\Omega\mu\nabla^2\chi' - \frac{2\Omega}{a^2}(1-\mu^2)\frac{\partial \chi'}{\partial \mu} \tag{2.12}$$

$$\alpha'\left[\nabla^2\frac{\partial \chi'}{\partial t}\right] + \nabla^2\phi' = 2\Omega\mu\nabla^2\psi' + \frac{2\Omega}{a^2}(1-\mu^2)\frac{\partial \psi'}{\partial \mu} - \alpha\left[\frac{2\Omega}{a^2}\frac{\partial \chi'}{\partial \varphi}\right] \tag{2.13}$$

$$\frac{\partial}{\partial t}\left(\frac{\partial \phi'}{\partial Z}\right) = -\bar{S}(z)\,\dot{Z}' \tag{2.14}$$

$$\nabla^2\chi' = -\left(\frac{\partial}{\partial Z} - 1\right)\dot{Z}' \tag{2.15}$$

with the lower boundary condition (taking w =0)

$$\dot{Z}' = -\frac{1}{R\bar{T}}\frac{\partial \phi'}{\partial t} \qquad \text{at } Z = 0. \tag{2.16}$$

$$\nabla^2 \equiv \frac{1}{a^2}\left[\frac{\partial}{\partial\mu}(1-\mu^2)\frac{\partial}{\partial\mu} + \frac{1}{1-\mu^2}\frac{\partial^2}{\partial\varphi^2}\right] \tag{2.17}$$

is the horizontal part of the spherical Laplacian operator, φ is longitude, and μ = sine(latitude). The primes indicate perturbation quantities and an overbar means basic state. The balance system in this linearized form is obtained by making $\alpha'=0$ and $\alpha=0$ ($\alpha=1$ will be discussed in chapter 7). This problem (with $\alpha'=\alpha=1$) is a very important one for both atmospheric and oceanic motions. These equations arise in the study of tides, the theory of which was originally formulated by Laplace (Lamb, 1932 (p.330 and 554); Taylor, 1936).

2.3 Horizontal and Vertical Structure

In order to separate out the vertical and horizontal structures we search for solutions of the form

$$\begin{aligned}
\psi'(\varphi,\mu,Z,t) &= \psi(\varphi,\mu,t)\,A(Z)\\
\chi'(\varphi,\mu,Z,t) &= \chi(\varphi,\mu,t)\,A(Z)\\
\phi'(\varphi,\mu,Z,t) &= \phi(\varphi,\mu,t)\,A(Z)\\
\dot{Z}(\varphi,\mu,Z,t) &= w(\varphi,\mu,t)\,B(Z)
\end{aligned} \tag{2.18}$$

When put into (2.12) - (2.15) these give

$$a^2\nabla^2\frac{\partial\psi}{\partial t} = -2\Omega\frac{\partial\psi}{\partial\varphi} - 2\Omega\mu a^2\nabla^2\chi - 2\Omega(1-\mu^2)\frac{\partial\chi}{\partial\mu} \tag{2.19}$$

$$\alpha'\left[a^2\nabla^2\frac{\partial\chi}{\partial t}\right] = -a^2\nabla^2\phi + 2\Omega\mu a^2\nabla^2\psi + 2\Omega(1-\mu^2)\frac{\partial\psi}{\partial\mu} - \alpha\left[2\Omega\frac{\partial\chi}{\partial\varphi}\right] \tag{2.20}$$

$$\frac{1}{W}\frac{\partial\phi}{\partial t} = -\left[\frac{\bar{S}(z)\,B(z)}{\frac{dA(z)}{dz}}\right] \tag{2.21}$$

$$\nabla^2\chi = -\left[\frac{\frac{dB(z)}{dz} - B(z)}{A(z)}\right]W \tag{2.22}$$

$$W = -\frac{A(0)}{R\bar{T}(0)\,B(0)}\frac{\partial\phi}{\partial t} \qquad \text{at } Z=0 \tag{2.23}$$

We set $A(Z) = \frac{dB(z)}{dz} - B(Z)$ (2.24)

and use (2.22) and (2.24) in (2.21):

$$\frac{1}{\nabla^2\chi}\frac{\partial\phi}{\partial t} = \left[\frac{\bar{S}(z)\,B(z)}{\frac{d^2B}{dz^2} - \frac{dB}{dz}}\right] = -c^2 \tag{2.25}$$

Here c^2 is a separation constant and has dimensions of $(\text{velocity})^2$.

The equations describing the horizontal structure are (2.19), (2.20) and

$$\frac{\partial\phi}{\partial t} = -c^2\nabla^2\chi \tag{2.26}$$

The vertical structure is dependent upon the mean temperature $\bar{T}(Z)$ and upon the thermal forcing that would appear in the right hand side of (2.27) in the case of a forced problem. One obtains

$$\frac{d^2D(z)}{dz^2} + \left(\frac{\bar{S}(z)}{c^2} - \frac{1}{4}\right)D(z) = 0 \tag{2.27}$$

subject to the lower boundary condition

$$\left[\frac{dD}{dZ} + \left(\frac{R\overline{T}(0)}{c^2} - \frac{1}{2} \right) D \right]_{Z=0} = 0 \tag{2.28}$$

where $D(Z) = B(Z) \exp(-Z/2)$, to determine the vertical structure. The upper boundary condition on $D(Z)$ is either that energy density be finite as $Z \to \infty$ or an imposed outward radiation condition as $Z \to \infty$ requiring the energy flux to be upwards. Discussions concerning the upper boundary condition may be found in Lindzen (1967), Chapman and Lindzen (1970), and Eliassen and Palm (1960).

3. TIDAL THEORY : A Summary

3.1 The Tidal Equations

It is our primary interest to study thoroughly the latitudinal structure of equations (2.19), (2.20), and (2.26). In order to do so, we look for solutions of the form

$$\left[\psi\ ,\chi\ ,\phi\right](\varphi,\mu,t) = Re\left[\left(P(\mu)\,;\,i\,Q(\mu)\,,2\Omega R(\mu)\right)e^{i(s\varphi-\sigma t)}\right] \tag{3.1}$$

The latitudinal dependence of those equations are then

$$-\lambda\,\mathcal{L}(P) + \mu\,\mathcal{L}(Q) + (1-\mu^2)\frac{dQ}{d\mu} + sP = 0 \tag{3.2}$$

$$\mu\,\mathcal{L}(P) + (1-\mu^2)\frac{dP}{d\mu} + \alpha\left[sQ\right] = \mathcal{L}(R) + \alpha'\left[\lambda\,\mathcal{L}(Q)\right] \tag{3.3}$$

$$\mathcal{L}(Q) = \lambda\epsilon R \tag{3.4}$$

where $\lambda = \dfrac{\sigma}{2\Omega}$ a non-dimensional frequency

$\epsilon = \dfrac{4\Omega^2 a^2}{c^2}$ a non-dimensional parameter (called Lamb's parameter by Longuet-Higgins)

$$\mathcal{L}(\ ) \equiv \left[\frac{d}{d\mu}(1-\mu^2)\frac{d}{d\mu} - \frac{s^2}{1-\mu^2}\right](\ )$$

Equations (3.2) - (3.4) with $\alpha' = \alpha = 1$ are referred to as Laplace's tidal equations and form an eigenvalue-eigenfunction problem (Longuet-Higgins, 1968). λ is real. Its spectrum depends on the separation constant c^2 (or ϵ), on the longitudinal wave number s, and on a latitudinal modal number n :

$$\lambda = \lambda(c^2, s, n) \tag{3.5}$$

In the case of a homogeneous ocean one gets the same equations but with $c^2 = gh$, where h is called the "equivalent depth" (Taylor, 1936). The eigenfunctions of Laplace's tidal equations are called "Hough Functions" on account of the important contribution made by Hough (1898) (Flattery, 1967; Lindzen, 1966, 1967, 1971).

The complete set of eigenfunctions in which a given forcing function can be expanded includes both positive and negative values of c^2. Negative values of c^2 are needed to represent forced modes and are needed in forced problems where the frequency λ, the longitudinal wave number s, and the latitudinal structure of the forcing are given. We should comment, in passing, that the use of the term "equivalent depth" for h has retarded the discovery of the "negative equivalent depth" ($\epsilon < 0$), the importance of which has been stressed by Lindzen (1966, 1971) [see also Dikii (1965) and Kato (1966)].

3.2 The Eigenvalues of Laplace's Tidal Equations

Figure 1 displays the general nature of the eigenvalues of Laplace's tidal equations as derived by Longuet-Higgins (1968). For each fixed mode the surface $n = n(\epsilon, \lambda, s)$ is shown as a function of ϵ, the frequency λ, and the wave number s. (Strictly speaking, the values that s assumes are discrete). The frequency ranges over $0<\lambda<\infty$ for positive ϵ but only over $0<\lambda<1$ for negative ϵ. [The interpretation of the signs of λ and s is as follows. (a) One can use the convention that λ takes on only positive values, and the wave number s can be positive (eastward propagating waves) or negative (westward propagating waves); i.e., $s=0,\pm1,\pm2,..$ (b) One can also take s to be a non-negative integer, in which case the frequency λ may either assume negative values (westward moving waves) or positive values (eastward moving waves). The first convention is most convenient for formulas and graphical representation, the second convention most convenient for numerical solution using spherical harmonics. The two choices are possible because (3.2) - (3.4) have the property that if $(P,Q,R;\lambda,s)$ is a solution, then $(P^*,-Q^*,R^*;-\lambda,-s)$ is also a solution having the same ψ, χ, ϕ.]

Figure 2 represents a cross-section of figure 1 at $\epsilon = 100$ and shows the relationship between the frequency and the longitudinal wave number. In this figure, where the various modes are indicated, the "mixed Rossby-gravity mode" is seen to behave either like a Rossby mode or like a gravity mode for large negative or large positive values of s, respectively. For small values of s it has a mixed character (Matsuno, 1966).

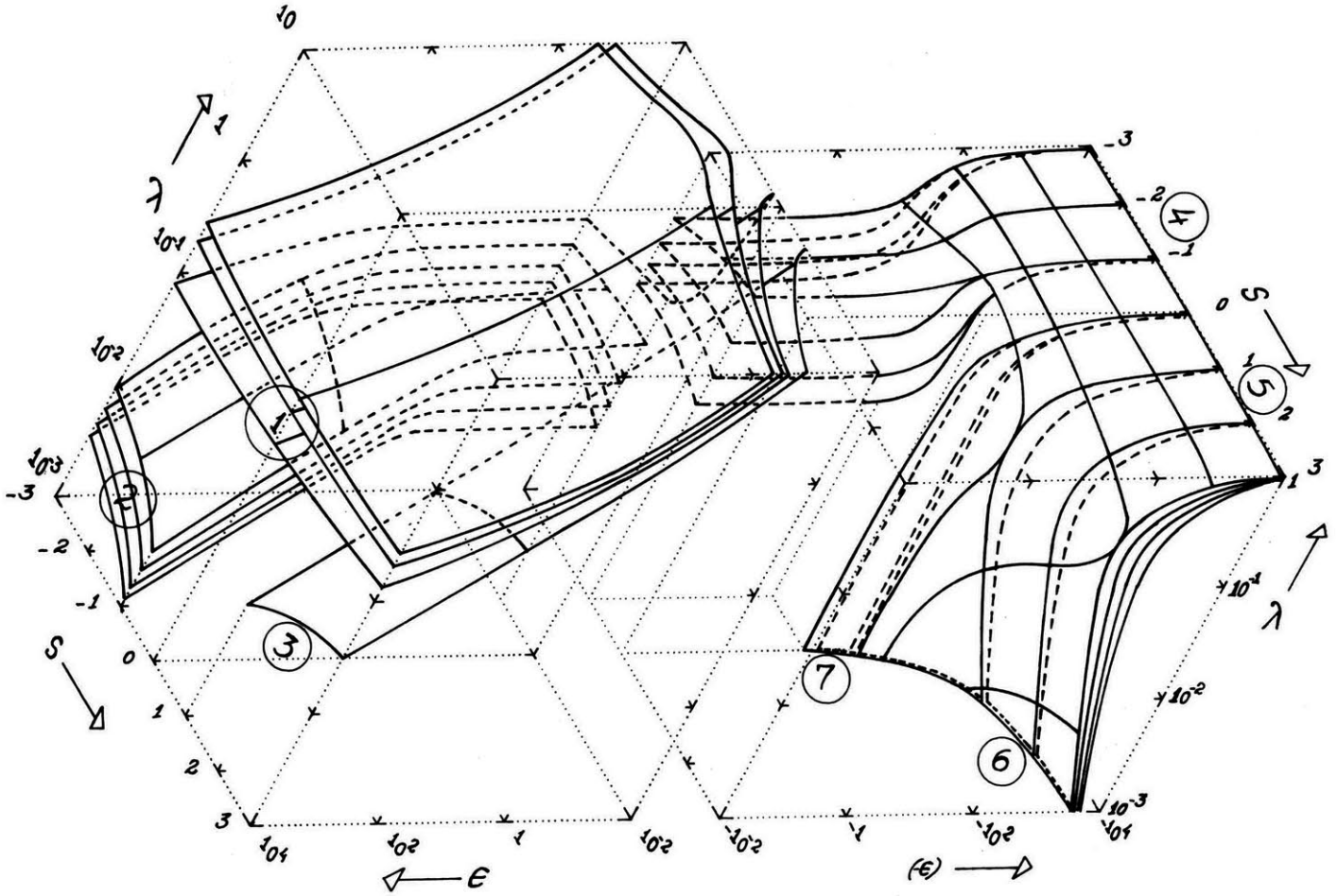


Fig. 1 Eigenvalues for Laplace's tidal equations constructed from the analysis by Longuet-Higgins. Surfaces are shown for selected latitudinal modes, as a function of frequency ($\lambda > 0$, on a log scale), longitudinal wave number (s), and Lamb's parameter ($\epsilon = 4\Omega^2 a^2/c^2$, also on a log scale). The encircled numbers refer to the seven limiting types described by Longuet-Higgins. Surfaces are drawn by continuity as if s could assume non-integer values except when the connection between s=0 and s=1 is not obvious.

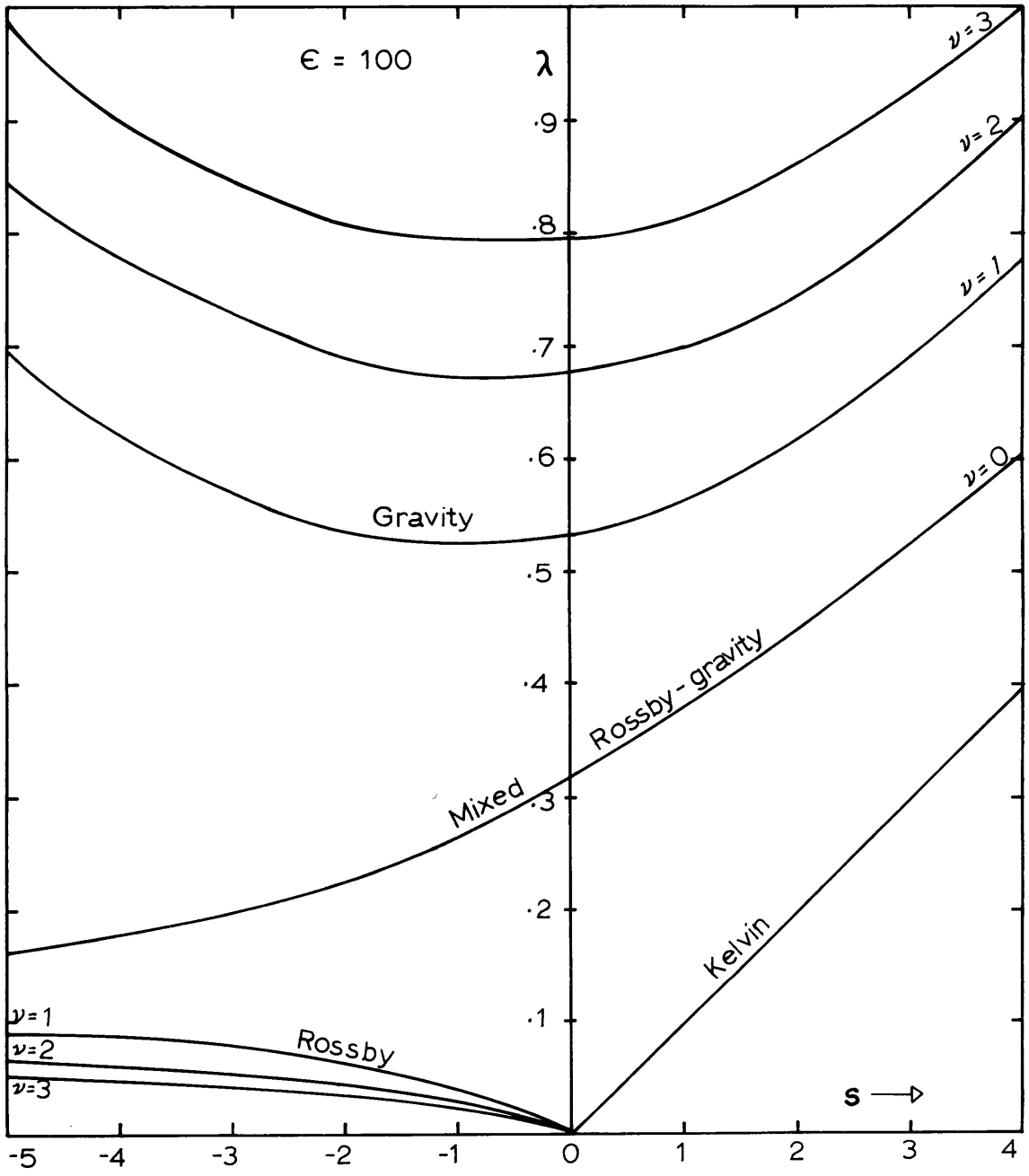


Fig. 2 Eigenvalues for Laplace's tidal equations for ϵ (= $4\Omega^2 a^2/c^2$) = 100. The frequency (λ) dependence on the longitudinal wave number (s) is shown for selected modes, as indicated in the figure.

Figures 3, 4, and 5 correspond to sections of figure 1 at s=0, s=1, and s=-1. They show the dependence of the frequency on the parameter ϵ for fixed values of s.

3.3 Asymptotic Solutions

The eigenvalues shown in figure 1 are a result of "exact" numerical calculations when P, Q, and R are expressed as series of surface spherical harmonics. These computations have revealed several asymptotic forms taken by the eigensolutions (Longuet-Higgins, 1968).

3.3.1 Asymptotic Solutions as $\epsilon \to 0$

As $\epsilon \to +0$ the solutions separate out into two families: waves of the first class (gravity waves)

$$\lambda = \left[\frac{n(n+1)}{\epsilon}\right]^{1/2} , \quad n = |s| + \nu , \quad \nu = 0,1,2,\ldots$$

and waves of the second class (non-divergent Rossby waves)

$$\lambda = -\frac{s}{n(n+1)} = \frac{-s}{s^2 - s(2\nu+1) + \nu(\nu+1)} ; \quad s < 0 , \quad \nu = 0,1,2,\ldots$$

The first family corresponds to irrotational motions with eigenfunctions given by $P(\mu) = 0$ and $Q(\mu) \propto P_n^{|s|}(\mu)$ whereas the second family corresponds to non-divergent motions with $Q(\mu) = 0$ and $P(\mu) \propto P_n^{-s}(\mu)$. $P_n^{-s}(\mu)$ is the associated Legendre "polynomial" of degree n and order s. These results are found in the work of Hough (1898).

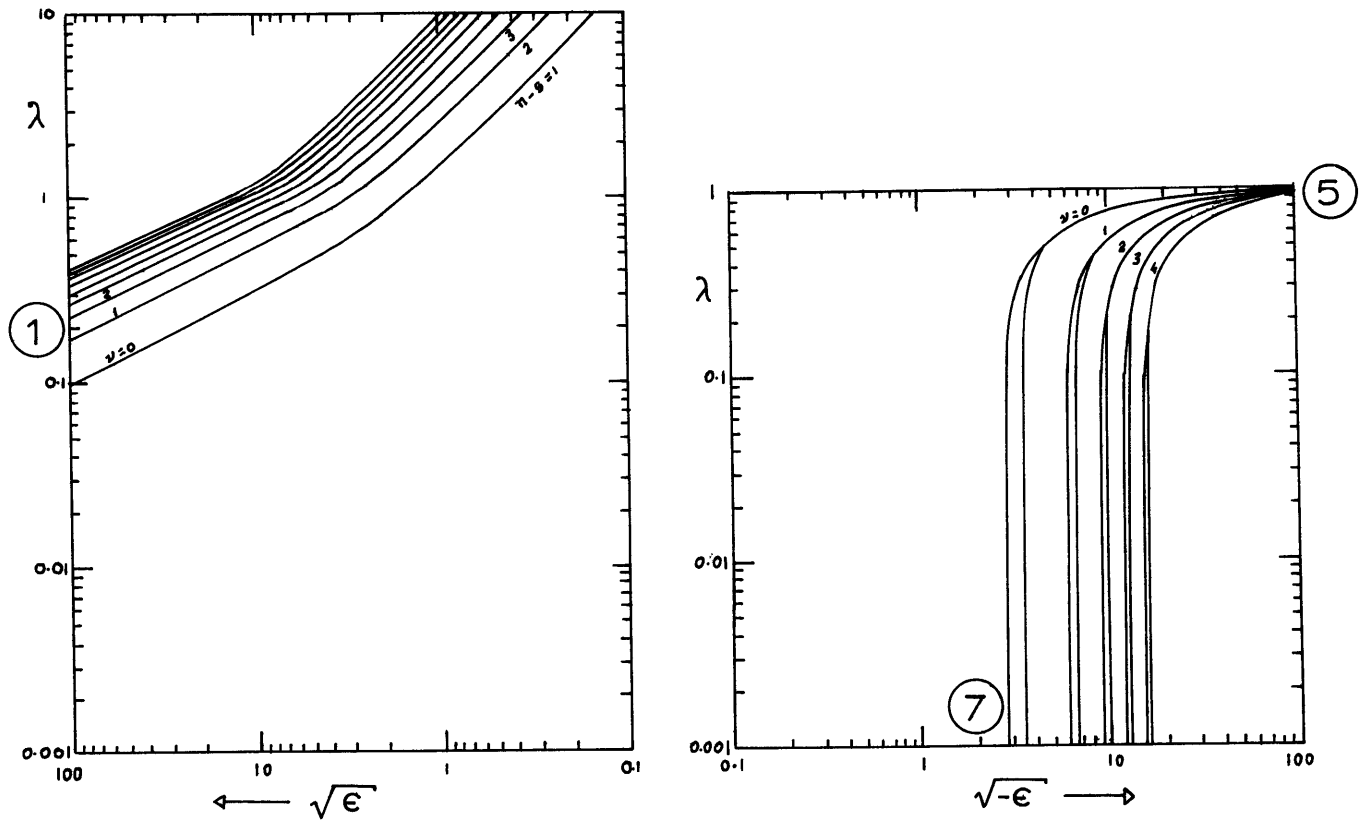


Fig. 3 Eigenvalues for Laplace's tidal equations for the longitudinal wave number equal to zero (s=0) constructed from the analysis by Longuet-Higgins. The frequency (λ) dependence on the parameter $\epsilon = 4\Omega^2 a^2/c^2$ is shown. The frequency is less than one for all negative values of ϵ . The encircled numbers refer to the limiting types described by Longuet-Higgins.

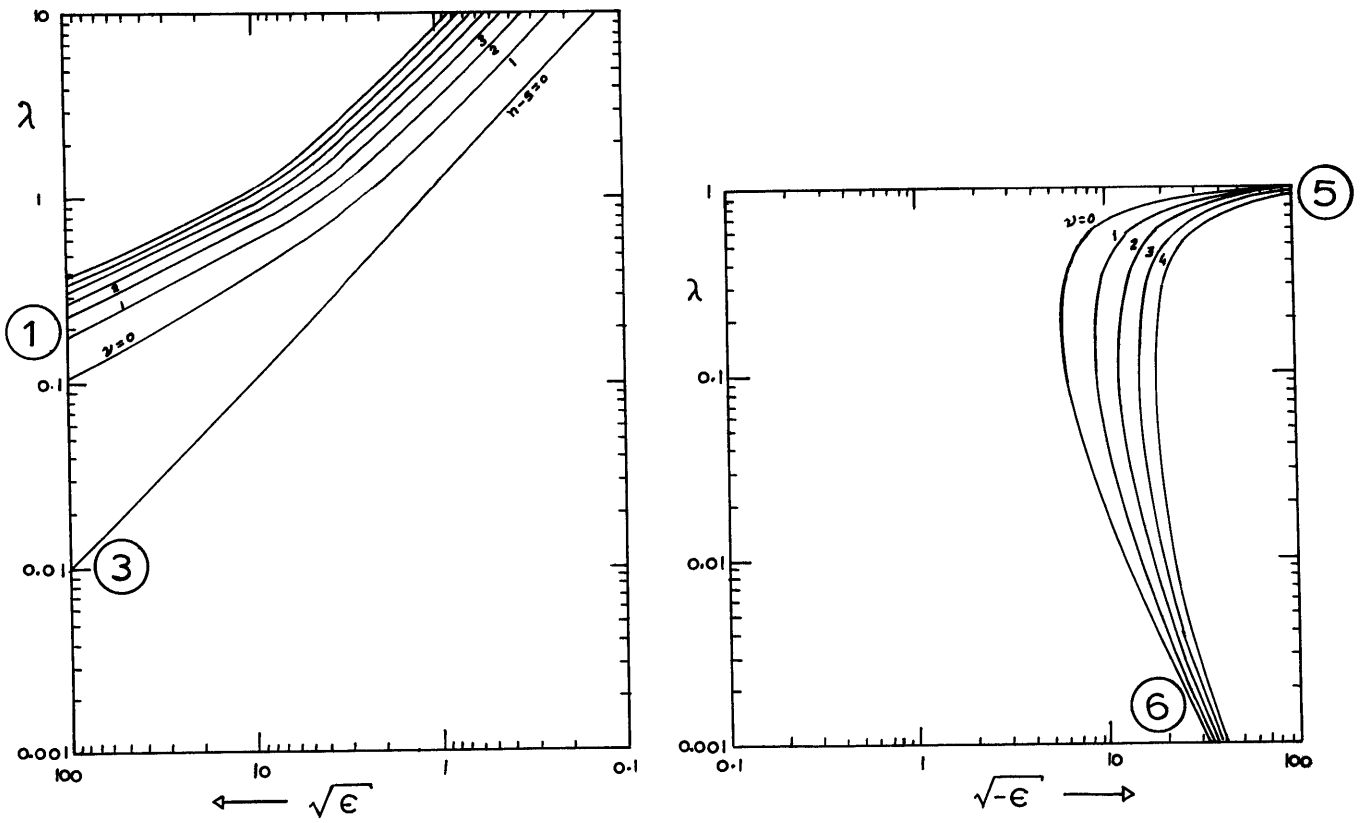


Fig. 4 Same as Fig. 3, but for the longitudinal wave number s=1.

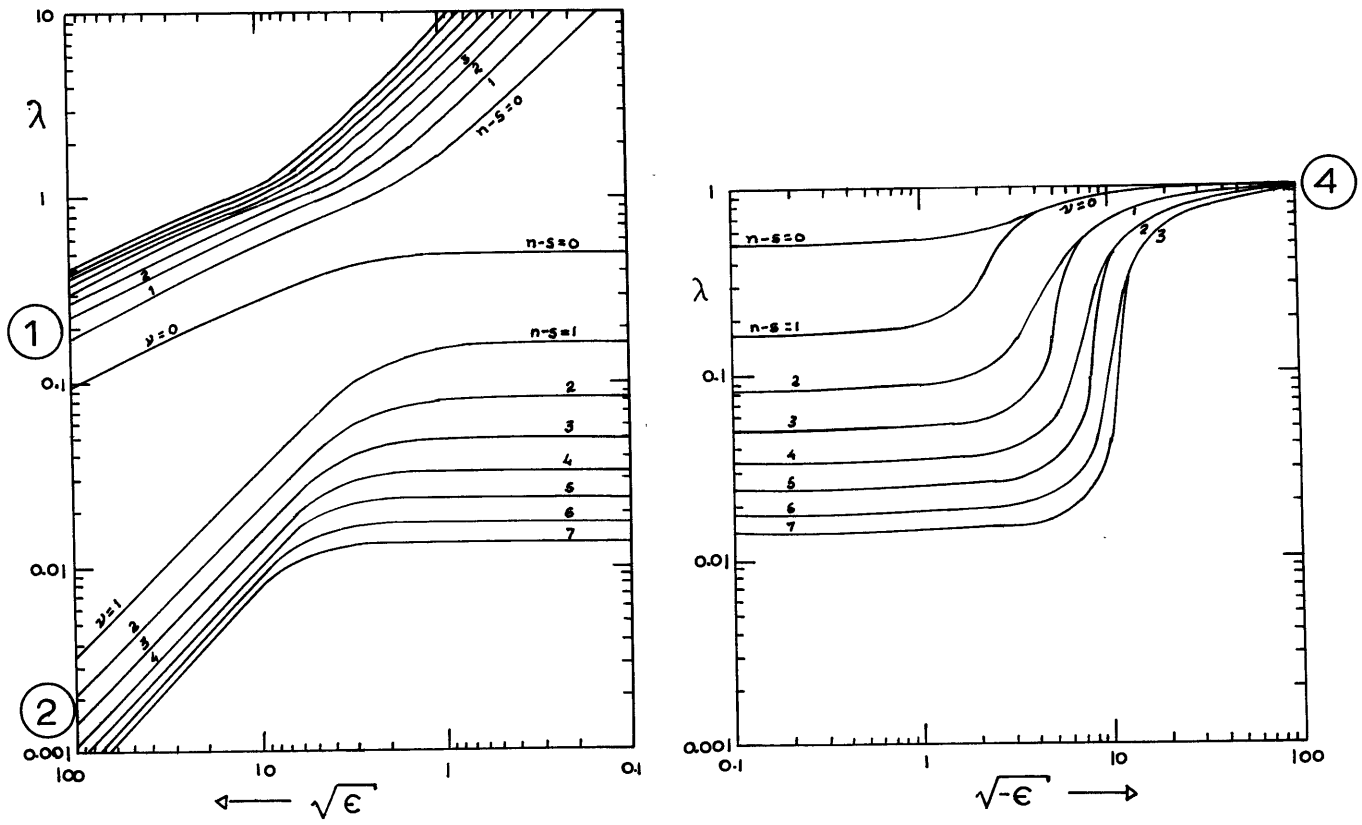


Fig. 5 Same as Fig. 3, but for the longitudinal wave number s = -1.

As $\epsilon \to -0$ the only limiting forms of solutions correspond to an analytical continuation of the waves of the second class.

3.3.2 Asymptotic Solutions as $\epsilon \to +\infty$

The solutions comprise three types of motions, all of which are described in terms of Hermite functions. They are confined to the equatorial region as $\epsilon \to +\infty$, and as such were first described by Matsuno (1966). The Hermite functions and the dispersion relation (a cubic equation for λ) appear as a result of the boundary conditions imposed on a parabolic cylinder equation for the meridional velocity, with exception of type 3.

Type 1: The motions of type 1 are inertial gravity waves with frequencies

$$\lambda = \frac{(2\nu + 1)^{1/2}}{\epsilon^{1/4}} + \frac{s}{2(2\nu + 1)} \quad ; \quad \nu = 0,1,2,\ldots$$

$s=0$, $s > 0$, or $s < 0$. The $\nu = 0$ mode is referred to as the mixed Rossby-gravity mode with properties already mentioned. The associated eigenfunctions are:

$$v(\eta) = -i\, e^{-\frac{1}{2}\eta^2} H_\nu(\eta) \quad ; \quad \eta = \epsilon^{1/4}\mu$$

$$u(\eta) = \pm \frac{1}{(2\nu+1)^{1/2}}\, e^{-\frac{1}{2}\eta^2} \left[\nu H_{\nu-1}(\eta) + \tfrac{1}{2} H_{\nu+1}(\eta)\right] \quad ; \quad \nu = 0,1,2,\ldots \quad (3.6)$$

$$-R(\eta) = \pm \left[\frac{1}{(2\nu+1)\epsilon}\right]^{1/2} e^{-\frac{1}{2}\eta^2} \left[\nu H_{\nu-1}(\eta) - \tfrac{1}{2} H_{\nu+1}(\eta)\right]$$

where $V(\mu) = i\left[(1-\mu^2)\frac{dQ}{d\mu} + sP\right]\frac{(1-\mu^2)^{-1/2}}{a}$ is the latitudinal dependence of the meridional velocity; $U(\mu) = -\left[(1-\mu^2)\frac{dP}{d\mu} + sQ\right]\frac{(1-\mu^2)^{-1/2}}{a}$ is the latitudinal dependence of the zonal velocity, and the sign choice is + for $s \geq 0$, - for $s < 0$.

Type 2: These correspond to equatorially trapped westward propagating Rossby waves with frequencies given by:

$$\lambda = -\frac{s}{(2\nu+1)\epsilon^{1/2}} \quad ; \quad \nu = 1,2,3,.. \quad , s < 0$$

and the eigenfunctions described by

$$\begin{aligned} U(\eta) &= \frac{2\nu+1}{2s}\epsilon^{1/4} e^{-\frac{1}{2}\eta^2}\left[H_{\nu-1}(\eta) - \frac{1}{2(\nu+1)}H_{\nu+1}(\eta)\right] \\ V(\eta) &= -i\, e^{-\frac{1}{2}\eta^2} H_\nu(\eta) \qquad (3.7) \\ R(\eta) &= -\frac{2\nu+1}{2s}\epsilon^{-1/4} e^{-\frac{1}{2}\eta^2}\left[H_{\nu-1}(\eta) + \frac{1}{2(\nu+1)}H_{\nu+1}(\eta)\right] \end{aligned}$$

[Note: The well-known decrease of Rossby wave frequencies with large (-s) is not shown by the above formula for λ, as described by Longuet-Higgins. An expansion in powers of $\epsilon^{-1/2}$ to the next order replaces $(2\nu+1)\epsilon^{1/2}$ in the denominator by $(2\nu+1)\epsilon^{1/2} + s^2(1 - (2\nu+1)^{-2}) - (2\nu^2 + 2\nu - 1) \div 4.$]

Type 3: This represents a "Kelvin wave" solution propagating eastward along the equator with very small meridional velocity. Kelvin waves propagate along coastal boundaries in rotating systems with constant Coriolis parameter, and the change of sign of the Coriolis parameter on the equator here plays the role of an "equatorial wall" for this Kelvin wave solution. The zonal velocity is geostrophically balanced

and has a Gaussian profile. The frequency is given by

$$\lambda = \frac{s}{\epsilon^{1/2}}\left[1 + \frac{1}{4\epsilon^{1/2}}\right] \quad , \; s \geq 0$$

and the eigenfunctions are:

$$\begin{aligned} v(\eta) &= i\eta e^{-\frac{1}{2}\eta^2} \\ u(\eta) &= \epsilon^{\frac{1}{2}} R(\eta) = \frac{2}{s}\epsilon^{3/4} e^{-\frac{1}{2}\eta^2} \end{aligned} \tag{3.8}$$

The asymptotic behavior of the eigensolutions as $\epsilon \to +\infty$ can be described by an ad-hoc equatorial β-plane approximation. This simplified geometry has been applied with success in the studies of Matsuno (1966) and Lindzen (1967). The Kelvin wave has meridional velocity identically equal to zero in this simplified geometry.

3.3.3 Asymptotic Solutions as $\epsilon \to -\infty$

The solutions as $\epsilon \to -\infty$ are asymptotically described in terms of generalized Laguerre polynomials. The energy of the motions is concentrated around the north and south poles and is small near the equator. This fact implies that the motions are hemispherically independent and explains the pairing of eigenvalues of symmetric and antisymmetric solutions evident on figures 4 and 5. (We correct several misprints on pages 553-6 of Longuet-Higgins).

Type 4: The motions of type 4 take place in inertial circles moving westward. The frequencies are:

$$\lambda = 1 + \frac{s - 2\nu}{(-\epsilon)^{1/2}} \quad ; \quad \nu = 0,1,2,\ldots \ , \ s < 0$$

and the eigenfunctions are:

$$\begin{aligned} u(\omega) &= -iv(\omega) = (-\epsilon)^{1/4} e^{-\frac{1}{2}\omega^2} \omega^{|s|-1} L_\nu^{(|s|-1)}(\omega^2) \\ R(\omega) &= (-\epsilon)^{-3/4}\left(\frac{1}{\omega}\frac{d}{d\omega} + \frac{s}{\omega^2}\right) i\omega v \qquad ; \omega = -(-\epsilon)^{1/4}\theta \end{aligned} \tag{3.9}$$

$L_\nu^s(x)$ is the generalized Laguerre polynomial of degree ν and order s.

Type 5: This type of motions is in inertial circles and propagate eastward for $s > 0$. The frequencies are:

$$\lambda = 1 - \frac{s + 2\nu + 2}{(-\epsilon)^{1/2}} \ , \ \nu = 0,1,2,\ldots \quad \text{and } s = 0,1,2,\ldots.$$

The eigenfunctions are

$$\begin{aligned} u(\omega) &= iv(\omega) = (-\epsilon)^{1/4} e^{-\frac{1}{2}\omega^2} \omega^{s+1} L_\nu^{(s+1)}(\omega^2) \\ R(\omega) &= -(-\epsilon)^{-3/4}\left(\frac{1}{\omega}\frac{d}{d\omega} + \frac{s}{\omega^2}\right) i\omega v \end{aligned} \tag{3.10}$$

The motions of type 4 and 5 have kinetic energy much larger than the total potential energy.

Type 6: This type of motion consists of waves propagating slowly eastward. The energy is mostly potential energy, concentrated around the poles ($\mu = \pm 1$). This type of motion is a linearized form of the motion analyzed by Burger (1958) under the scaling assumptions of negligible acceleration and very large horizontal scale. Phillips (1963)

in his discussion of "geostrophic motion of type 2", anticipated that if Burger's motion did exist in the atmosphere, it must be forced. This is consistent with the negative values of ϵ for type 6.

The eigenfrequencies and the eigenfunctions are:

$$\lambda = \frac{s}{(-\epsilon)} \left[1 + \frac{2(s + 2\nu + 1)}{(-\epsilon)^{1/2}} \right] \; ; \quad \nu = 0,1,2,\ldots \; ; \quad s \geq 1$$

$$s R(\omega) = -i\omega V(\omega) = e^{-\frac{1}{2}\omega^2} \omega^s L_\nu^{(s)}(\omega^2) \tag{3.11}$$

$$U(\omega) = (-\epsilon)^{1/4} \frac{dR}{d\omega}$$

The geostrophic character of this type of motion is expressed by the last of these relations.

3.3.4 Asymptotic Solutions for s=0 and $\lambda \to 0$

The numerical calculations by Longuet-Higgins (1968) also suggested an asymptotic behavior for s=0 and very small frequencies ($\lambda \to 0$). The asymptotic solutions appear as an eigenvalue problem for ϵ, the values of which are found to be finite, negative numbers. This asymptotic behavior is classified as type 7 by Longuet-Higgins.

3.4 Relevance of the Solutions

Theory and applications of atmospheric tides have been very well discussed in Chapman and Lindzen (1970). Among the various forced tides let us show how the "negative equivalent depths" appear in the context of figure 1. The solar semi-diurnal thermal tide for example, needs only the positive ϵ eigensolutions for the forcing

to be expanded (the line s=-2 and λ =1 only intercepts surfaces of positive ϵ in figure 1). On the other hand, the solar diurnal thermal tide does need both the positive and the negative ϵ eigensolutions (the line s= -1 and λ = 0.5 intercepts both surfaces of positive and of negative ϵ in figure 1). The importance of the negative ϵ eigensolutions for this problem was first recognized by Lindzen (1966).

Tidal theory has also been applied with success in the analysis of stratospheric equatorial motions. Yanai and Maruyama (1966) have found observational evidence of stratospheric wave disturbances over the tropical Pacific with $s \approx -4$ and $\lambda \simeq 0.1 - 0.125$, being identified as a mixed Rossby-gravity mode (Maruyama, 1967). Wallace and Kousky (1968) have observed and identified the Kelvin wave with $\lambda \simeq 0.03 - 0.05$ with suggested small s. They suggest that this wave has an upward flux of eastward momentum large enough to account for the biennial oscillation. Tropospheric wave analyses have also been made by Wallace (1971), where a review of tropical wave studies is also presented.

4. BALANCE EQUATIONS: Eigenvalues and Asymptotic Relations

Our attention is again focused upon equations (3.2) - (3.4) but with $\alpha' = \alpha = 0$. These determine the latitudinal dependence of the linearized balance equations.

The eigenvalues and eigenfunctions of these equations are to be compared with those of the Laplace's tidal equations described in chapter 3. The possible asymptotic solutions to the equations will also be studied. But, as pointed out by Charney (1962), because the equations form a highly implicit system it is very hard (if not impossible) to obtain a single equation for one of the variables, as is readily done for the tidal equations. This fact makes the asymptotic study of the eigensolutions quite difficult.

Before describing the results from the calculations for this eigenvalue problem, a relationship between the frequency and the eigenfunctions is presented.

4.1 Integral Theorem for the Balance Equations

Analogous to the way one proceeds to form an energy equation, one gets an explicit equation for the frequency by multiplying equation (3.2) by P*, (3.3) by Q* ($\alpha'=0$), and (3.4) by R*. The three equations are then added and the resulting expression is written in flux form

$$\lambda\left(s^2 \frac{P P^*}{1-\mu^2} + (1-\mu^2)\frac{dP}{d\mu}\frac{dP^*}{d\mu} + \epsilon R R^*\right) = -s P P^* + \alpha\left[s Q Q^*\right] + \tag{4.1}$$

$$+\frac{d}{d\mu}\left[(1-\mu^2)\left(\lambda P^* \frac{dP}{d\mu} + \mu Q \frac{dP^*}{d\mu} - \mu P^* \frac{dQ}{d\mu} + R^* \frac{dQ}{d\mu} - Q \frac{dR^*}{d\mu}\right)\right]$$

Taking advantage of the fact that the last term appears in flux form we integrate (4.1) from $\mu=-1$ to $\mu=+1$. This flux term gives no contribution at $|\mu|=1$, since all the functions are required to be finite at both poles.

The following integral theorem is obtained

$$\lambda = \frac{-s I_1 + \alpha (s I_5)}{s^2 I_2 + I_3 + \epsilon I_4} \tag{4.2}$$

where
$$I_1 = \int_{-1}^{1} |P|^2 d\mu$$
$$I_2 = \int_{-1}^{1} \frac{|P|^2}{1-\mu^2} d\mu$$
$$I_3 = \int_{-1}^{1} (1-\mu^2) \left|\frac{dP}{d\mu}\right|^2 d\mu \tag{4.3}$$
$$I_4 = \int_{-1}^{1} |R|^2 d\mu$$
$$I_5 = \int_{-1}^{1} |Q|^2 d\mu$$

The spectrum of possible frequencies is represented by (4.2), where λ is expressed by means of positive integrals of the eigenfunctions, the wave number s, and the parameter ϵ.

An important result from (4.2) is that for the balance equations ($\alpha = 0$) only westward propagating modes are solutions when ϵ is positive. (This powerful constraint is no longer true if $\alpha = 1$.) For s=0 the only solutions are $\lambda = 0$, except for some finite negative values of ϵ for which the denominator of (4.2) vanishes. These values of ϵ are discussed in section 4.2.6 and correspond to the asymptotic type 7 (section 3.3.4). From this behavior of the eigenvalues for s=0 we may infer that if the balance equations are to

have part of the mixed Rossby-gravity mode as a solution, it cannot "cross" the s=0 axis (see figure 2).

It might be pointed out that the denominator of (4.2) is essentially the sum of solenoidal kinetic plus total potential energy, whereas the numerator comes from the variability of the Coriolis parameter in equations (2.7) and (2.8). Thus, the dispersion relation (4.2) shows the importance of "β" = $-a^{-1}\frac{df}{d\theta}$ in case one further attempts to simplify the set of equations (e.g. studying asymptotic behaviors).

In our numerical study of the eigensolutions we have also derived an equivalent integral theorem for a truncated matrix (Appendix B).

4.2 The Eigenvalues of the Balance Equations

4.2.1 Method of Solution

Solutions of (3.2) - (3.4) are obtained in the conventional manner by expanding $P(\mu)$ and $Q(\mu)$ in surface spherical harmonics $P_n^s(\mu)$ (defined in Appendix A), and then solving a system of algebraic equations for the coefficients.

$$P = \sum_{n=s}^{\infty} B_n^s P_n^s(\mu)$$
$$Q = \sum_{n=s}^{\infty} A_n^s P_n^s(\mu) \qquad (4.4)$$

We now use convention (b) of section 3.2 for computational convenience, in which $s \geq 0$, but λ may be negative.

Making use of the properties of $P_n^s(\mu)$ we get

$$R(\mu) = -\frac{1}{\lambda\epsilon}\sum_{n=s}^{\infty} n(n+1)\,A_n^s\,P_n^s(\mu) \tag{4.5}$$

and the following recurrence relations for A_n^s and B_n^s

$$\left(\lambda n(n+1)+s\right)B_n^s - \left(\frac{n(n+2)(n+s+1)}{2n+3}\right)A_{n+1}^s - \left(\frac{(n-1)(n+1)(n-s)}{2n-1}\right)A_{n-1}^s = 0 \tag{4.6}$$

$$\left(\frac{n^2(n+1)^2}{\lambda\epsilon} - \alpha(s)\right)A_n^s + \left(\frac{n(n+2)(n+s+1)}{2n+3}\right)B_{n+1}^s + \left(\frac{(n-1)(n+1)(n-s)}{2n-1}\right)B_{n-1}^s = 0 \tag{4.7}$$

Equation (4.7) (with $\alpha = 0$) is solved for A_n^s and the result used in (4.6) to give (see Appendix A where the α term is kept).

$$d_{n-2}\,B_{n-2}^s + \left(a_n + b_n - \lambda\right)B_n^s + c_{n+2}\,B_{n+2}^s = 0 \tag{4.8}$$

where

$$a_n = -\lambda\epsilon\left[\frac{n(n-s+1)(n+s+1)}{(n+1)^3(2n+1)(2n+3)} + \frac{(n+1)(n-s)(n+s)}{n^3(2n-1)(2n+1)}\right]$$

(for $s=0$, $n=1,2,3,\ldots$; $a_1 = -\frac{\lambda\epsilon}{30}$)

$$b_n = -\frac{s}{n(n+1)} \qquad (\text{for } s=0\,,\ b_n = 0) \tag{4.9}$$

$$c_n = -\lambda\epsilon\left[\frac{(n+1)(n+s-1)(n+s)}{(n-1)^2 n(2n-1)(2n+1)}\right]$$

$$d_n = -\lambda\epsilon\left[\frac{n(n-s+1)(n-s+2)}{(n+1)(n+2)^2(2n+1)(2n+3)}\right]$$

There are two separate types of motions described by the algebraic system (4.8). One for which (n-s) is even will be denominated antisymmetric modes (v and P are even functions of μ ; u,Q,R are odd

functions of μ) and another for which (n-s) is odd will be denominated symmetric modes (v and P are odd functions; u,Q,R are even functions of μ).

$$\begin{pmatrix} (a_s+b_s-\lambda) & (c_{s+2}) & 0 & \cdots \\ (d_s) & (a_{s+2}+b_{s+2}-\lambda) & (c_{s+4}) & 0 \cdots \\ 0 & (d_{s+2}) & (a_{s+4}+b_{s+4}-\lambda) & \ddots \\ \vdots & 0 & (d_{s+4}) & \ddots \\ & \vdots & 0 & \\ & & \vdots & \end{pmatrix} \begin{pmatrix} B^s_s \\ B^s_{s+2} \\ B^s_{s+4} \\ \vdots \end{pmatrix} = \begin{pmatrix} 0 \\ 0 \\ 0 \\ \vdots \end{pmatrix} \tag{4.10}$$

$$\begin{pmatrix} (a_{s+1}+b_{s+1}-\lambda) & (c_{s+3}) & 0 & \cdots \\ (d_{s+1}) & (a_{s+3}+b_{s+3}-\lambda) & (c_{s+5}) & 0 \cdots \\ 0 & (d_{s+3}) & (a_{s+5}+b_{s+5}-\lambda) & \ddots \\ \vdots & 0 & (d_{s+5}) & \ddots \\ & \vdots & 0 & \\ & & \vdots & \end{pmatrix} \begin{pmatrix} B^s_{s+1} \\ B^s_{s+3} \\ B^s_{s+5} \\ \vdots \end{pmatrix} = \begin{pmatrix} 0 \\ 0 \\ 0 \\ \vdots \end{pmatrix} \tag{4.11}$$

System (4.11) describes motions with no crossing flow at the equator.

In order to solve the two homogeneous systems (4.10) and (4.11) we will fix values of the product $\lambda\epsilon$ and treat the consequent ordinary eigenvalue problem for λ. There is an infinite number of eigenvalues from which we are interested only in the lowest modes. The procedure is to truncate the tridiagonal matrices taking only the first N x N elements. The value of N is dictated by the convergence of the eigenvalues being sought. Appendix A describes the numerical problem and Appendix B gives a consistent way to truncate the matrices.

We now pass to the discussion of the computed eigenvalues as the parameter ϵ is varied. The corresponding eigenfunctions will be described in the next chapter.

4.2.2 Discussion of the Computed Eigenvalues

Figure 6 is the counterpart of figure 1 for the balance equations, showing the surfaces $n = n(\lambda,s,\epsilon)$.

For positive values of ϵ only westward propagating modes ($s < 0$) are solutions. λ is confined to the range (0,1/2) and the westward gravity waves are absent. Referring for further details to figure 9 (for s=-1), we note the following facts about the remaining (Rossby) modes. First, there is excellent agreement with the tidal theory for small positive values of ϵ (waves of the second class). As ϵ is increased the highest frequency mode begins to have a somewhat higher frequency than the mixed Rossby-gravity mode of the tidal equations. The lower frequency modes have good agreement for the antisymmetric modes, but the symmetric modes begin to assume

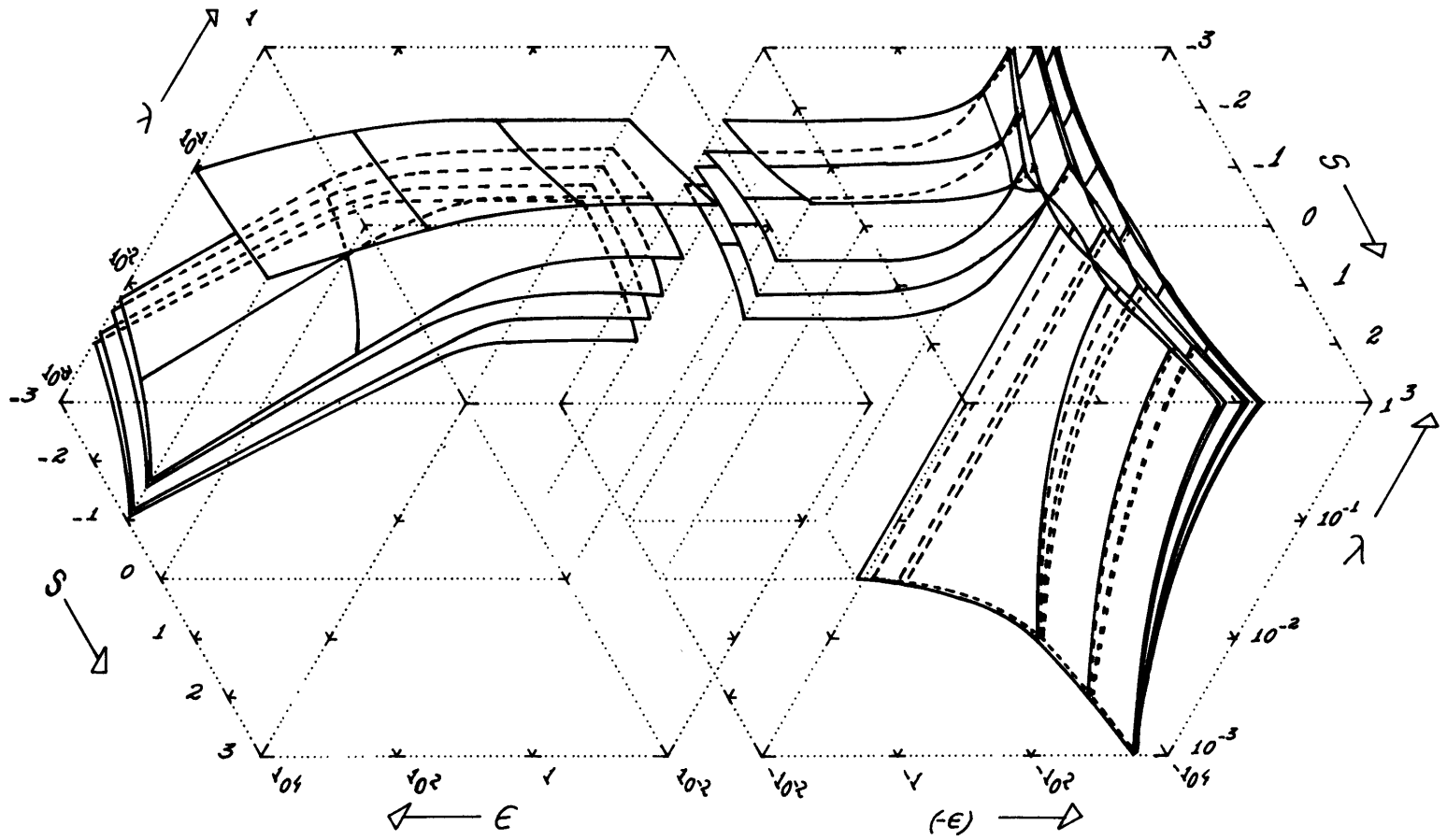


Fig. 6 Eigenvalues for the balance equations. Surfaces are shown for selected latitudinal modes (see legend to Fig. 1). The surfaces for negative ϵ continue upwards above $\lambda = 1$ instead of accumulating at $\lambda = 1$ as they do in Fig. 1.

the frequency appropriate to the neighboring antisymmetric mode.

For negative values of ε there are eastward and westward propagating solutions, but λ has the range $(0,\infty)$ instead of the range $(0,1)$ of the tidal equations. The westward modes (figure 9) are an analytical continuation of the modes of second class for small negative ε, but instead of showing an accumulation at $\lambda = 1$ (section 3.3.3, type 4) as $(-\varepsilon)$ is increased, symmetric and antisymmetric modes "cross" and become independent of λ at finite negative values of ε.

For $s = 0$ and $\varepsilon < 0$, the allowable values of ε are independent of λ (see figure 7). This independence of λ appears in the matrices (4.10) and (4.11) where $s = 0$ makes b_n vanish, allowing λ to be divided out of each row in the matrix. The ε values appear to be numerically identical with the numerical values given by Longuet-Higgins for the asymptotic type 7 ($\varepsilon<0$, $s=0$, $\lambda\to0$). For $\varepsilon<0$ and $s>0$ (eastward propagation) we have recovered (figure 8) the limiting low frequency "Burger" solutions corresponding to the type 6 of Longuet-Higgins (section 3.3.3). As the frequency is increased, however, the pairing described in section 3.3.3 for type 6 does not occur. Instead, both symmetric and antisymmetric modes at large λ have eigenvalues $(-\varepsilon)$ independent of λ.

We now parallel Longuet-Higgins' approach by examining the asymptotic behavior suggested by the numerical results.

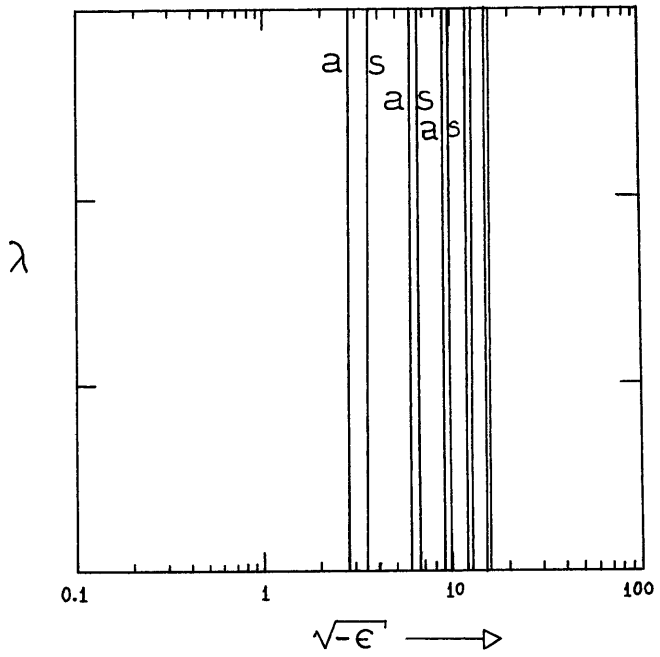


Fig. 7 Eigenvalues for the balance equations for the longitudinal wave number s = 0. They correspond to the asymptotic type 7 ($\epsilon < 0, \lambda \to 0$) described by Longuet-Higgins (compare with Fig. 3). Here the eigenvalues (ϵ) are independent of the frequency (λ). The letters a and s stand for modes with geopotential antisymmetric and symmetric about the equator.

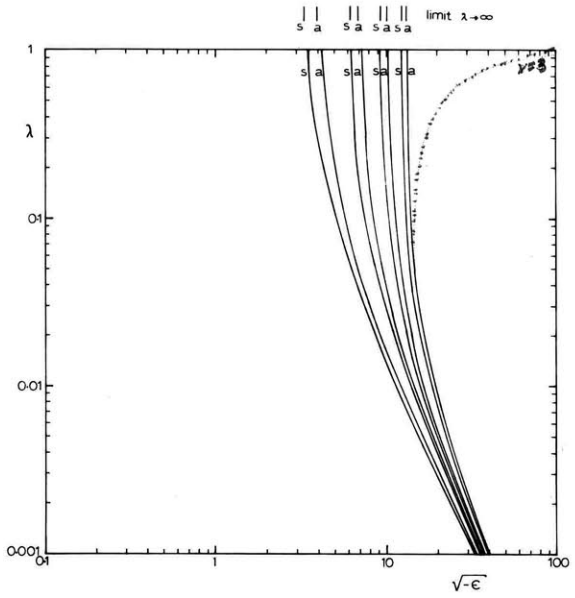


Fig. 8 Eigenvalues for the balance equations for s = 1. The limiting solutions for small frequencies agree with Longuet-Higgins' type 6 (compare with Fig. 4). However, for high frequencies, the modal curves continue upwards above $\lambda = 1$ and become independent of λ, with the limiting solutions ($\lambda \to \infty$) indicated. (These modes are here called "Burger" modes).

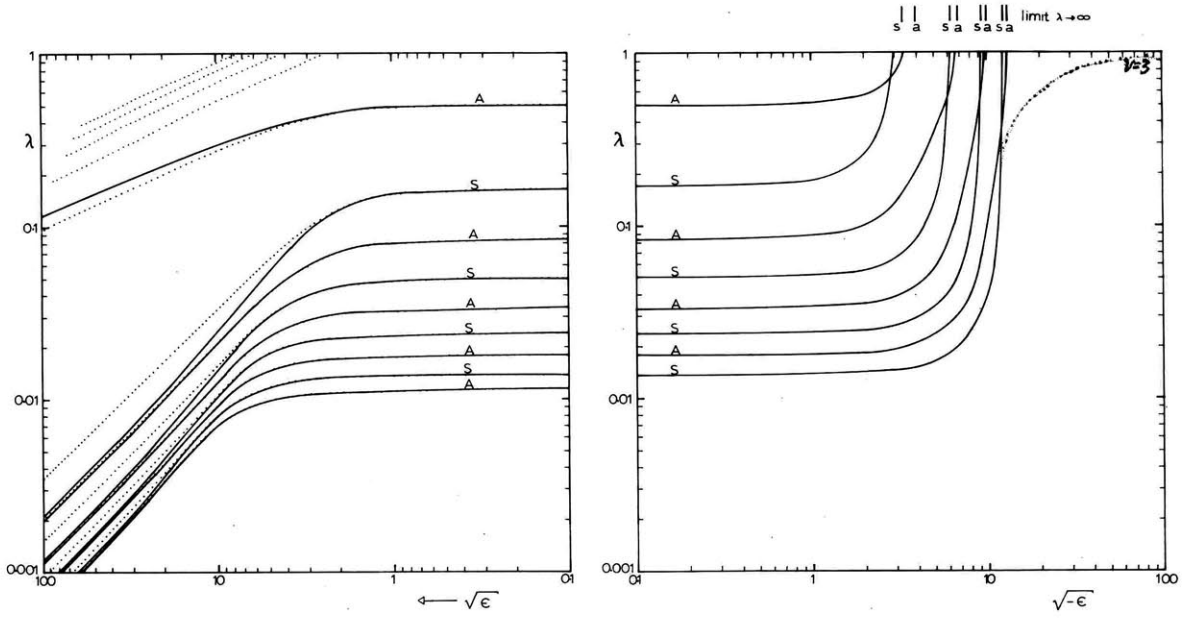


Fig. 9 Eigenvalues for the balance equations for s = -1. The frequencies are in the range (0, ½) for positive values of ϵ . The curves for negative values of ϵ have symmetric (S) and antisymmetric (A) modes crossing and continue upwards above $\lambda = 1$, with the limiting solutions ($\lambda \to \infty$) indicated (compare with Fig. 5). The dotted curves correspond to some of the eigenvalues for the Laplace's tidal equations.

4.2.3 Asymptotic Solutions as $\varepsilon \to 0$

These asymptotic solutions are obtained directly from the systems (4.10) and (4.11) as $\lambda\varepsilon \to 0$. The square matrices become diagonally dominant (c_n, $d_n \to 0$) and the eigenvalues become those for the "second class" Rossby waves

$$\lambda = \frac{-s}{n(n+1) + \epsilon\left[\frac{(n+1)^2(n-s)(n+s)}{n^2(2n-1)(2n+1)} + \frac{n^2(n-s+1)(n+s+1)}{(n+1)^2(2n+1)(2n+3)}\right]} \quad ; \; s < 0 \qquad (4.12)$$

[The term multiplied by ε in the denominator comes from the first order terms in the expansion in powers of ε for small ε as described in Appendix E.]

The waves of the first class (gravity waves) do not appear as solutions in this limiting value of ε. In this sense the gravity waves are "filtered out" by the use of the balance system. Figure 9 shows this asymptote for the case s = -1.

4.2.4 Asymptotic Solutions as $\varepsilon \to -\infty$

There exist solutions with small frequencies as $\varepsilon \to -\infty$ (figure 8). They are obtained from an expansion in power series of $(-\varepsilon)^{-\frac{1}{2}}$ as follows:

$$\lambda = s(-\varepsilon)^{-1}\left[\lambda_o + (-\varepsilon)^{-\frac{1}{2}}\lambda_1 + \ldots\right]$$

$$P = \left[P_o + (-\varepsilon)^{-\frac{1}{2}}P_1 + \ldots\right]$$

$$Q = (-\varepsilon)^{-\frac{1}{2}}\left[Q_o + (-\varepsilon)^{-\frac{1}{2}}Q_1 + \ldots\right]$$

$$R = [\, R_o + (-\varepsilon)^{-\frac{1}{2}} R_1 + \ldots \,]$$

Since the solutions are expected to be confined to the vicinity of the poles we use the stretched coordinate $\omega = (-\varepsilon)^{\frac{1}{4}}\theta$ (or $\omega = (-\varepsilon)^{\frac{1}{4}}(\pi-\theta)$ for the South pole). In order to find the solutions it is necessary to go up to first order in the expanding parameter. The zeroth order corresponds to a β-plane approximation, which geometry we know to be incapable of describing these motions [see Phillips (1963), p. 161]. It is then expected that the solutions emanate from additional constraints in higher order terms in $(-\varepsilon)^{-\frac{1}{2}}$. Appendix C gives the detailed derivation of these solutions. The eigensolutions are, asymptotically:

$$\lambda = \frac{s}{(-\epsilon)}\left[1 + \frac{2(s+2\nu+1)}{(-\epsilon)^{1/2}}\right] \quad ; \nu = 0,1,2,\ldots, s>0 \tag{4.13}$$

$$P = R = e^{-\frac{1}{2}\omega^2}\omega^s L_\nu^{(s)}(\omega^2)$$

$$\left(\omega^2\frac{d^2}{d\omega^2} + \omega\frac{d}{d\omega} - s^2\right)Q = -s(-\epsilon)^{-1/2}\omega^2 P \tag{4.14}$$

The solutions correspond to Longuet-Higgins' type 6 as discussed in section 3.3.3.

It was pointed out earlier that this type of wave follows from the scale analysis of Burger (1958). His scale analysis assumed that the divergence and vorticity were of equal magnitude, so that the vorticity equation reduces to

$$f\,\nabla\cdot\vec{v} = -\beta v \text{ , or}$$

$$\nabla\cdot\vec{v} = -\tan\theta\left(\frac{v}{a}\right) = \nabla\cdot\vec{v}_{g\tilde{e}\tilde{o}} \tag{4.15}$$

The balance equations on the other hand are derived (from the point of view of accuracy) by assuming that the vorticity (or stream function) is greater than the divergence (or velocity potential), and equation (4.14) verifies that this is indeed true for these motions. The apparent paradox with (4.15) is solved by noting that the solutions are concentrated near the pole, where $\tan\theta$ is small and the geostrophic wind is non-divergent.

4.2.5 Asymptotic Solutions as $\varepsilon \to +\infty$

Our attempts to describe this asymptotic behavior analytically have not been completely successful. In order to study this case we proceed as for the case of $\varepsilon \to -\infty$ but with the stretched coordinate now being $\eta = \varepsilon^{\frac{1}{4}}\mu$ (i.e., the solutions are expected to be concentrated about the equator), and the expanding parameter is $\varepsilon^{-\frac{1}{2}}$. The following expansion is made:

$$\begin{aligned} \lambda &= \varepsilon^{-\frac{1}{2}}[\lambda_o + \varepsilon^{-\frac{1}{2}}\lambda_1 + \ldots] \\ P &= \quad [P_o + \varepsilon^{-\frac{1}{2}}P_1 + \ldots] \\ Q &= \varepsilon^{-\frac{1}{4}}[Q_o + \varepsilon^{-\frac{1}{2}}Q_1 + \ldots] \\ R &= \varepsilon^{-\frac{1}{4}}[R_o + \varepsilon^{-\frac{1}{2}}R_1 + \ldots] \end{aligned} \tag{4.16}$$

A detailed derivation is presented in Appendix D, arriving at the equations

$$\lambda_o U_o + \eta V_o = sR_o + sA\eta + C \tag{4.17}$$

$$-\eta U_o = \frac{dR_o}{d\eta} + A \tag{4.18}$$

$$sU_o - \frac{dV_o}{d\eta} = \lambda_o R_o \tag{4.19}$$

Inthese equations $U_o = -\frac{dP_o}{d\eta}$ and $V_o = \frac{dQ_o}{d\eta} + sP_o$ play the role of zonal and meridional velocities. A and C are integration constants: $A = -(\frac{dR_o}{d\eta})_{\eta=0}$; $C = (\lambda_o U_o - sR_o)_{\eta=0}$. Note that if they were zero, (4.17) - (4.19) would correspond directly to the original equations of motion with $\frac{\partial v}{\partial t} = 0$.

The following equation for V_o is obtained from (4.17) - (4.19), when $\lambda_o \neq s^2$:

$$\left(\frac{d^2}{d\eta^2} - \frac{s}{\lambda_o} - \eta^2\right) V_o = -A(s\eta^2 - \lambda_o) - C\eta \tag{4.20}$$

If A = C = 0, (4.20) leads immediately to Longuet-Higgins' solutions of type 2 (section 3.3.2).

However, we know from the accurate matrix solutions shown on figure 9 that the <u>symmetric</u> modes of the balance equations differ from this at large ε. Let us write (4.20) separately for symmetric ($V_o^{(s)}$) and for antisymmetric modes ($V_o^{(a)}$).

<u>Symmetric modes</u> (R_o , U_o , Q_o even ; V_o , P_o odd)

$$\left(\frac{d^2}{d\eta^2} - \frac{s}{\lambda_o} - \eta^2\right) V_o^{(s)} = -C\eta \tag{4.21}$$

Antisymmetric modes (R_o , U_o , Q_o odd ; V_o , P_o even)

$$\left(\frac{d^2}{d\eta^2} - \frac{s}{\lambda_o} - \eta^2\right) V_o^{(a)} = - A (s\eta^2 + \lambda_o) \tag{4.22}$$

The boundary conditions on V_o are that $V_o \to 0$ as $|\eta| \to \infty$ (i.e., V_o must decay rapidly away from the equator for the β-plane (zeroth-order) to be a valid approximation). The homogeneous solutions of the parabolic cylinder equation (4.20) obeying these boundary conditions are the Hermite functions $e^{-\frac{1}{2}\eta^2} H_\nu(\eta)$ with the imposed eigenvalue condition $-\frac{s}{\lambda_o} = 2\nu + 1$, where ν is equal to a positive integer.

Our matrix computations have revealed that the eigensolutions for the antisymmetric modes are well described by (4.22) with $A = -(\frac{dR_o}{d\eta})_{\eta=0} \neq 0$. This implies that although R_o is an odd function of η it has a zero slope at $\eta = 0$ (as in fact happens for the type 2 solutions of the Laplace tidal equation). That in turn tells us that the zonal motions are likely to be geostrophically balanced in the equatorial region for both kind of symmetries (clearly seen from (4.18)).

On the other hand, the (matrix) computed eigensolutions for the symmetric modes show quite different results. They evidently cannot be described by equation (4.21) with $C = 0$, contrary to what happens in tidal theory (type 2 solutions with $\nu = 1,3,5, \ldots$). The eigenvalues show noticeable discrepancy when contrasted to those of Laplace's tidal equations, as shown in figure 9. The matrix computed eigenfunctions for the meridional velocity (discussed in chapter 5)

show that at large positive ε the antisymmetric modes are confined to low latitudes, agreeing well with the tidal solutions, but the meridional velocity for the symmetric modes has an appreciably larger amplitude in high latitudes than do the tidal solutions. The equatorial expansion in η evidently breaks down to some extent for these solutions.

In chapter 7 it will be shown that these symmetric modes, when calculated for the modified balance system (α=1), agree much better with Longuet-Higgins' results.

4.2.6 Behavior of the Solutions for s = 0

The eigenvalues for s = 0 are independent of frequency. They correspond to finite negative values of ε which agree with those of type 7 ($\lambda \to 0$; section 3.3.4) and are such that the denominator of (4.2) vanishes (i.e., $I_3 = -\epsilon I_4$). The same results are found if α=1, since s also multiplies this term in (4.2). Let us call $u_* = (1-\mu^2)\frac{dP}{d\mu}$ and $\lambda v_* = (1-\mu^2)\frac{dQ}{d\mu}$ and write equations (3.1) - (3.4) with s = 0 (α'=0)

$$-\lambda \frac{du_*}{d\mu} + \lambda \frac{d\mu v_*}{d\mu} = 0 \qquad (4.23a)$$

$$\frac{d\mu u_*}{d\mu} = \frac{d}{d\mu}(1-\mu^2)\frac{dR}{d\mu} \qquad (4.24a)$$

$$\lambda \frac{dv_*}{d\mu} = \lambda\epsilon R \qquad (4.25a)$$

These equations are now independent of λ (for $\lambda = 0$ the solution is $v_* = 0$ and zonal geostrophy $\mu u_* = (1-\mu^2)\frac{dR}{d\mu}$) and when integrated give:

$$-u_* + \mu v_* = E \tag{4.23b}$$

$$\mu u_* = (1-\mu^2)\frac{dR}{d\mu} + F \tag{4.24b}$$

$$\frac{dv_*}{d\mu} = \epsilon R \tag{4.25b}$$

The integration constants E and F are identically equal to zero if u_* and v_* are to be equal to zero at both poles (with $\frac{dR}{d\mu}$ finite there). We get the following equation for v_*

$$(1-\mu^2)\frac{d^2 v_*}{d\mu^2} - \epsilon \mu^2 v_* = 0 \tag{4.26}$$

This apparently simple eigenvalue problem (ϵ is the eigenvalue with $v_* = 0$ at $\mu = \pm 1$) is the same as that for Longuet-Higgins' type 7. The values of ϵ are shown in figure 7.

4.2.7 Asymptotic Behavior as $\lambda \to \infty$

There are no free solutions (positive ϵ) with frequencies greater than $\lambda = 1/2$; high frequency response of the balance equations occurs only in the case of forcing (negative ϵ).

Our numerical computations of the eigenvalues have revealed the existence of high frequency solutions for both westward and eastward propagating waves. In addition, the eigenvalues tend to become

independent of λ for finite negative values of ϵ. In order to show this, we let $Q = \lambda Q_*$ and write (3.2) - (3.4) with $\alpha' = \alpha = 0$

$$-\frac{d}{d\mu}(1-\mu^2)\frac{dP}{d\mu} + \mathcal{L}_0(Q_*) + (1-\mu^2)\frac{dQ_*}{d\mu} + \left(\frac{s^2}{1-\mu^2} + \frac{s}{\lambda}\right)P = 0 \tag{4.27}$$

$$\mu\mathcal{L}_0(P) + (1-\mu^2)\frac{dP}{d\mu} = \mathcal{L}_0(R) \tag{4.28}$$

$$\mathcal{L}_0(Q_*) = \epsilon R \tag{4.29}$$

When the limit $\lambda \to \infty$ is now taken, $\frac{s}{\lambda}$ is neglected in comparison with $\frac{s^2}{1-\mu^2}$. The variability of the Coriolis parameter in the original equations is represented by this $\frac{s}{\lambda}$ term and by the $\frac{dQ_*}{d\mu}$ and $\frac{dP}{d\mu}$ terms. The former, as evidenced by its dominant role in the $\epsilon \to 0$ solutions (4.12), which correspond to Rossby's (1939) and Haurwitz's (1940) non-divergent treatments, is historically thought of as the principal effect of the variable Coriolis parameter. It is perhaps worthwhile to note that in the present limit of $\lambda \to \infty$, it is the other terms which contain the effect of rotation on the eigenfunctions and eigenvalues.

The resulting equations are unfortunately as complicated to solve as the system (3.2) - (3.4). The limiting eigenvalues are shown in figures 7, 8, 9 and summarized in figure 10.

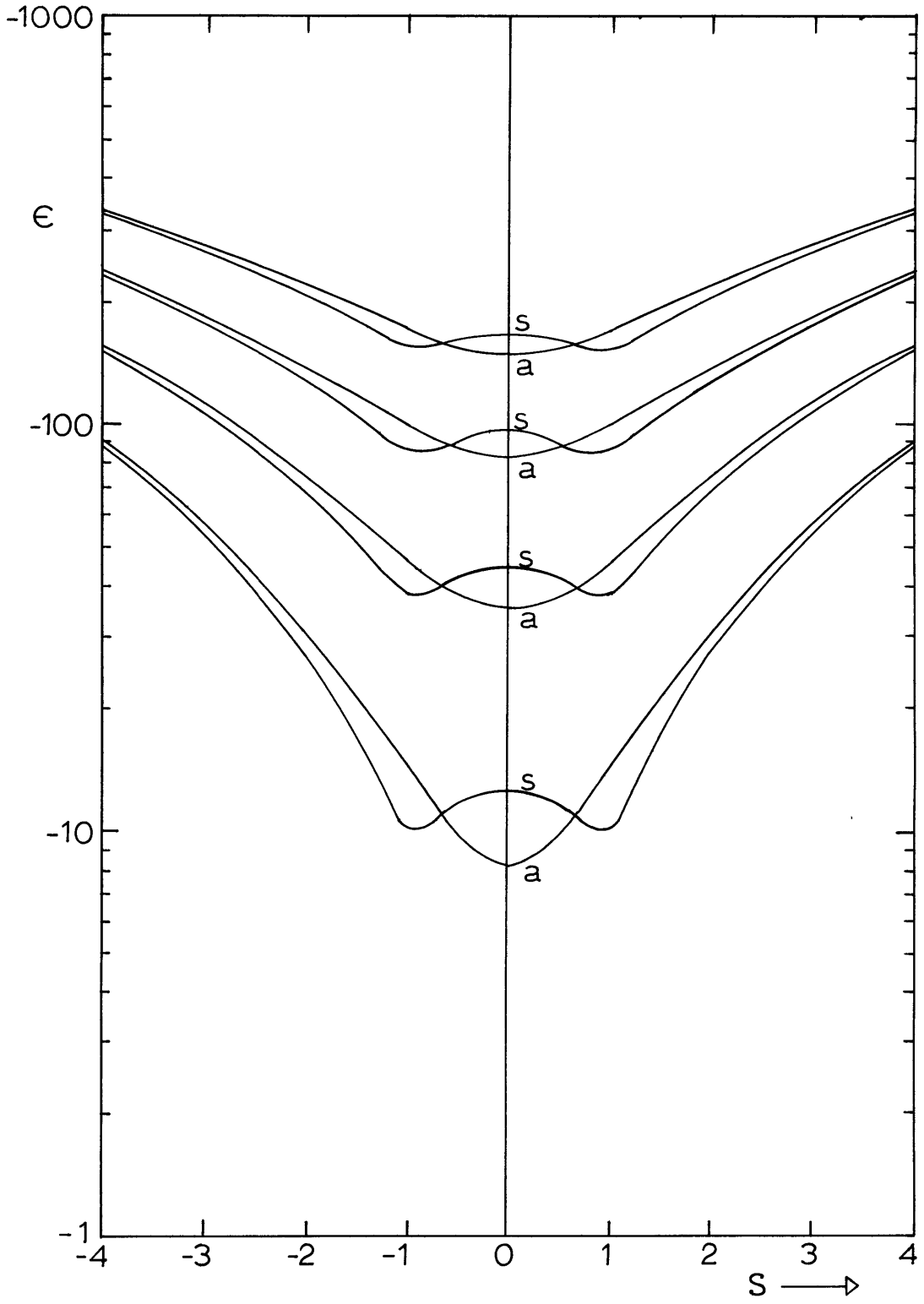


Fig. 10 Eigenvalues for the balance equations for $\lambda = 10$. These solutions appear for negative values of ϵ only. The curves show crossings of symmetric and antisymmetric modes.

5. EIGENFUNCTIONS

The eigenfunctions of the linearized balance equations are presented graphically in this chapter. The normalization factor used makes the total energy (rotational kinetic plus potential) integrated over the globe equal to $\frac{\pi}{2}$. This in turn ensures that

$$s^2 I_2 + I_3 + |\epsilon| I_4 = 1$$

where I_2, I_3, I_4 are the integrals defined in section 4.1 and the absolute value of ϵ is taken for $\epsilon < 0$ modes. This normalization procedure (discussed in Appendix A) is similar to that used by Longuet-Higgins (1968). We have chosen to present the variables $|\epsilon|^{1/2}R$, representing the latitudinal dependence of the geopotential, $U_{ROT} = -(1-\mu^2)^{1/2}\frac{dP}{d\mu}$ corresponding to the latitudinal dependence of the rotational part of the zonal velocity, and $V_{ROT} = s(1-\mu^2)^{-1/2}P$ corresponding to the latitudinal dependence of the rotational part of the meridional velocity. The formulas used for these are those at the end of Appendix A with 50 elements in each expansion and evaluation of the series made at an evenly distributed set of 41 points between $\mu=0$ and $\mu=1$. [To numerically check the eigenfunctions and eigenvalues obtained from the series, we have also introduced these values into a second-order finite-difference analog of (3.2) - (3.4). The resulting finite difference equations were typically in error of order $(1/40)^2$.]

The results are shown in figures 11-22. Only the first four modes are presented for s=1 and s=-1. The changes in the modal structure are shown as a function of the parameter ϵ. The eigenfunctions

have significant amplitude at all latitudes, for small positive or negative values of ε . However, as $|\varepsilon|$ is increased, the solutions get trapped to some extent in equatorial or polar latitudes, depending on the sign of ε .

At low frequencies, the rotational part of the zonal and meridional velocities generally accounts for most of the total zonal and meridional velocities. One exception appears for the mixed mode (see figure 11) as ε is increased. In this case the total U and V velocities are confined more to low latitudes. At high frequencies (which occur only with negative values of ε), the divergent part of U and V dominate over the rotational parts. These eigenfunctions are, of course, unrealistic in light of the balance approximation assumption that divergence << vorticity. Fortunately they would only appear in an expansion if high frequency forcings are imposed upon the system.

Figure 23 illustrates our discussion concerning the symmetric and antisymmetric modes of the asymptotic expansion $\varepsilon \to +\infty$ (section 4.2.5). The total meridional velocities of the first and second "equatorial Rossby" modes (symmetric and antisymmetric, respectively) for s=-1 are plotted in contrast with the asymptotic solutions of type 2 (section 3.3.2). It is apparent that the first symmetric mode (as computed from the matrix 4.11) cannot be described by (3.7) with ν =1 due to the large disagreement. It has an extra zero crossing between μ=0 and μ=1 and significant amplitude even at high latitudes. On the other hand, the antisymmetric mode agrees very well with the corresponding asymptotic solution, except for small discrepancy at extra-equatorial latitudes. It can be fairly well described by (3.7) with ν =2.

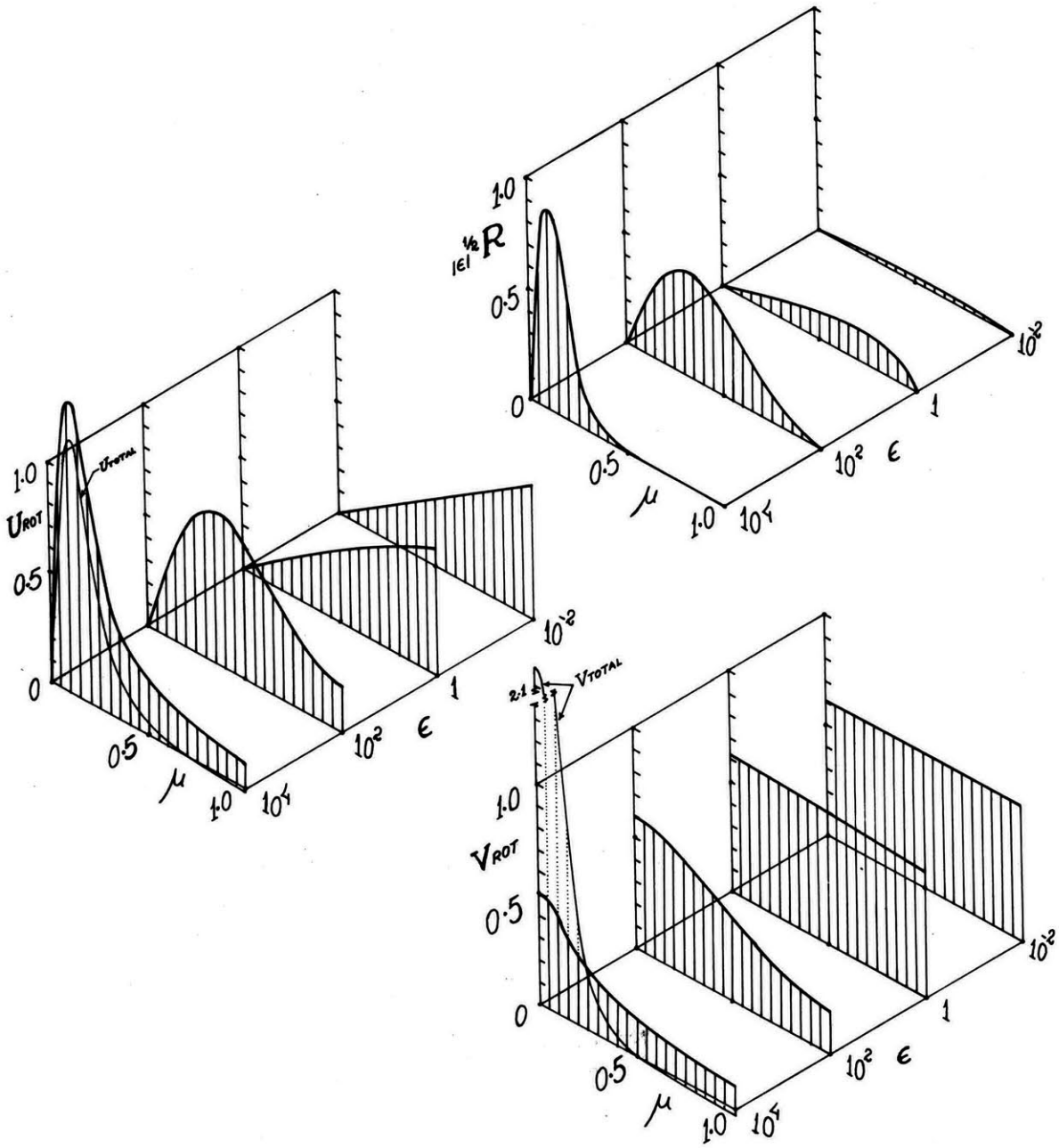


Fig. 11 Eigenfunctions for the balance equations for the "mixed Rossby-gravity" ($\epsilon > 0$) mode (n-s=0), with s = -1, showing the latitudinal distributions of the geopotential (R) and the rotational parts of the zonal (U_{ROT}) and meridional (V_{ROT}) velocities. The solutions become more confined to low latitudes as ϵ is increased. At large values of ϵ , the divergent part of the meridional velocity becomes larger than the rotational part for this mode.

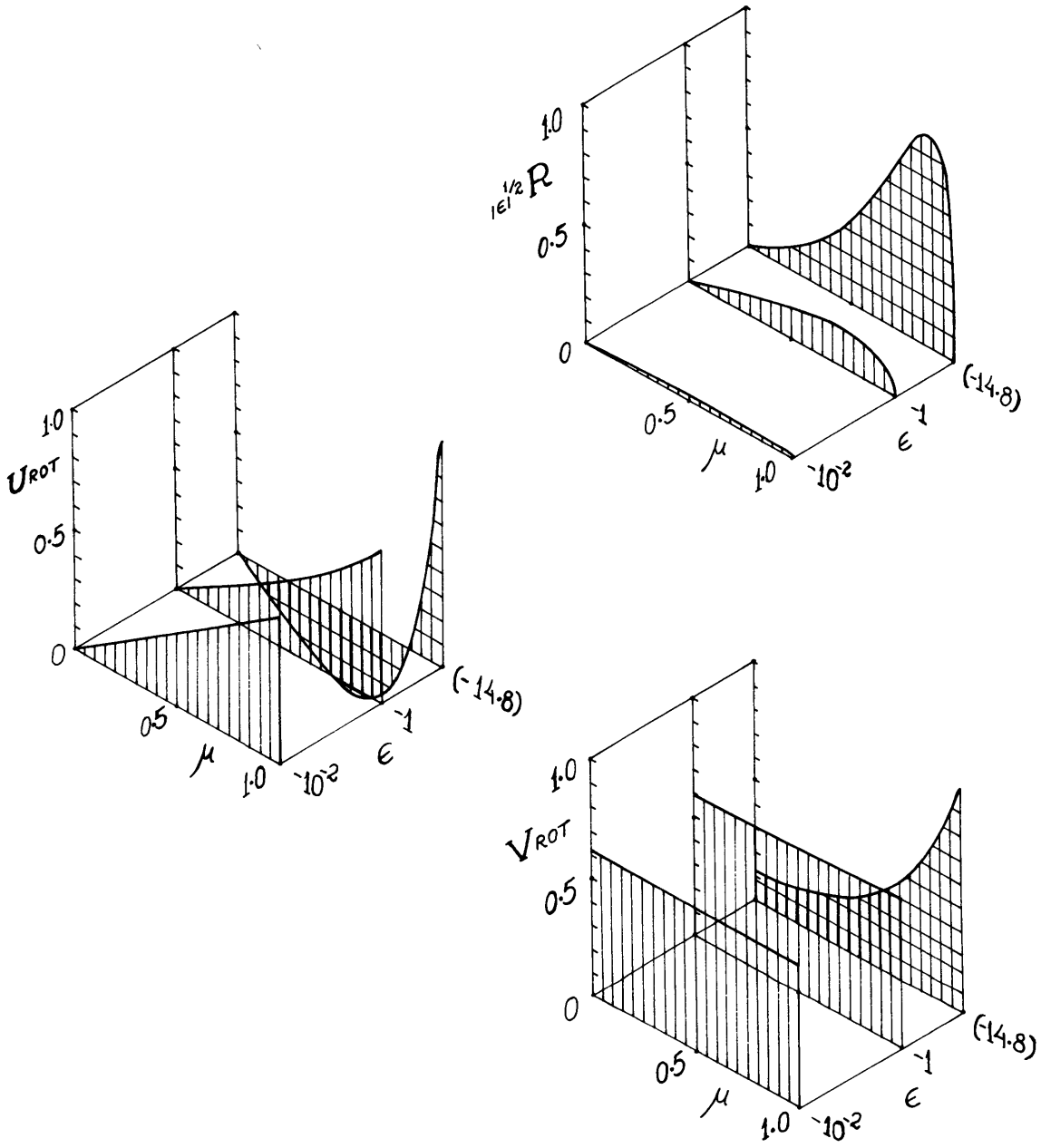


Fig. 12 Eigenfunctions for the balance equations for the continuation ($\epsilon < 0$) of the "Mixed Rossby-Gravity" mode, with s = -1, showing the latitudinal distributions of the geopotential (R) and the rotational parts of the zonal (U_{ROT}) and meridional (V_{ROT}) velocities. The cross-hatched eigenfunctions correspond to the limiting $\lambda \to \infty$ ($\epsilon < 0$) solutions.

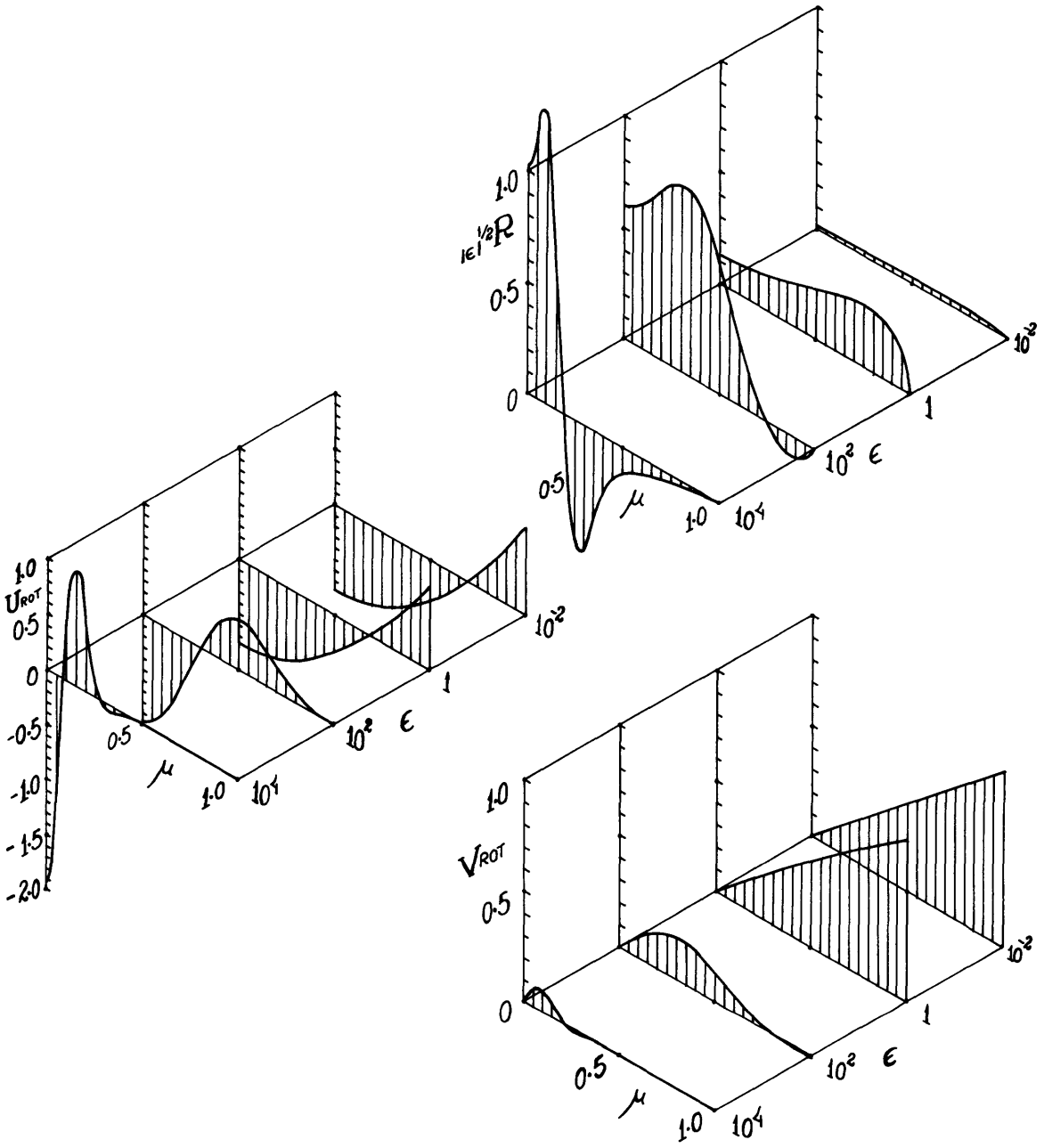


Fig. 13 Eigenfunctions for the balance equations for the (n-s) = 1 Rossby mode, with s = -1. The latitudinal structure of the geopotential (R) and the rotational parts of the zonal (U_{ROT}) and meridional (V_{ROT}) velocities are shown for several positive values of ϵ . This mode, at large ϵ , differs from Laplace's tidal solutions of type 2 for $\nu = 1$.

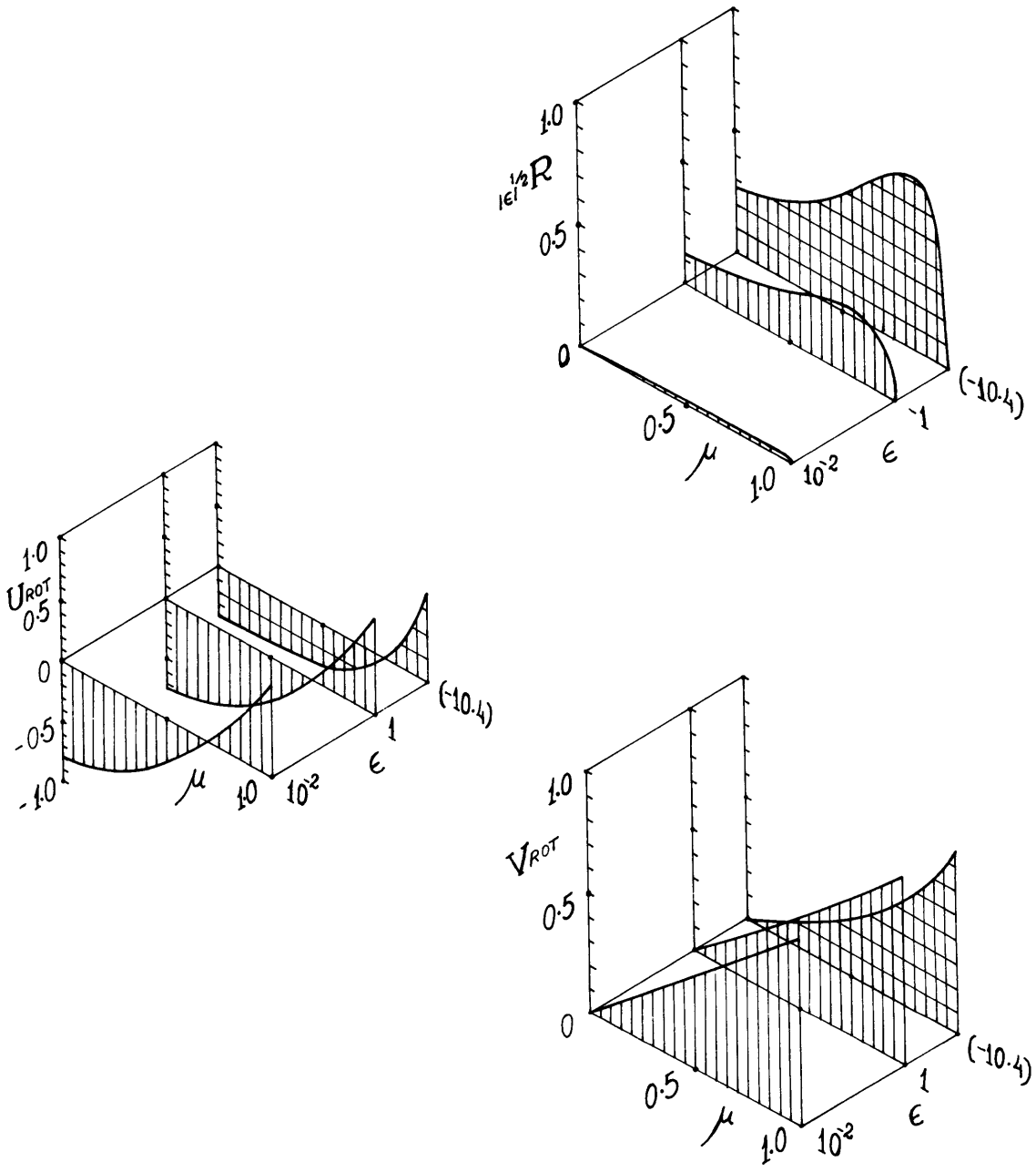


Fig. 14 Eigenfunctions for the balance equations for the continuation ($\epsilon < 0$) of the (n-s) = 1 Rossby mode, with s = -1, showing the latitudinal structure of the geopotential (R) and the rotational parts of the zonal (U_{ROT}) and meridional (V_{ROT}) velocities. The cross-hatched eigenfunctions correspond to the limiting $\lambda \to \infty$ ($\epsilon < 0$) solutions.

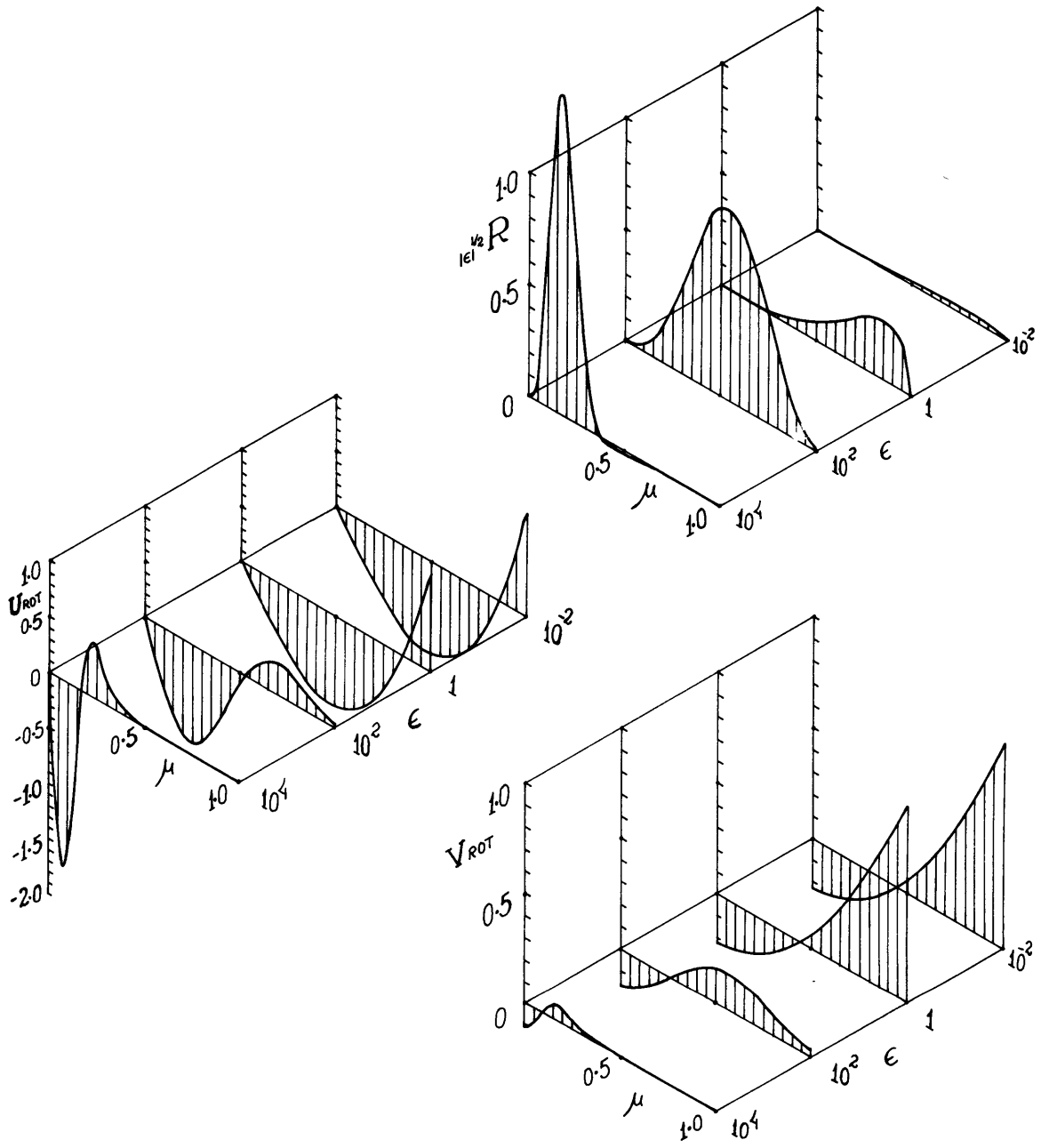


Fig. 15 Same as Fig. 13, but for the (n-s) = 2 Rossby mode. This mode, at large ϵ , agrees well with the limiting type 2 solutions with $\nu = 2$ (Longuet-Higgins).

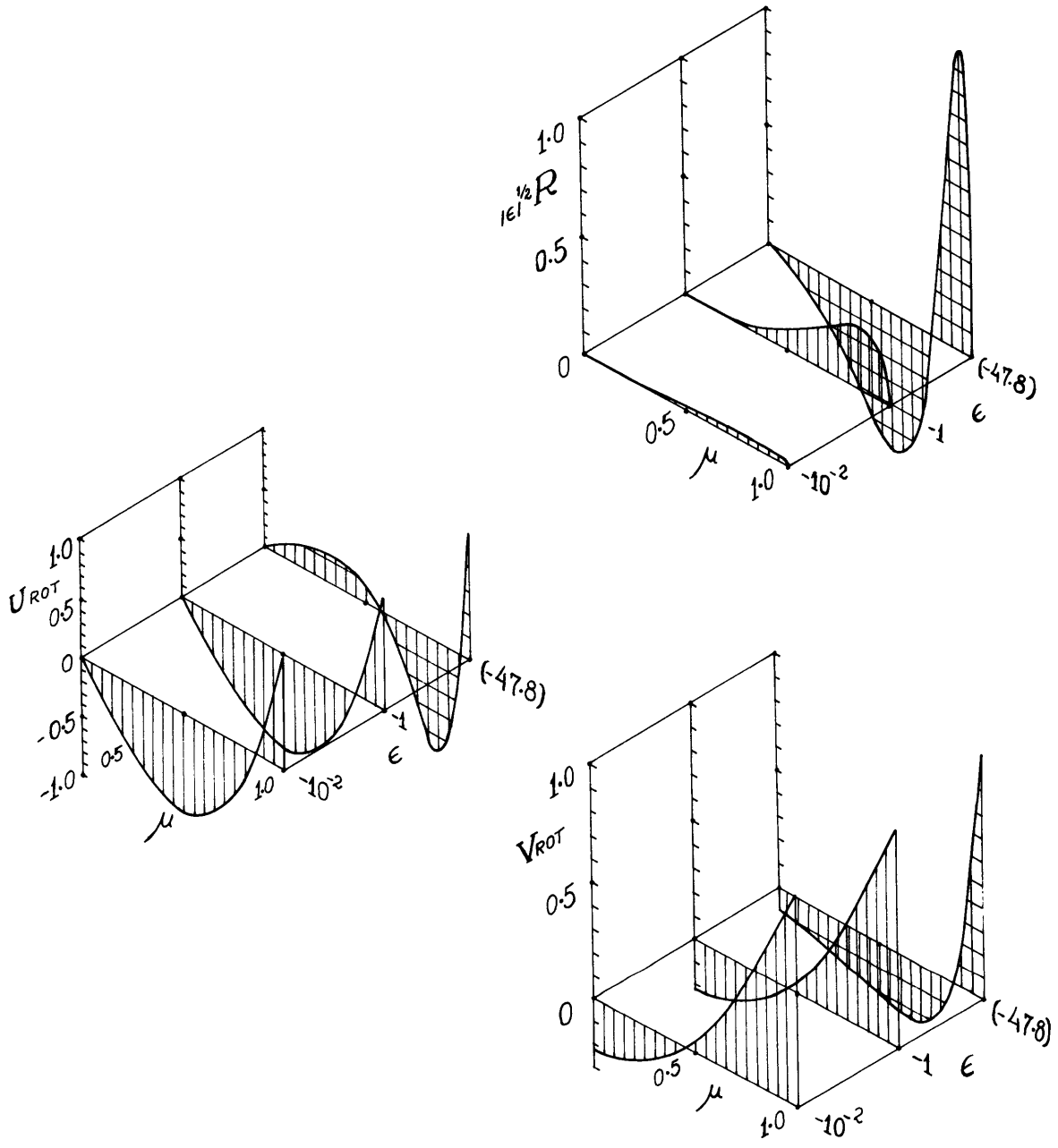


Fig. 16 Same as Fig. 14, but for the continuation ($\epsilon < 0$) of the (n-s) = 2 Rossby mode.

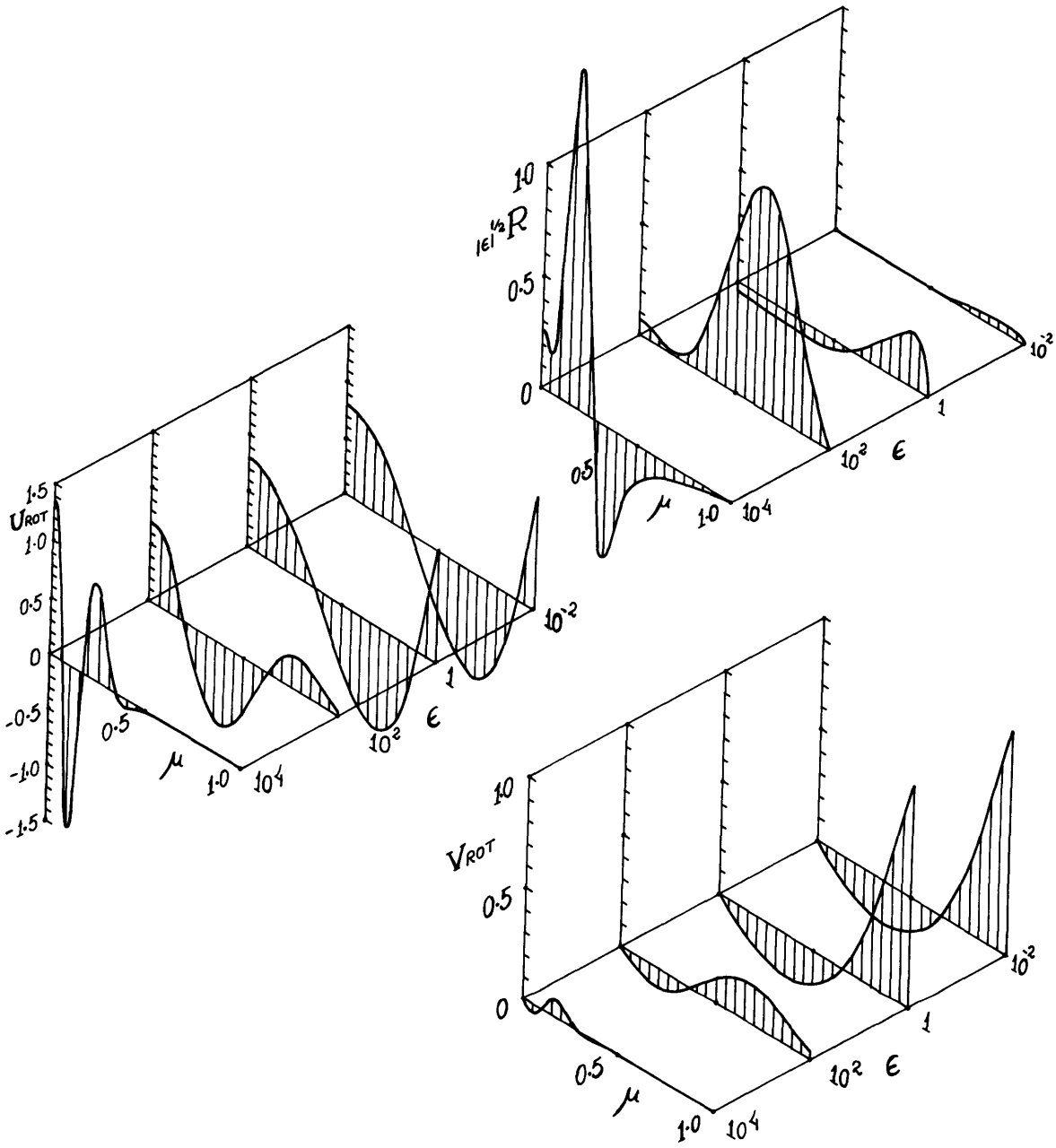


Fig. 17 Same as Fig. 13, but for the (n-s) = 3 Rossby mode.

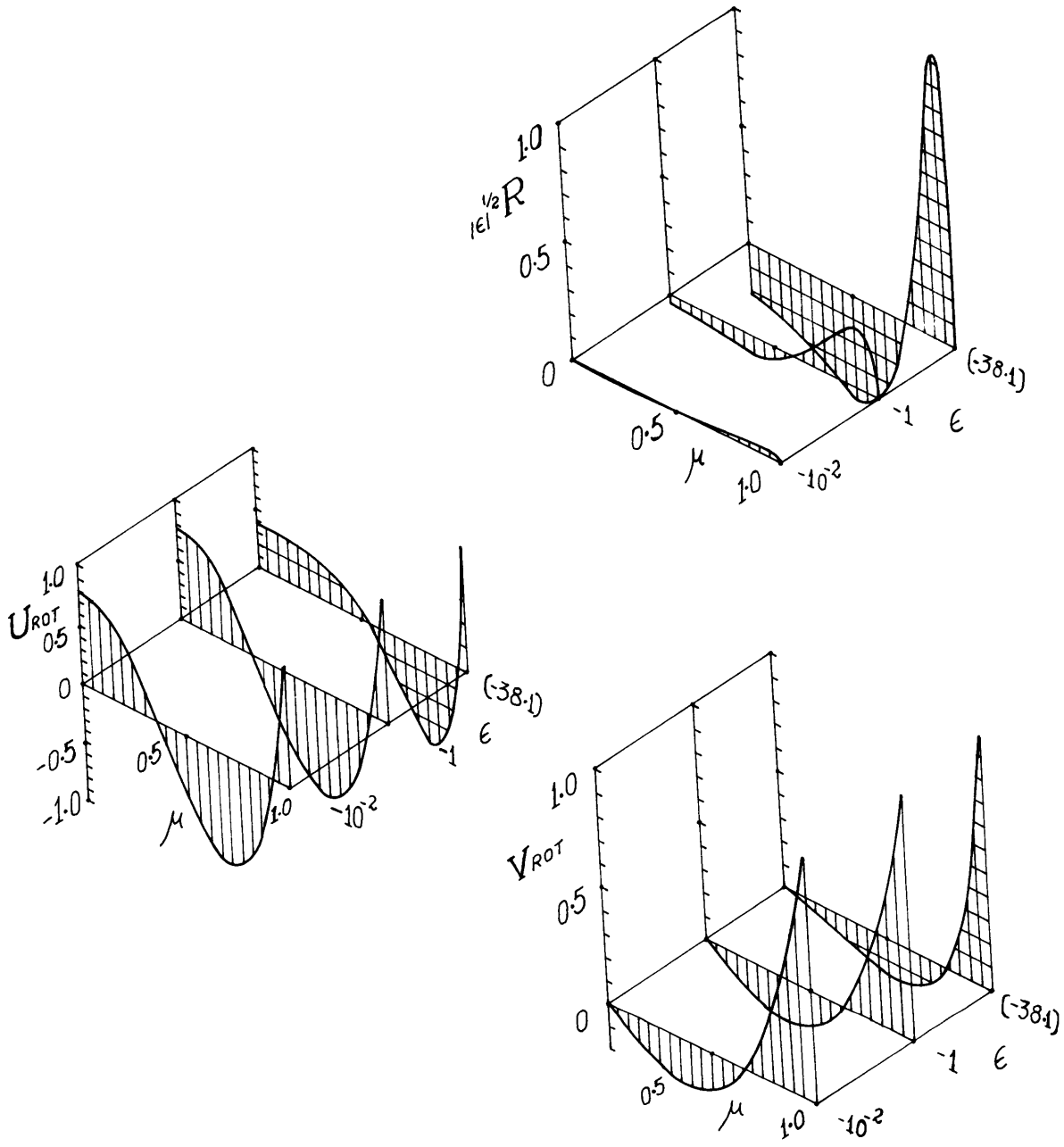


Fig. 18 Same as Fig. 14, but for the continuation ($\epsilon < 0$) of the (n-s) = 3 Rossby mode.

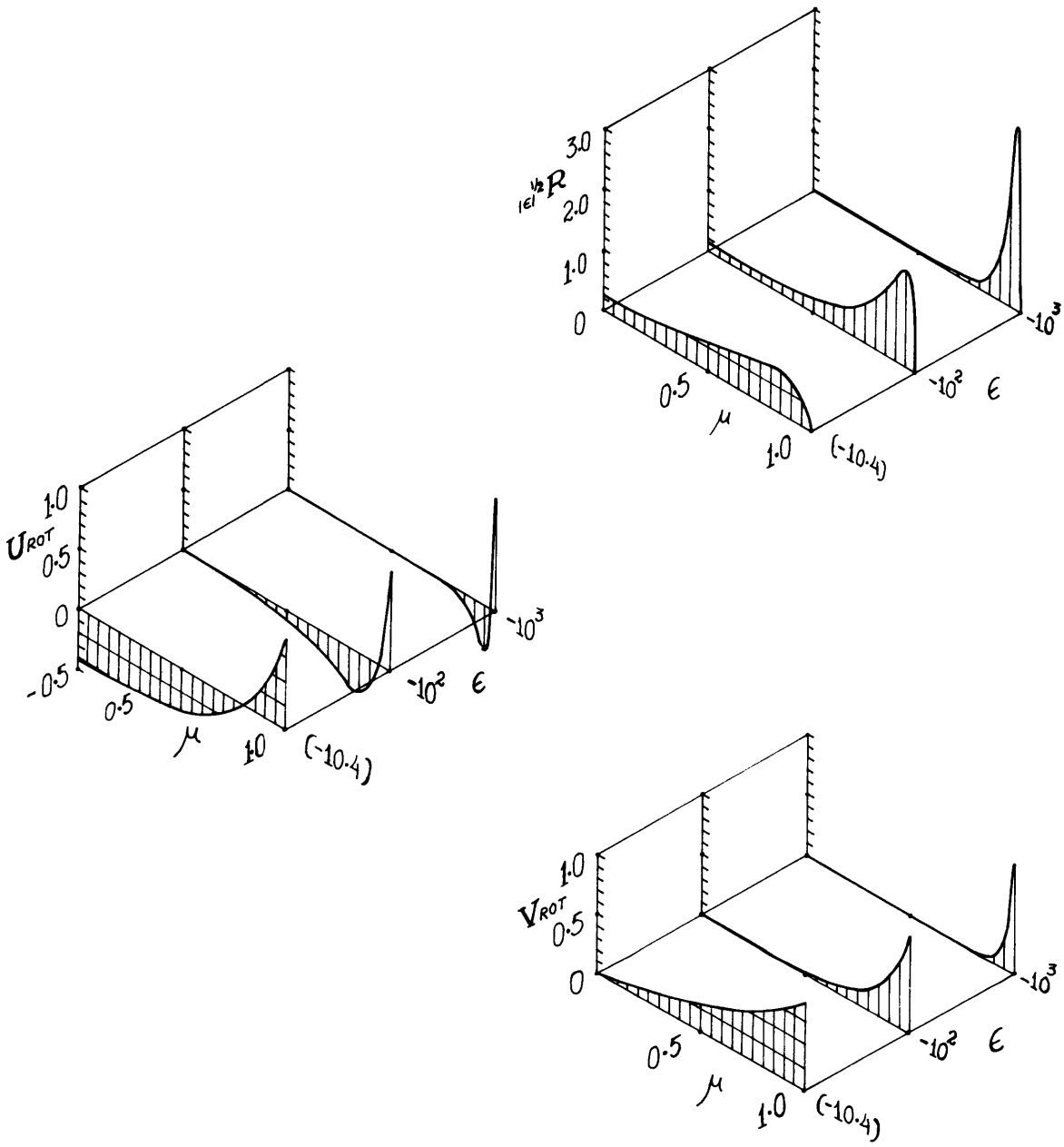


Fig. 19 Eigenfunctions ($|\epsilon|^{1/2}R$, U_{ROT}, V_{ROT}) for the balance equations for the "Burger 0" mode ($\epsilon < 0$), with $s = 1$. The cross-hatched eigenfunctions correspond to the limiting ($\lambda \to \infty$; $\epsilon < 0$) solutions. At low frequencies, this mode agrees with the limiting type 6 solutions by Longuet-Higgins.

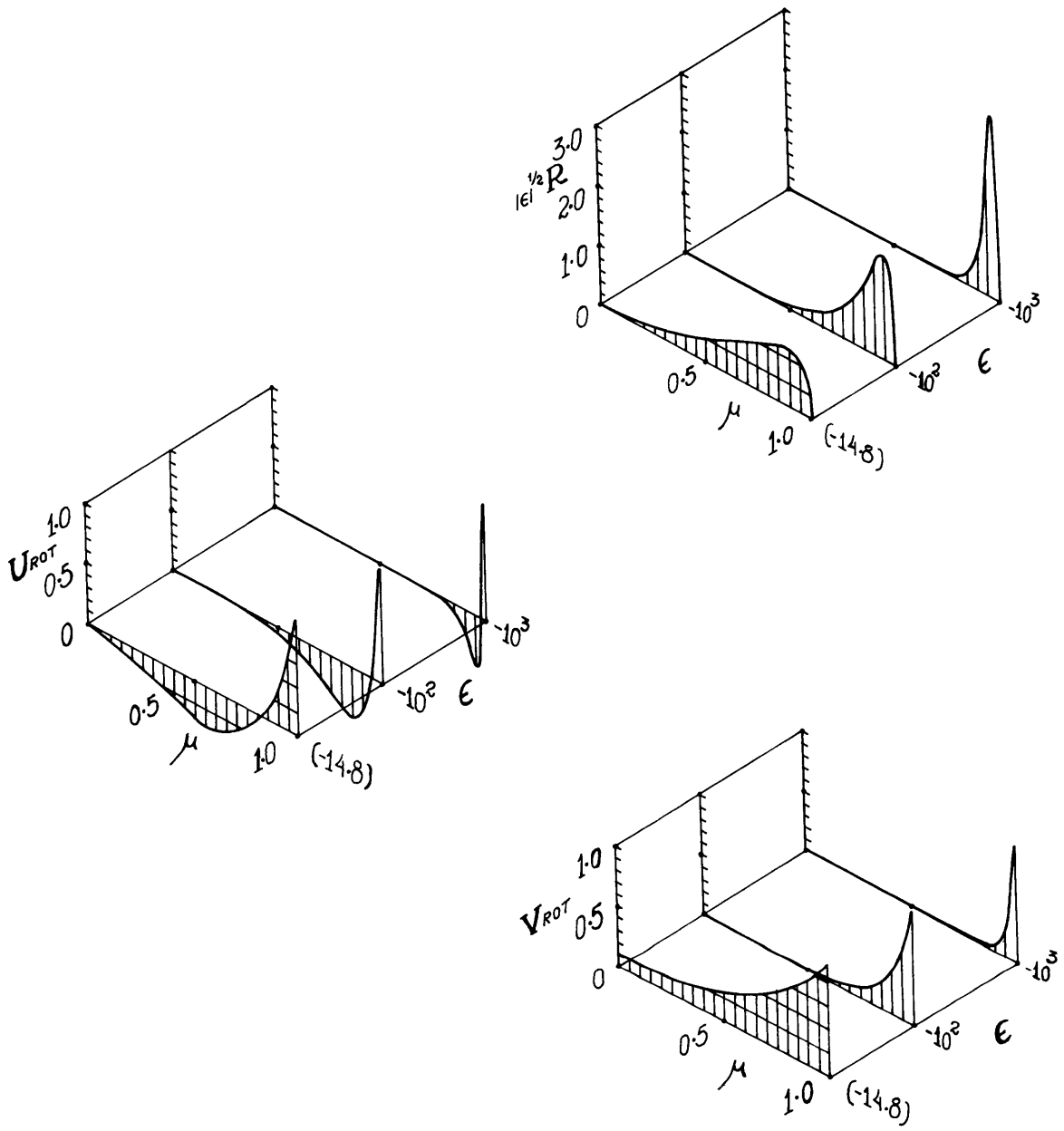


Fig. 20 Same as Fig. 19, but for the "Burger 1" ($\epsilon < 0$) mode.

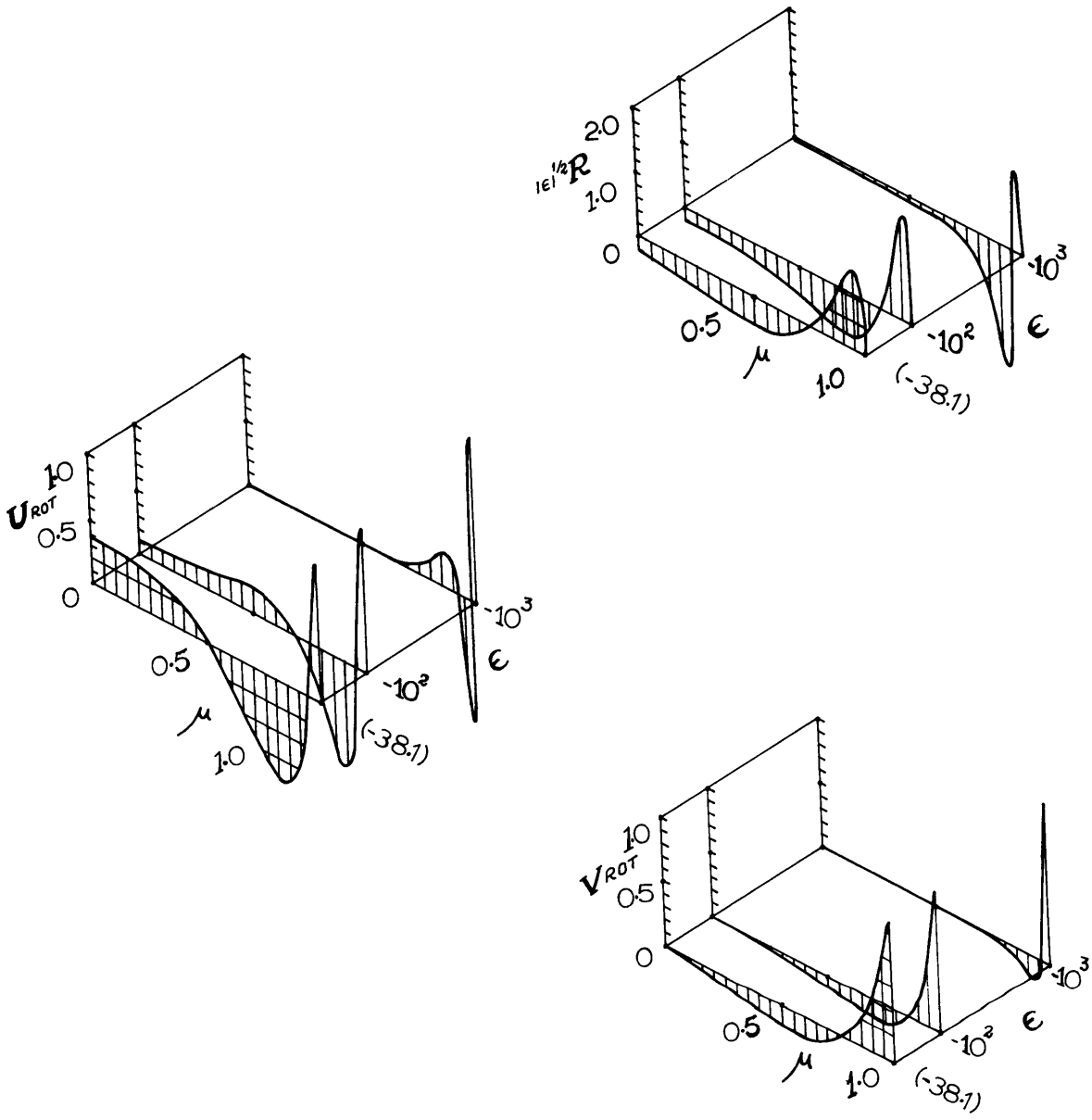


Fig. 21 Same as Fig. 19, but for the "Burger 2" ($\epsilon < 0$) mode.

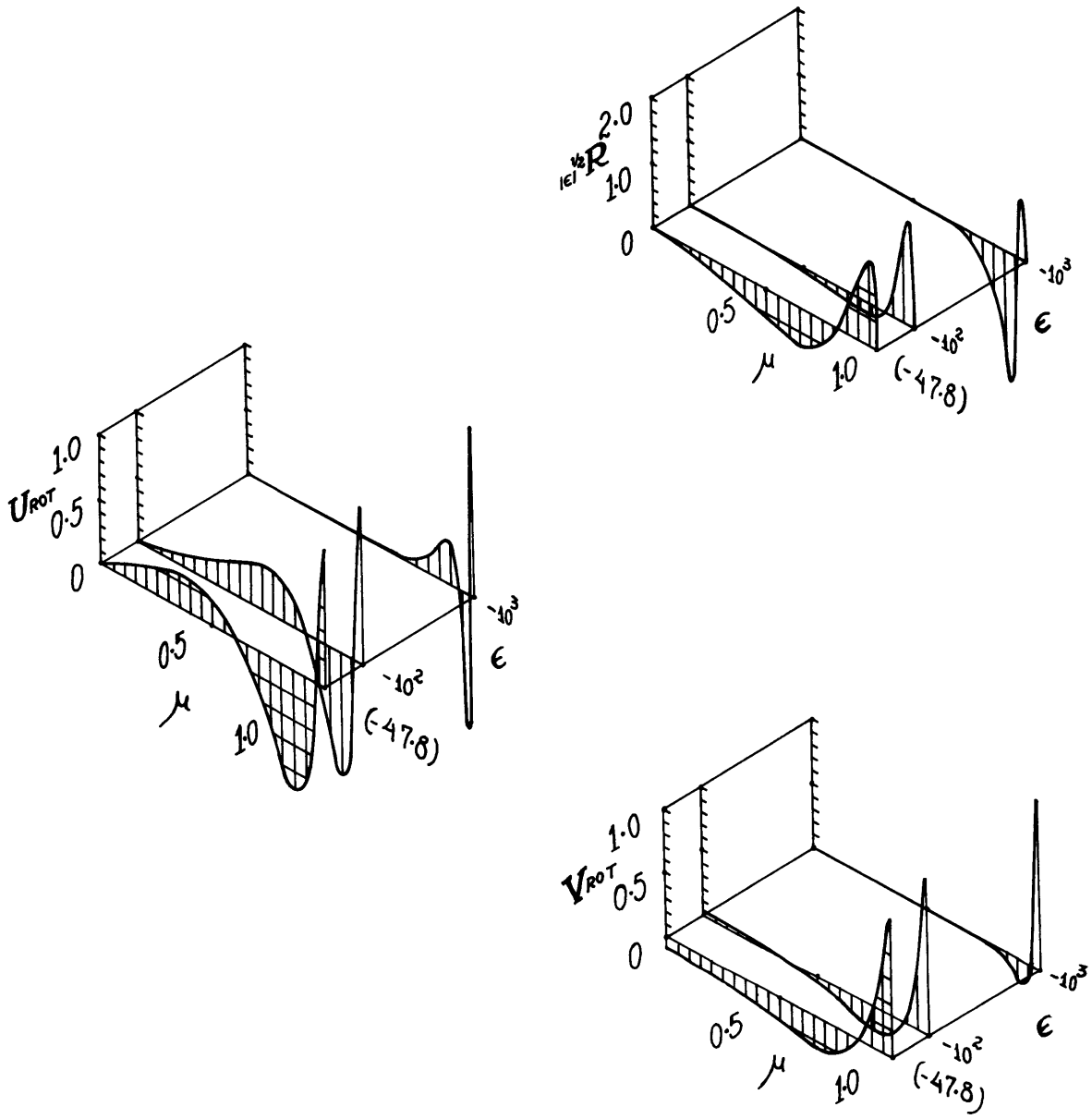


Fig. 22 Same as Fig. 19, but for the "Burger 3" ($\epsilon < 0$) mode.

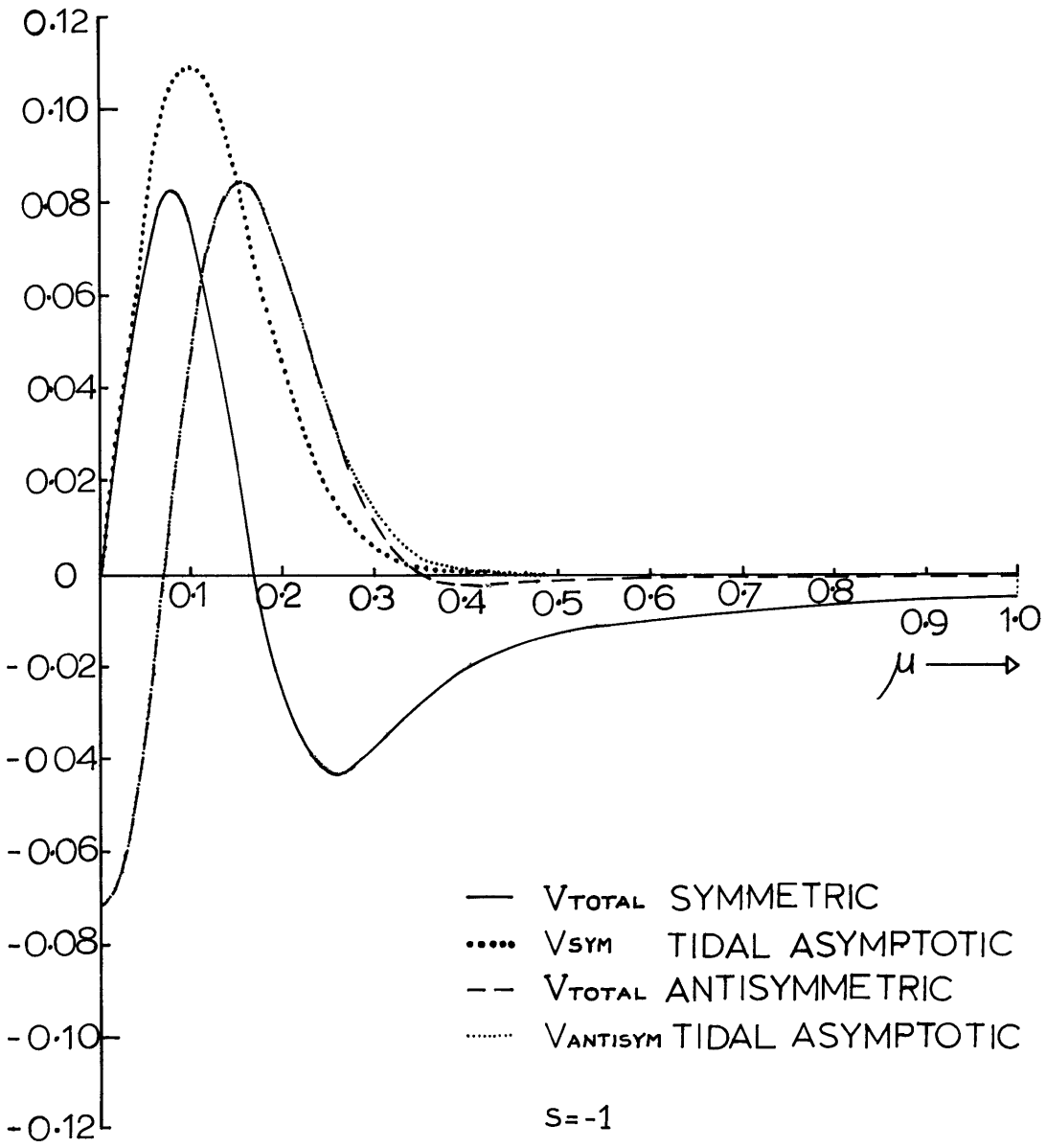


Fig. 23 Comparison of the total meridional velocity (V_{TOTAL}) of the balance equations with the asymptotic solutions of type 2 for $s = -1$ described by Longuet-Higgins. The discrepancy between the V_{TOTAL} Symmetric of the balance equations for $\epsilon = 1.07 \times 10^{-4}$, $\lambda = 1.97 \times 10^{-3}$ and the asymptotic solution of type 2 for $\epsilon = 1.07 \times 10^{-4}$ and $\nu = 1$ is shown. The good agreement between the V_{TOTAL} Antisymmetric of the balance equations for $\epsilon = 1.02 \times 10^{-4}$, $\lambda = 1.95 \times 10^{-3}$ and the type 2 solution for $\epsilon = 1.02 \times 10^{-4}$ and $\nu = 2$ is also shown.

6. STABILITY STUDY OF A BASIC ZONAL VELOCITY PROFILE

In the previous chapters we have studied the latitudinal structure of the solutions of the balance equations on a resting basic state. We have shown that all possible frequencies are real (integral theorem (4.2)).

The inclusion of a basic zonal flow in the equations (2.7) - (2.11) may allow for complex values among the possible frequencies. Some of the modal solutions will then be damped while others will grow exponentially with time. The perturbation solutions with a positive growth rate (imaginary part of the frequency > 0) are said to be unstable. If the growing disturbances derive their energy from the zonal kinetic energy available due to a horizontal shear of the basic zonal flow, the basic flow is said to be barotropically unstable with respect to those disturbances. But if the growing disturbances owe their energy source to the available potential energy in the horizontal basic temperature gradient (which by hydrostatic and geostrophic balance requires a vertical shear of the basic zonal profile), the basic zonal flow is baroclinically unstable and the perturbations are called growing baroclinic waves.

We will focus our attention on the baroclinic instability problem with a simple family of zonal profiles $\overline{U} = a\alpha(p)\sqrt{1-\mu^2}\,(1+\delta\mu^2)$. The use of this basic zonal velocity in the continuous equations (2.7) - (2.11), however, makes the separation of vertical and horizontal structures impossible. In order to handle this difficulty we will make use of a simple two-layer model, which is still able to provide

the conversion of available potential energy to feed the growing perturbations.

6.1 The Model Equations

The version of (2.7) – (2.10) with the α index equal to zero, $\vec{F}=0$, $q=0$ and linearized about the basic state in pressure coordinates are

$$\frac{\partial}{\partial t}\nabla^2\psi' = -\hat{k}\times\nabla\overline{\psi}\cdot\nabla(\nabla^2\psi') - \hat{k}\times\nabla\psi'\cdot\nabla(\nabla^2\overline{\psi}+f) - \nabla\cdot(\gamma\nabla^2\overline{\psi}+f)\nabla\chi' - \gamma\nabla\cdot\left(\tilde{\omega}'\nabla\frac{\partial\overline{\psi}}{\partial p}\right) \tag{6.1}$$

$$\nabla^2\phi' = \nabla\cdot(f+\gamma\nabla^2\overline{\psi})\nabla\psi' + \gamma\nabla\cdot\left[\nabla^2\psi'\nabla\overline{\psi} - \nabla(\nabla\overline{\psi}\cdot\nabla\psi')\right] \tag{6.2}$$

$$\frac{\partial}{\partial t}\left(\frac{\partial\phi'}{\partial p}\right) = -\hat{k}\times\nabla\overline{\psi}\cdot\nabla\left(\frac{\partial\phi'}{\partial p}\right) - \hat{k}\times\nabla\psi'\cdot\nabla\left(\frac{\partial\overline{\Phi}}{\partial p}\right) + \tilde{\omega}'\left[\frac{R}{p_{oo}}\left(\frac{p_{oo}}{p}\right)^{1-\chi}\frac{d\Theta_s(p)}{dp}\right] \tag{6.3}$$

$$\nabla^2\chi' = -\frac{\partial\tilde{\omega}'}{\partial p} \tag{6.4}$$

where the primes are used for perturbation variables and the basic state variables (functions of latitude and pressure alone) are indicated by overbars. The latter satisfy the relations

$$\nabla\overline{\psi} = -\hat{j}\,a\,\alpha(p)\,(1-\mu^2)^{1/2}(1+\delta\mu^2) \tag{6.5}$$

$$\nabla\overline{\Phi} = -\hat{j}\,a\,\alpha(p)\,\mu(1-\mu^2)^{1/2}(1+\delta\mu^2)\left[2\Omega+\gamma\alpha(p)(1+\delta\mu^2)\right] \tag{6.6}$$

$$f+\nabla^2\overline{\psi} = 2\mu\left[\Omega+\alpha(p)(1-\delta+2\delta\mu^2)\right] \tag{6.7}$$

$$\overline{\chi} = \overline{\tilde{\omega}} = 0 \tag{6.8}$$

in which $\alpha(p)$ is the functional variation of the basic state zonal velocity with respect to pressure. The index γ, which takes the values 0 or 1, is used in order to compare the two sets of equations (6.1) - (6.4) with and without the γ terms. These γ terms arise from the underlined terms in (2.7) and (2.8). In equation (6.3) the advection term due to the divergent part of the velocity was not included because in the last term of (6.3) we are taking the potential temperature $\Theta_s(p)$ for a standard atmosphere. This is necessary for the energy consistency requirement (see Lorenz (1960)). (Note that (6.1) - (6.4) with γ =1 or γ =0 reduces to the same set of equations if the basic state is a resting one. Thus, the linearized study presented in the previous chapters applies to both systems).

Inserting (6.5) - (6.7) into (6.1) - (6.4) we obtain

$$\frac{\partial}{\partial t}\mathcal{L}\psi' = -\alpha(p)(1+\delta\mu^2)\frac{\partial}{\partial\varphi}\mathcal{L}\psi' - 2\left[\Omega+\alpha(p)(1-\delta+6\delta\mu^2)\right]\frac{\partial\psi'}{\partial\varphi} - $$
$$-2\mu\left[\Omega+\gamma\alpha(p)(1-\delta-2\delta\mu^2)\right]\mathcal{L}\chi' - 2(1-\mu^2)\left[\Omega+\gamma\alpha(p)(1-\delta+6\delta\mu^2)\right]\frac{\partial\chi'}{\partial\mu} +$$
$$+\gamma a^2\frac{d\alpha(p)}{dp}\frac{\partial}{\partial\mu}\left[(1-\mu^2)(1+\delta\mu^2)\tilde{\omega}'\right] \tag{6.9}$$

$$\mathcal{L}\phi' = 2\mu\left[\Omega+\gamma\alpha(p)(1-\delta+2\delta\mu^2)\right]\mathcal{L}\psi' + 2(1-\mu^2)\left[\Omega+\gamma\alpha(p)(1-\delta+6\delta\mu^2)\right]\frac{\partial\psi'}{\partial\mu}$$
$$+2\gamma\alpha(p)\mu(1-\delta+2\delta\mu^2)\mathcal{L}\psi' - \gamma\alpha(p)(1-\mu^2)(1-\delta\mu^2)\frac{\partial}{\partial\mu}\mathcal{L}\psi' +$$
$$+\gamma\alpha(p)\,\mathcal{L}\left[(1-\mu^2)(1+\delta\mu^2)\frac{\partial\psi'}{\partial\mu}\right] \tag{6.10}$$

$$\frac{\partial}{\partial t}\left(\frac{\partial\phi'}{\partial p}\right) = -\alpha(p)(1+\delta\mu^2)\frac{\partial}{\partial\varphi}\left(\frac{\partial\phi'}{\partial p}\right) + 2\frac{d\alpha(p)}{dp}\mu(1+\delta\mu^2)\left[\Omega+\gamma\alpha(p)(1+\delta\mu^2)\right]\frac{\partial\psi'}{\partial\varphi}$$
$$+\left[\frac{R}{p_{oo}}\left(\frac{p_{oo}}{p}\right)^{1-\chi}\frac{d\Theta_s(p)}{dp}\right]\tilde{\omega}', \tag{6.11}$$

$$\mathcal{L}\chi' = -a^2 \frac{\partial \tilde{\omega}'}{\partial p} \tag{6.12}$$

$$\mathcal{L} \equiv a^2 \nabla^2 \quad \text{and} \quad \varepsilon \quad \text{is a parameter.} \tag{6.13}$$

6.2 Two-layer Model

The pressure dependence of the perturbation variables will be expressed in finite-difference form by means of a two-layer model, schematically shown in figure 24.

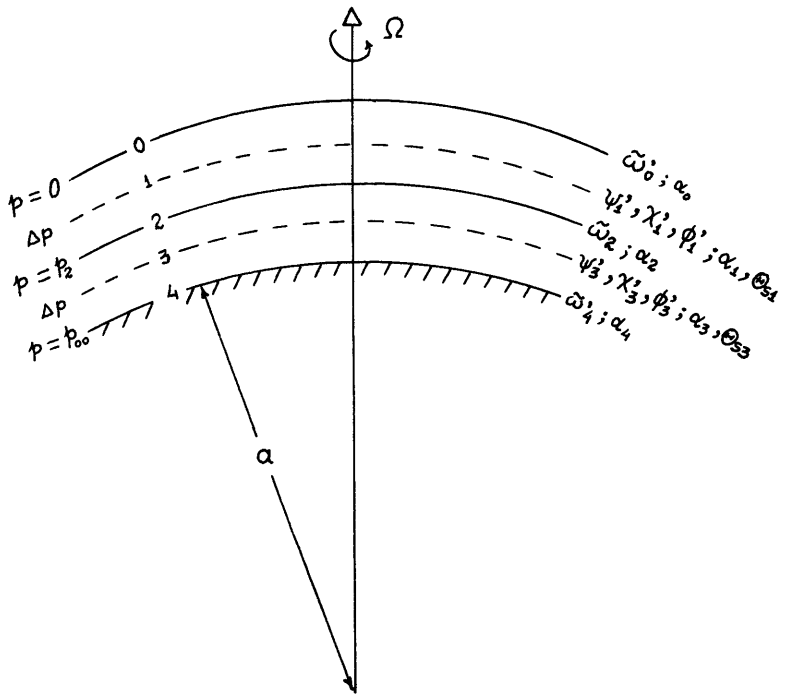


Figure 24 – Scheme of a two-layer model

Equations (6.9), (6.10), and (6.12) are written for levels 1 and 3 while equation (6.11) is written for level 2 to give:

$$\frac{\partial}{\partial t}\mathcal{L}\psi_1' = -\alpha_1(1+\delta\mu^2)\frac{\partial}{\partial\varphi}\mathcal{L}\psi_1' - 2\left[\Omega+\alpha_1(1-\delta+6\delta\mu^2)\right]\frac{\partial\psi_1'}{\partial\varphi} - \\ -2\mu\left[\Omega+\gamma\alpha_1(1-\delta+2\delta\mu^2)\right]\mathcal{L}\chi_1' - 2(1-\mu^2)\left[\Omega+\gamma\alpha_1(1-\delta+6\delta\mu^2)\right]\frac{\partial\chi_1'}{\partial\mu} + \\ +\gamma a^2\frac{\alpha_2-\alpha_0}{\Delta p}\frac{\partial}{\partial\mu}\left[(1-\mu^2)(1+\delta\mu^2)\tilde{\omega}_1'\right] \tag{6.14}$$

$$\frac{\partial}{\partial t}\mathcal{L}\psi_3' = -\alpha_3(1+\delta\mu^2)\frac{\partial}{\partial\varphi}\mathcal{L}\psi_3' - 2\left[\Omega+\alpha_3(1-\delta+6\delta\mu^2)\right]\frac{\partial\psi_3'}{\partial\varphi} - \\ -2\mu\left[\Omega+\gamma\alpha_1(1-\delta+2\delta\mu^2)\right]\mathcal{L}\chi_3' - 2(1-\mu^2)\left[\Omega+\gamma\alpha_3(1-\delta+6\delta\mu^2)\right]\frac{\partial\chi_3'}{\partial\mu} + \\ +\gamma a^2\frac{\alpha_4-\alpha_2}{\Delta p}\frac{\partial}{\partial\mu}\left[(1-\mu^2)(1+\delta\mu^2)\tilde{\omega}_3'\right] \tag{6.15}$$

$$\mathcal{L}\phi_1' = 2\mu\left[\Omega+\gamma\alpha_1(1-\delta+2\delta\mu^2)\right]\mathcal{L}\psi_1' + 2(1-\mu^2)\left[\Omega+\gamma\alpha_1(1-\delta+6\delta\mu^2)\right]\frac{\partial\psi_1'}{\partial\mu} + \\ +2\gamma\alpha_1\mu(1-\delta+2\delta\mu^2)\mathcal{L}\psi_1' - \gamma\alpha_1(1-\mu^2)(1+\delta\mu^2)\frac{\partial}{\partial\mu}\mathcal{L}\psi_1' + \\ +\gamma\alpha_1\mathcal{L}\left[(1-\mu^2)(1+\delta\mu^2)\frac{\partial\psi_1'}{\partial\mu}\right] \tag{6.16}$$

$$\mathcal{L}\phi_3' = 2\mu\left[\Omega+\gamma\alpha_3(1-\delta+2\delta\mu^2)\right]\mathcal{L}\psi_3' + 2(1-\mu^2)\left[\Omega+\gamma\alpha_3(1-\delta+6\delta\mu^2)\right]\frac{\partial\psi_3'}{\partial\mu} \\ +2\gamma\alpha_3\mu(1-\delta+2\delta\mu^2)\mathcal{L}\psi_3' - \gamma\alpha_3(1-\mu^2)(1+\delta\mu^2)\frac{\partial}{\partial\mu}\mathcal{L}\psi_3' + \\ +\gamma\alpha_3\mathcal{L}\left[(1-\mu^2)(1+\delta\mu^2)\frac{\partial\psi_3'}{\partial\mu}\right] \tag{6.17}$$

$$\frac{\partial}{\partial t}\frac{\phi_1'-\phi_3'}{\Delta p} = -\alpha_2(1+\delta\mu^2)\frac{\partial}{\partial\varphi}\frac{\phi_1'-\phi_3'}{\Delta p} - 2\frac{\alpha_3-\alpha_1}{\Delta p}\mu(1+\delta\mu^2)\left[\Omega+\gamma\alpha_2(1+\delta\mu^2)\right]\frac{\partial\psi_2'}{\partial\varphi} \\ +\left\{\frac{R}{p_{00}}\left(\frac{p_{00}}{p_2}\right)^{1-\chi}\frac{\Theta_{s1}-\Theta_{s3}}{\Delta p}\right\}\tilde{\omega}_2' \tag{6.18}$$

$$\mathcal{L}\chi_1' = -a^2\frac{\tilde{\omega}_2'-\tilde{\omega}_0'}{\Delta p} \tag{6.19}$$

$$\mathcal{L}\chi_3' = -a^2\frac{\tilde{\omega}_4'-\tilde{\omega}_2'}{\Delta p} \tag{6.20}$$

The boundary conditions in the vertical are:

$$\tilde{\omega}_0' = \tilde{\omega}_4' = 0$$

Equations (6.19) and (6.20) give us then $X_1' = -X_3'$

Let us now define:

$$\begin{aligned}
\chi &= \chi_1' = -\chi_3' \\
\tau &= (\phi_1' - \phi_3')/4\Omega \\
\mathcal{H} &= (\phi_1' + \phi_3')/4\Omega \\
\Psi &= (\psi_1' + \psi_3')/2 \\
\Theta &= (\psi_1' - \psi_3')/2 \\
t' &= 2\Omega t \\
\omega &= (\alpha_1 + \alpha_3)/4\Omega \\
\Lambda &= (\alpha_1 - \alpha_3)/4\Omega
\end{aligned} \tag{6.21}$$

and assume

$$\begin{aligned}
\tilde{\omega}_3' &= \tilde{\omega}_1' = \tilde{\omega}_2'/2 \\
\psi_2' &= (\psi_1' + \psi_3')/2 \\
\alpha_4 - \alpha_2 &= \alpha_2 - \alpha_0 = \alpha_3 - \alpha_1 = -4\Omega\Lambda
\end{aligned} \tag{6.22}$$

After using (6.21) and (6.22) into (6.14) - (6.20) and combining the resulting equations we get

$$\begin{aligned}
\frac{\partial}{\partial t'}\mathcal{L}\Psi = {} & -\omega(1+\delta\mu^2)\frac{\partial}{\partial\varphi}\mathcal{L}\Psi - \Lambda(1+\delta\mu^2)\frac{\partial}{\partial\varphi}\mathcal{L}\Theta - \left[1+2\omega(1-\delta+6\delta\mu^2)\right]\frac{\partial\Psi}{\partial\varphi} - \\
& - 2\Lambda(1-\delta+6\delta\mu^2)\frac{\partial\Theta}{\partial\varphi} - 2\gamma\Lambda\mu(1-\delta+2\delta\mu^2)\mathcal{L}\chi - 2\gamma\Lambda(1-\mu^2)(1-\delta+6\delta\mu^2)\frac{\partial\chi}{\partial\mu} + \\
& + \gamma\Lambda\frac{\partial}{\partial\mu}\left[(1-\mu^2)(1+\delta\mu^2)\mathcal{L}\chi\right]
\end{aligned} \tag{6.23}$$

$$\frac{\partial}{\partial t'}\mathcal{L}\Theta = -\omega(1+\delta\mu^2)\frac{\partial}{\partial\varphi}\mathcal{L}\Theta - \Lambda(1+\delta\mu^2)\frac{\partial}{\partial\varphi}\mathcal{L}\Psi - \left[1+2\omega(1-\delta+6\delta\mu^2)\right]\frac{\partial\Theta}{\partial\varphi} -$$
$$-2\Lambda(1-\delta+6\delta\mu^2)\frac{\partial\Psi}{\partial\varphi} - \mu\left[1+2\gamma\omega(1-\delta+2\delta\mu^2)\right]\mathcal{L}\chi -$$
$$-(1-\mu^2)\left[1+2\gamma\omega(1-\delta+6\delta\mu^2)\right]\frac{\partial\chi}{\partial\mu} \qquad (6.24)$$

$$\frac{\partial\tau}{\partial t'} = -\omega(1+\delta\mu^2)\frac{\partial\tau}{\partial\varphi} + \Lambda\mu(1+\delta\mu^2)\left[1+2\gamma\omega(1+\delta\mu^2)\right]\frac{\partial\Psi}{\partial\varphi} - S\mathcal{L}\chi \qquad (6.25)$$

$$\mathcal{L}\tau = \mu\left[1+2\gamma\omega(1-\delta+2\delta\mu^2)\right]\mathcal{L}\Theta + 2\gamma\Lambda\mu(1-\delta+2\delta\mu^2)\mathcal{L}\Psi +$$
$$+(1-\mu^2)\left[1+2\gamma\omega(1-\delta+6\delta\mu^2)\right]\frac{\partial\Theta}{\partial\mu} + 2\gamma\Lambda(1-\mu^2)(1-\delta+6\delta\mu^2)\frac{\partial\Psi}{\partial\mu} +$$
$$+2\gamma\omega\mu(1-\delta+2\delta\mu^2)\mathcal{L}\Theta + 2\gamma\Lambda\mu(1-\delta+2\delta\mu^2)\mathcal{L}\Psi -$$
$$-\gamma\omega(1-\mu^2)(1+\delta\mu^2)\frac{\partial}{\partial\mu}\mathcal{L}\Theta - \gamma\Lambda(1-\mu^2)(1+\delta\mu^2)\frac{\partial}{\partial\mu}\mathcal{L}\Psi +$$
$$+\gamma\omega\mathcal{L}\left[(1-\mu^2)(1+\delta\mu^2)\frac{\partial\Theta}{\partial\mu}\right] + \gamma\Lambda\mathcal{L}\left[(1-\mu^2)(1+\delta\mu^2)\frac{\partial\Psi}{\partial\mu}\right] \qquad (6.26)$$

$$\mathcal{L}\mathcal{H} = \mu\left[1+2\gamma\omega(1-\delta+2\delta\mu^2)\right]\mathcal{L}\Psi + 2\gamma\Lambda\mu(1-\delta+2\delta\mu^2)\mathcal{L}\Theta +$$
$$+(1-\mu^2)\left[1+2\gamma\omega(1-\delta+6\delta\mu^2)\right]\frac{\partial\Psi}{\partial\mu} + 2\gamma\Lambda(1-\mu^2)(1-\delta+6\delta\mu^2)\frac{\partial\Theta}{\partial\mu} +$$
$$+2\gamma\omega\mu(1-\delta+2\delta\mu^2)\mathcal{L}\Psi + 2\gamma\Lambda\mu(1-\delta+2\delta\mu^2)\mathcal{L}\Theta -$$
$$-\gamma\omega(1-\mu^2)(1+\delta\mu^2)\frac{\partial}{\partial\mu}\mathcal{L}\Psi - \gamma\Lambda(1-\mu^2)(1+\delta\mu^2)\frac{\partial}{\partial\mu}\mathcal{L}\Theta +$$
$$+\gamma\omega\mathcal{L}\left[(1-\mu^2)(1+\delta\mu^2)\frac{\partial\Psi}{\partial\mu}\right] + \gamma\Lambda\mathcal{L}\left[(1-\mu^2)(1+\delta\mu^2)\frac{\partial\Theta}{\partial\mu}\right] \qquad (6.27)$$

$$\tilde{\omega}_2' = -\frac{\Delta p}{a^2}\mathcal{L}\chi \qquad (6.28)$$

and $S \equiv \frac{\Delta p\, R}{8\Omega^2 a^2 p_{00}}\left(\frac{p_{00}}{p_2}\right)^{1-\chi}(\Theta_{s1}-\Theta_{s3})$ is the non-dimensional static stability.

Equations (6.23) - (6.26) form a closed system in the variables Ψ , Θ , $\mathcal{T}$, and χ .

6.3 Comparison of the Two Systems of Equations with $\gamma=0$ and $\gamma=1$

We now turn our attention to the comparison of the two systems of equations (6.23) - (6.26) for $\gamma=0$ and $\gamma=1$. This comparison will be made using only the basic zonal velocity profile $\overline{U} = a\,\alpha(p)\sqrt{1-\mu^2}$; i.e., by letting $\underline{\delta=0}$ in those equations. This profile is able to accentuate the differences between the two sets of equations, since it has large amplitudes in low latitudes, where the behavior of the two sets is most distinct. It corresponds to a state of solid rotation within each layer.

We then seek solutions of the form

$$\begin{pmatrix} \Psi \\ \Theta \\ \chi \\ \mathcal{T} \end{pmatrix} = \mathrm{Re}\left\{ e^{is\varphi - i\omega s t'} \sum_{n=s}^{N} P_n^s(\mu) \begin{pmatrix} \Psi_n^s(t') \\ \Theta_n^s(t') \\ i\,X_n^s(t') \\ T_n^s(t') \end{pmatrix} \right\} \quad ; \; s=1,2,3,.. \tag{6.30}$$

where the latitudinal dependence has been truncated in the associated Legendre "polynomial" expansion for computational purposes.

After using the properties (A.2)-(A.5) (Appendix A), equations (6.23) - (6.26) become:

$$\dot{\Psi}_n^s = e_n \Psi_n^s + f_n \Theta_n^s + A_n X_{n-1}^s - B_n X_{n+1}^s \tag{6.31}$$

$$\dot{\Theta}_n^s = e_n \Theta_n^s + f_n \Psi_n^s + C_n X_{n-1}^s + D_n X_{n+1}^s \tag{6.32}$$

$$\dot{T}_n^s = S_{n(n+1)} \left[-w_n \left(c_n \psi_{n-1}^s + d_n \psi_{n+1}^s \right) - X_n^s \right] \tag{6.33}$$

$$T_n^s = S_{n(n+1)} \left[w_n \left(a_n \Theta_{n-1}^s + b_n \Theta_{n+1}^s \right) + \Gamma_n \left(a_n \psi_{n-1}^s + b_n \psi_{n+1}^s \right) \right] \tag{6.34}$$

where $(\dot{}) \equiv i\frac{\partial}{\partial t'}$ and the coefficients a_n, b_n, ... etc. are given in Appendix F.

T_n^s is eliminated between (6.33) and (6.34) and the result is used to eliminate X_{n-1}^s and X_{n+1}^s in (6.31) and (6.32) to yield the following matrix equation:

$$\underset{\sim}{A}\,\dot{\underset{\sim}{Y}} = \underset{\sim}{B}\,\underset{\sim}{Y} \tag{6.35}$$

In Appendix F one finds a description of the matrices $\underset{\sim}{A}$, $\underset{\sim}{B}$ and $\underset{\sim}{Y}$ as well as the numerical method used to solve this matrix equation and the energetics of the model.

If the inverse of $\underset{\sim}{A}$ exists, equation (6.35) can be multiplied by it to give

$$\dot{\underset{\sim}{Y}} = \underset{\sim}{A}^{-1}\,\underset{\sim}{B}\,\underset{\sim}{Y}$$

By letting $\underset{\sim}{C} = \underset{\sim}{A}^{-1}\,\underset{\sim}{B}$ and $\underset{\sim}{Y}(t') = e^{-i\sigma t'}\underset{\sim}{\mathcal{Y}}$ we obtain

$$\left(\underset{\sim}{C} - \sigma\,\underset{\sim}{I}\right)\underset{\sim}{\mathcal{Y}} = 0 \tag{6.36}$$

which becomes an ordinary eigenvalue-eigenfinction problem for σ if ω , Λ , s, and S have assigned values. The frequency σ is a complex quantity: $\sigma = \lambda + i\nu$. λ is the real part of the frequency and ν is the exponential growth rate. $\nu > 0$ are associated with unstable modes, $\nu = 0$ with neutral modes, and $\nu < 0$ with decaying modes. The e-folding time in days is equal to $(4\pi\nu)^{-1}$. Because the matrix $\underset{\sim}{C}$ is real, for each complex eigenvalue σ , its complex conjugate σ^* is also a solution. (6.36) comprises two separate matrix systems with regard to the symmetry of the solutions, as even or odd functions of μ = sine (latitude).

Figures 25·a and 25·b (for stream functions symmetric and antisymmetric about the equator, respectively) present the growth rate of the unstable modes as a function of the discrete zonal wave number s and the mean meridional wave number m (defined as the number of zeros between the equator and pole of the real part of ϕ_1' plus one) for S = 0.005 and $\omega = \Lambda = 0.01$. Both systems $\gamma = 1$ and $\gamma = 0$ are shown for comparison. The maximum growth rate for this case is seen to be for s = 4 and m = 3 with corresponding eigenfunctions having stream-function (ψ) symmetric about the equator.

Figure 26·a displays the amplitudes and phases of the eigen-functions ϕ_1' and ϕ_3' for the most unstable mode (s = 4, m = 3) shown in figure 25·a for $\gamma = 1$. Figure 26·b presents the corresponding momentum and heat transports by the baroclinic eddies. Figure 27·a and 27·b are the counterpart of figures 26·a and 26·b for $\gamma = 0$. The two solutions are remarkably alike, except that the amplitudes of ϕ_3' and $\overline{U_3'V_3'}^*\cos^2(\text{lat.})$ in the lower layer (level 3) are relatively larger for $\gamma = 0$.

The $\overline{U}\ \alpha\cos(\text{lat})$ profile on a sphere is, in some ways, an analog of $\overline{U}$ = constant on a β-plane. It is the simplest profile for a baroclinic instability study on a sphere, since it is always stable to barotropic disturbances (See the energetics discussion in Appendix F.2). The most unstable perturbations for $\overline{U}$ = constant on a β-plane analysis give no net transport of momentum across latitude circles, as shown by Phillips (1954). Our results, however, show a momentum transport ($\overline{u_1'v_1'}*\cos^2(\text{lat})$ and $\overline{u_3'v_3'}*\cos^2(\text{lat})$) polewards for all latitudes (figure 27·b), even when $\overline{U}$ is in solid rotation at each level. The curvature effects are evidently very important in this case. The ratio $\max.\overline{u_1'v_1'}*\cos^2(51°)/\max.\overline{v_2T_2}*\cos(60°)$ is approximately 1.6 m $\sec^{-1}{}^{\circ}C^{-1}$, while the observed ratio (mean annual values) $\max.\overline{u'v'}*\cos^2(35°)/\max.\overline{v'T'}*\cos(50°)$ is approximately 1.56 m$\sec^{-1}{}^{\circ}C$ (Oort and Rasmusson, 1971).

The properties of the baroclinic eddies and their transports will be discussed in the next section, where only the system of equations with $\gamma=0$ will be used (because of the good agreement with the $\gamma=1$ set for $\overline{U} \propto \cos(\text{lat.})$ and mathematical simplicity) with the parameter δ being varied, for different profiles.

6.4 Study of Curvature Effects on Baroclinic Instability

We will now examine the influence of curvature effects on some important aspects of the baroclinic instability problem. Taking specific members of the family of profiles $\overline{U}\propto\sqrt{1-\mu^2}\ (1+\delta\mu^2)$, we will draw conclusions to partly answer questions concerning the meridional scale of the most unstable mode, the eigenfunctions' latitudinal

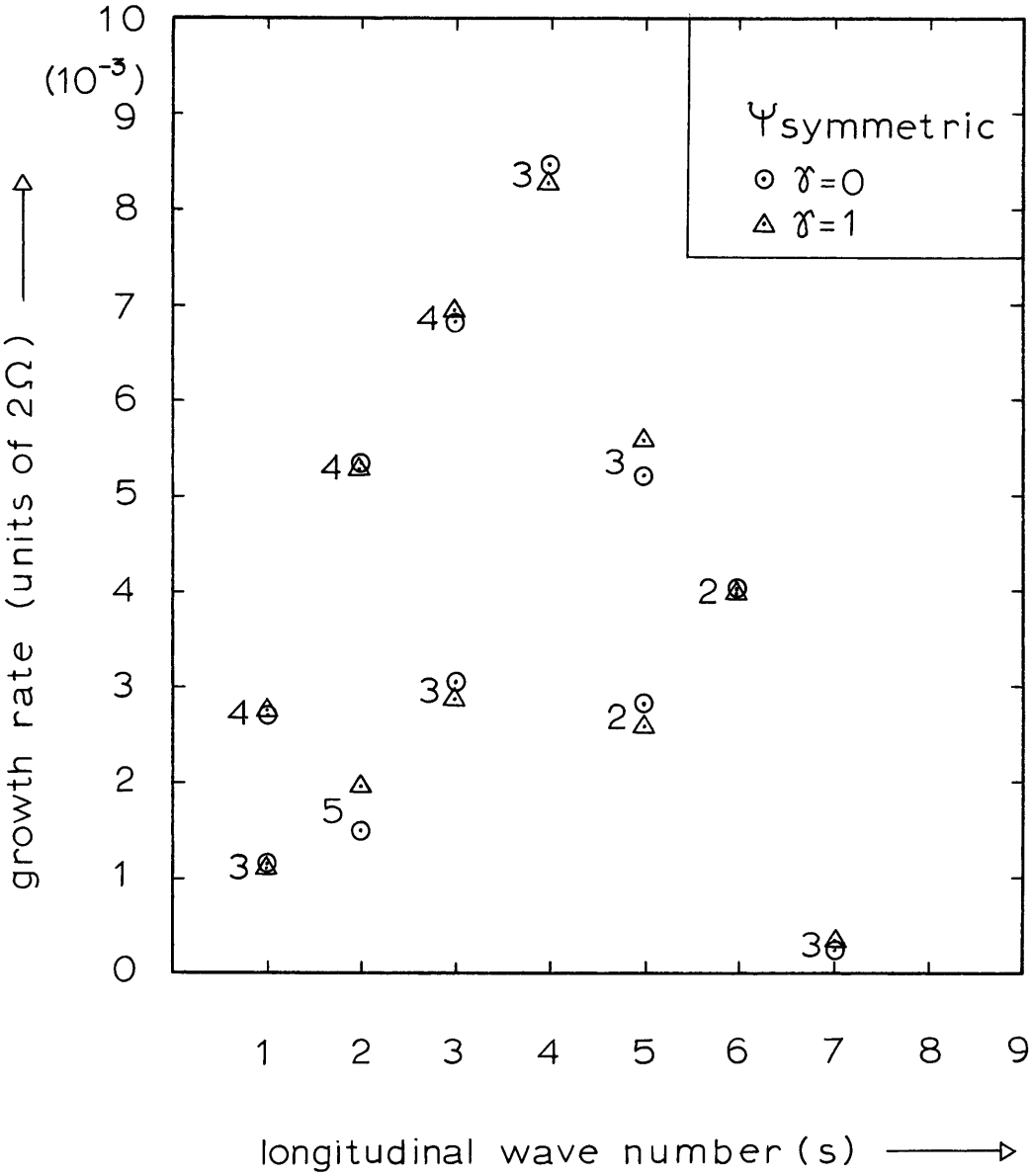


Fig. 25.a Growth rates (units of 2Ω) for the unstable solutions with stream function symmetric about the equator as a function of the longitudinal wave number (s) and the meridional modal number (m) (shown on the left of the circles and triangles) for the $\bar{U} \propto \cos(\text{lat})$ profile. The values obtained using the two sets of equations ($\gamma = 0$, and $\gamma = 1$) are shown for comparison. Numerical values of the parameters are $S = 0.005$; $\omega = \Lambda = 0.01$.

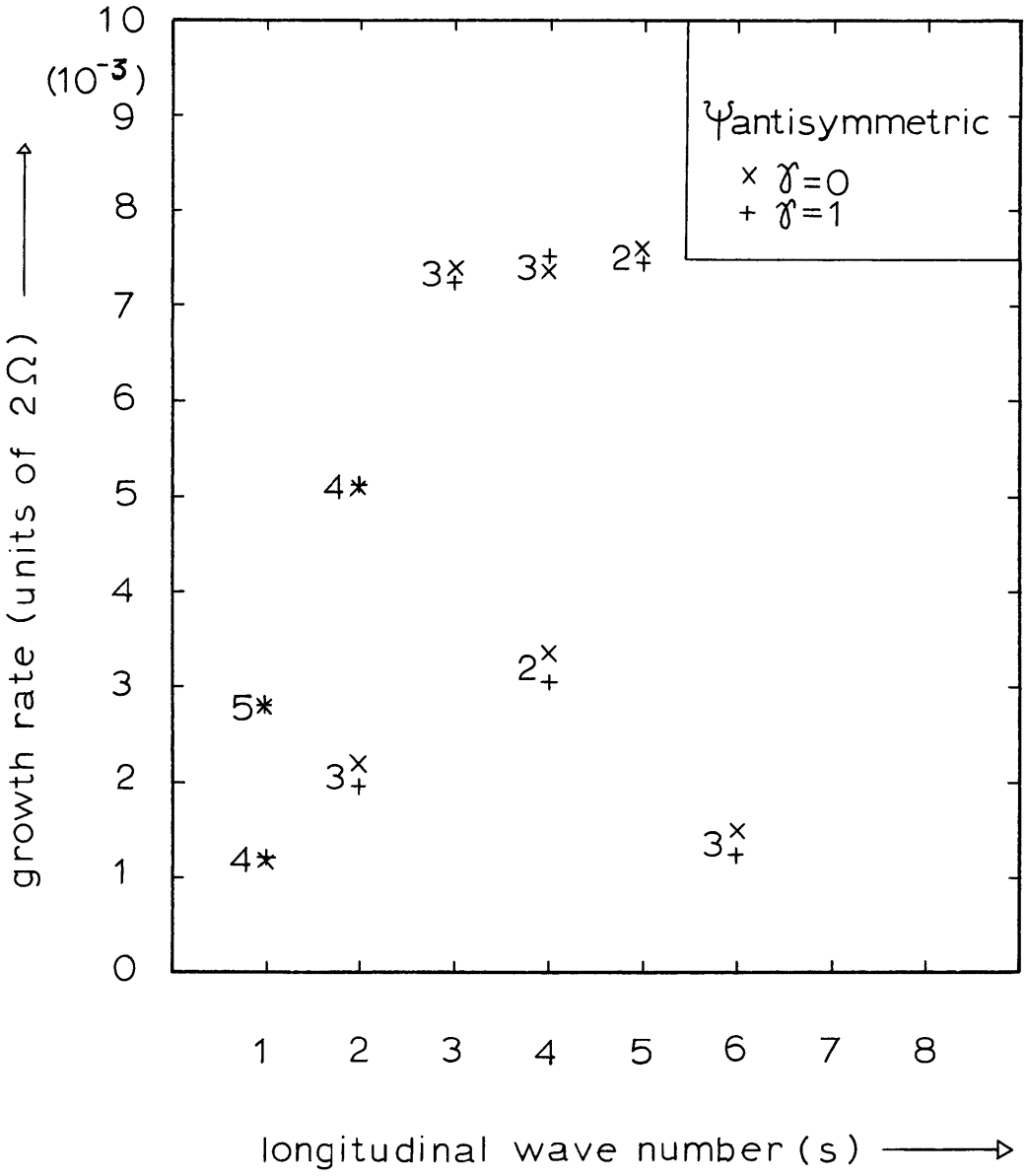


Fig. 25.b Same as Fig. 25.a, but for the unstable solutions with stream function antisymmetric about the equator.

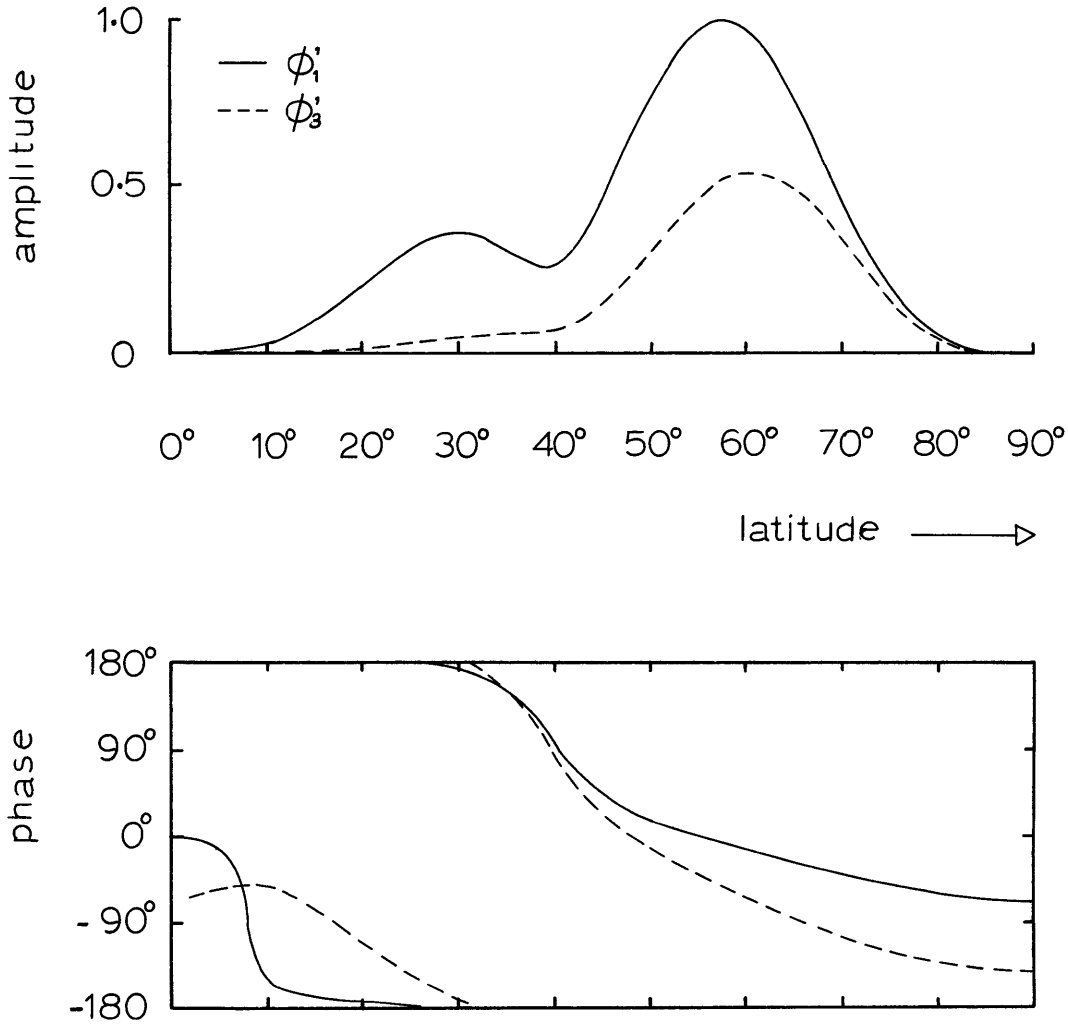
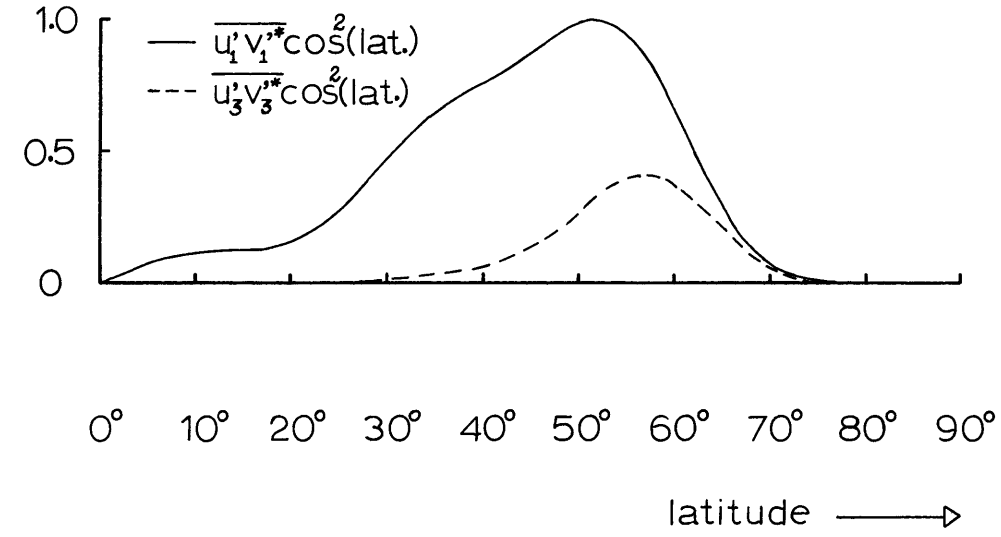


Fig. 26.a Eigenfunctions ϕ_1' and ϕ_3' for the most unstable mode for the profile ② (Fig. 29), using the balance equations ($\gamma = 1$). Numerical values of the parameters are: S = 0.005; $\omega = \Lambda = 0.01$. This mode has σ = -0.03145 + i 0.008280, s = 4, m = 3, and SYM = 0 (symmetric stream function).



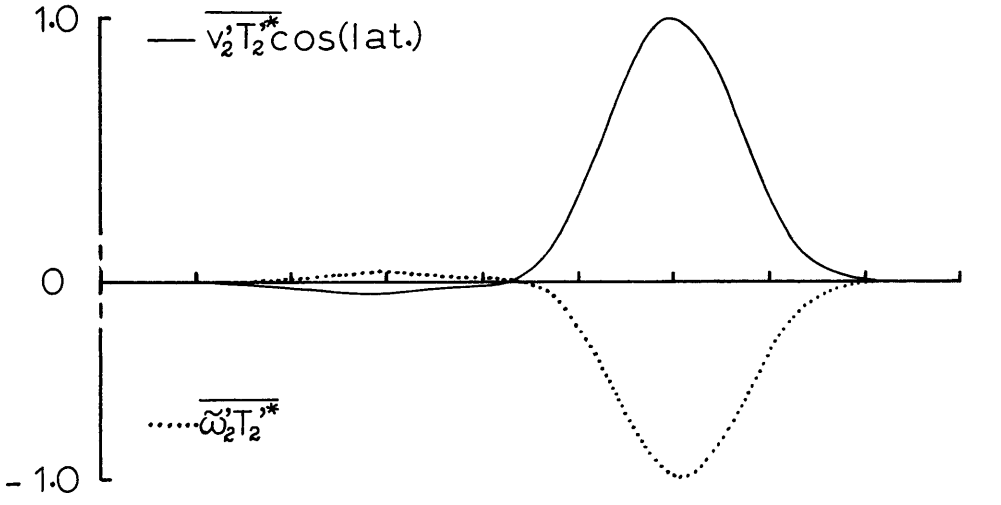


Fig. 26.b Angular momentum and heat transports corresponding to Fig.26.a.

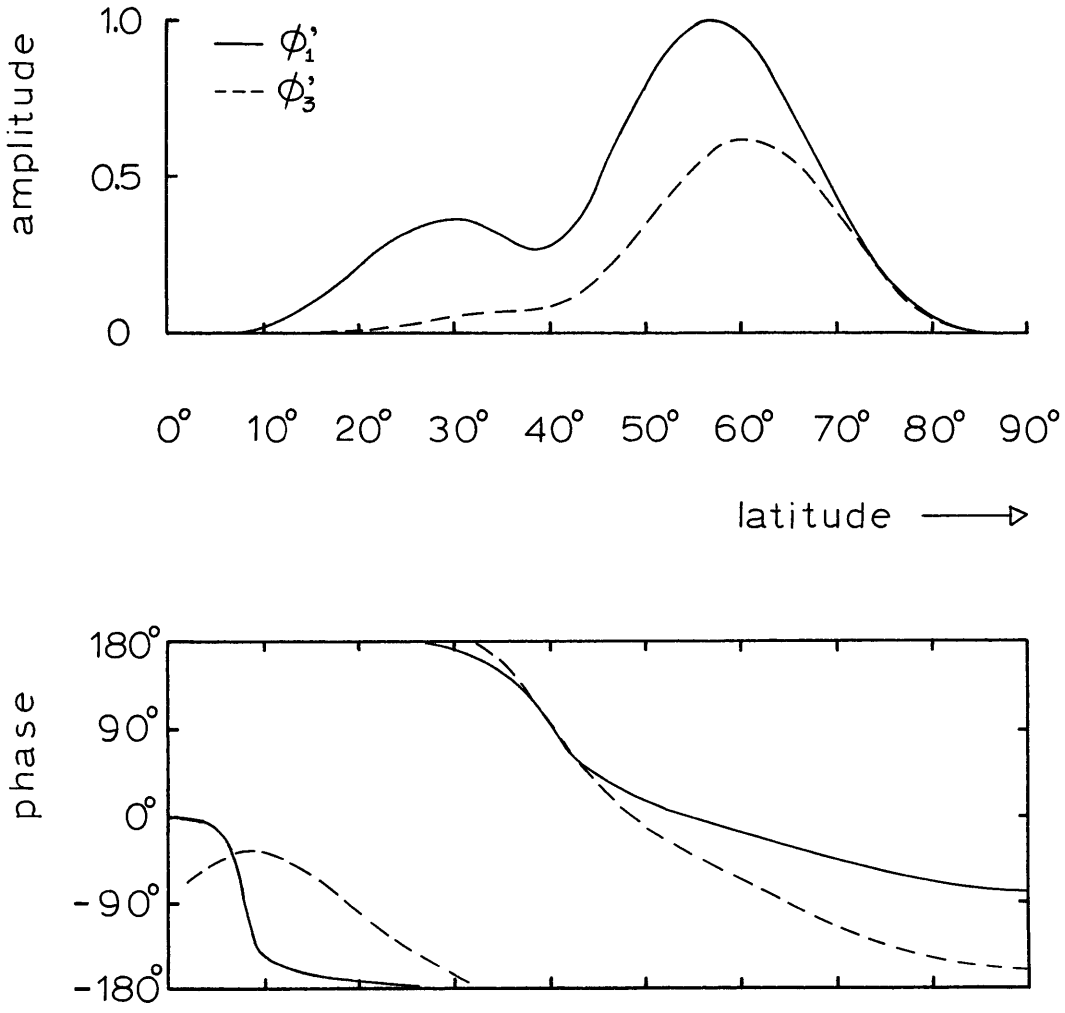
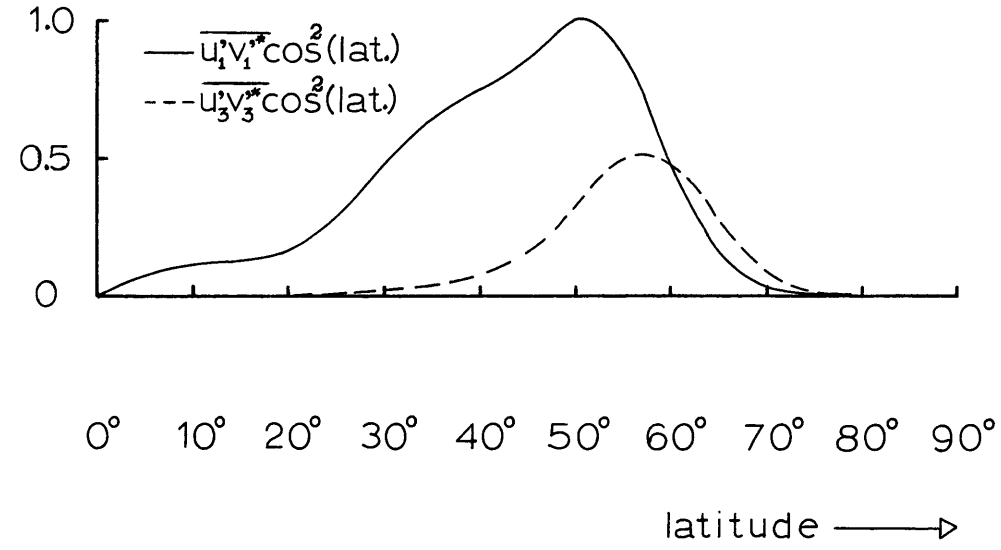


Fig. 27.a Eigenfunctions ϕ_1' and ϕ_3' for the most unstable mode for the profile ② (Fig. 29), using the set of equations $\gamma = 0$. Numerical values of the parameters are: S = 0.005; $\omega = \Lambda = 0.01$; $\delta = 0$. This mode has $\sigma = -0.03132 + i\ 0.008424$; s = 4; m = 3; SYM = 0. (Compare with Fig. 26.a)



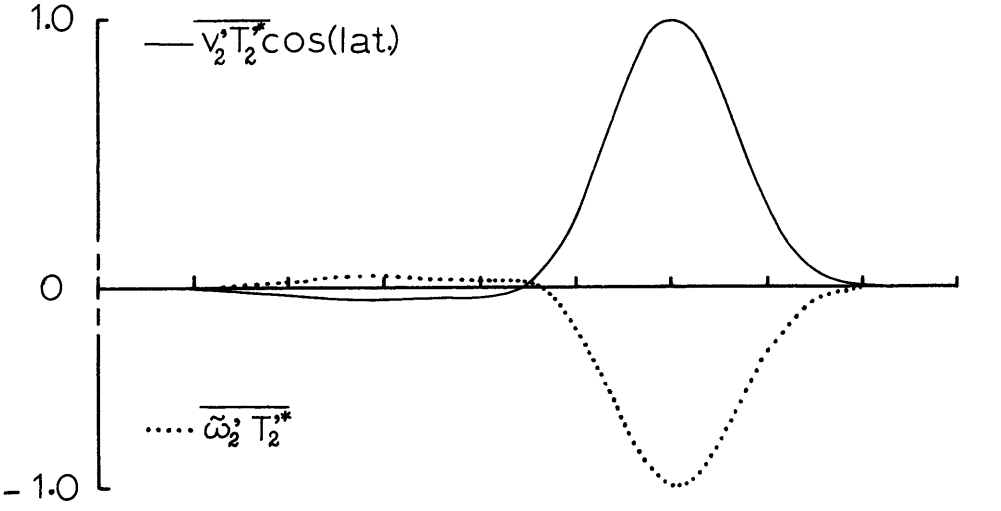


Fig. 27.b Angular momentum and heat transports corresponding to Fig. 27.a. (Compare with Fig. 26.b)

structure, and momentum and heat transports by the baroclinic eddies. Our solutions near and far from neutral stability will be compared with the results of some two-layer, quasi-geostrophic, β-plane investigations (Phillips, 1954; Pedlosky, 1964.a,b; Stone, 1969, 1974; Simmons, 1974). All the profiles used are stable to barotropic disturbances for the range of parameters used (See energetics discussion in Appendix G.2).

Let us return to equations (6.23)-(6.26) with $\gamma = 0$ and seek solutions of the form (6.30). After using the properties (A.2)-(A.5), we obtain

$$\dot{\psi}_n^s = b_n \psi_{n-2}^s + a_n \psi_n^s + c_n \psi_{n+2}^s + e_n \Theta_{n-2}^s + d_n \Theta_n^s + f_n \Theta_{n+2}^s \tag{6.37}$$

$$\dot{\Theta}_n^s = b_n \Theta_{n-2}^s + a_n \Theta_n^s + c_n \Theta_{n+2}^s + e_n \psi_{n-2}^s + d_n \psi_n^s + f_n \psi_{n+2}^s + g_n X_{n-1}^s + h_n X_{n+1}^s \tag{6.38}$$

$$\dot{T}_n^s = j_n T_{n-2}^s + i_n T_n^s + k_n T_{n+2}^s + \ell_n \psi_{n-3}^s + p_n \psi_{n-1}^s + q_n \psi_{n+1}^s + r_n \psi_{n+3}^s + s_n X_n^s \tag{6.39}$$

$$T_n^s = g_n \Theta_{n-1}^s + h_n \Theta_{n+1}^s \tag{6.40}$$

where $\dot{(\ )} \equiv i\frac{\partial}{\partial t}$, . Appendix G gives the coefficients a_n, b_n, ... etc. as well as a discussion of the numerical solutions of the problem.

T_n^s is eliminated from (6.39) by means of (6.40), which result is used to substitute for X_{n-1}^s and X_{n+1}^s in (6.38). A matrix equation is obtained in the form of (6.35), but with the matrices $\underset{\sim}{A}$ and $\underset{\sim}{B}$ now given in Appendix G.

We then look for solutions of the resulting eigenvalue-eigenfunction problem (in the form of (6.36)) with maximized growth rates with respect to zonal wave number (s), mean meridional wave number (m), and symmetry, for fixed values of ω, Λ, and S.

Figures 29 and 30 show the profiles used for our calculations far from and near neutral stability, respectively, including the cos(lat) profiles. These figures also show the observed mean annual values of $\overline{U}$ at 200 mb minus $\overline{U}$ at 700 mb (Oort and Rasmusson, 1971) and the local baroclinic instability criterion $(\overline{U}_1-\overline{U}_3 \geq 4\Omega aS \cos(\text{lat.})/\sin^2(\text{lat.}))$, derived for the profile $\overline{U}$ = constant on a β-plane analysis (Phillips, 1954; Pedlosky, 1964.a). Profiles ③ and ⑤ in figure 29 show less shear at low latitudes, with maximum shear approximately equal to the observed maximum shear, but at higher latitudes. These profiles are locally unstable at all high latitudes. Profile ④, however, is locally unstable only in middle latitudes. Profiles ② and ③ in figure 30 are unstable at polar latitudes only, while profile ④ is below (but near) the curve of marginal instability at all latitudes.

Horizontal shear in the basic zonal velocity profile does not seem to affect the threshold of instability (Pedlosky, 1964.b; Stone, 1969), defined as the local value of the shear where the shear profile first exceeds the curve $4\Omega aS \cos(\text{lat})/\sin^2(\text{lat})$. It is worthwhile,

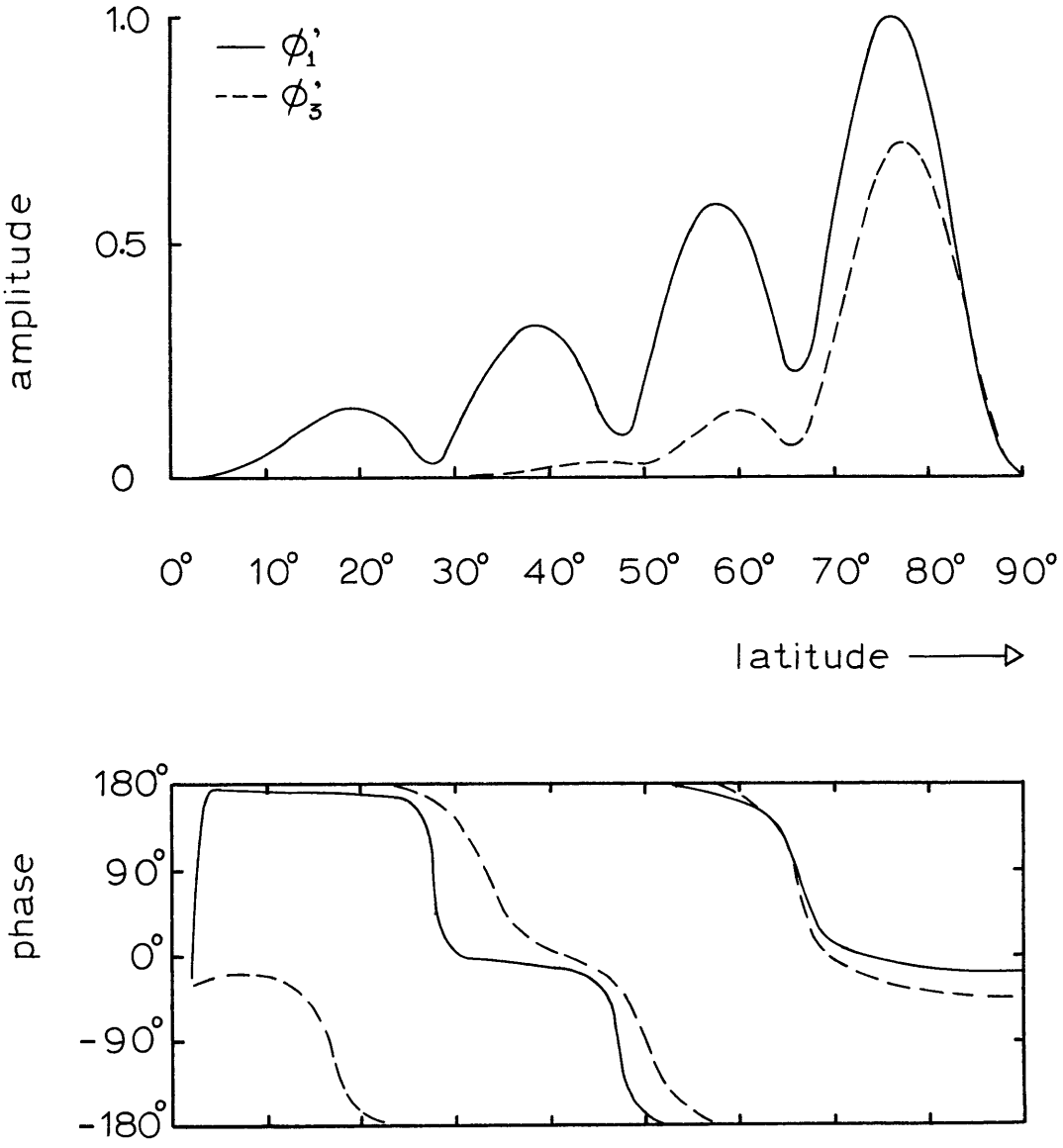


Fig. 28.a Eigenfunctions ϕ_1' and ϕ_3' for the most unstable mode for the profile ② (Fig. 30), using the set of equations $\gamma = 0$. Numerical values of the parameters are: S = 0.005; $\omega = \Lambda = 0.006$; $\delta = 0$. This mode has $\sigma = -0.01055 + i\ 0.0007142$; s = 2; m = 5; SYM = 0.

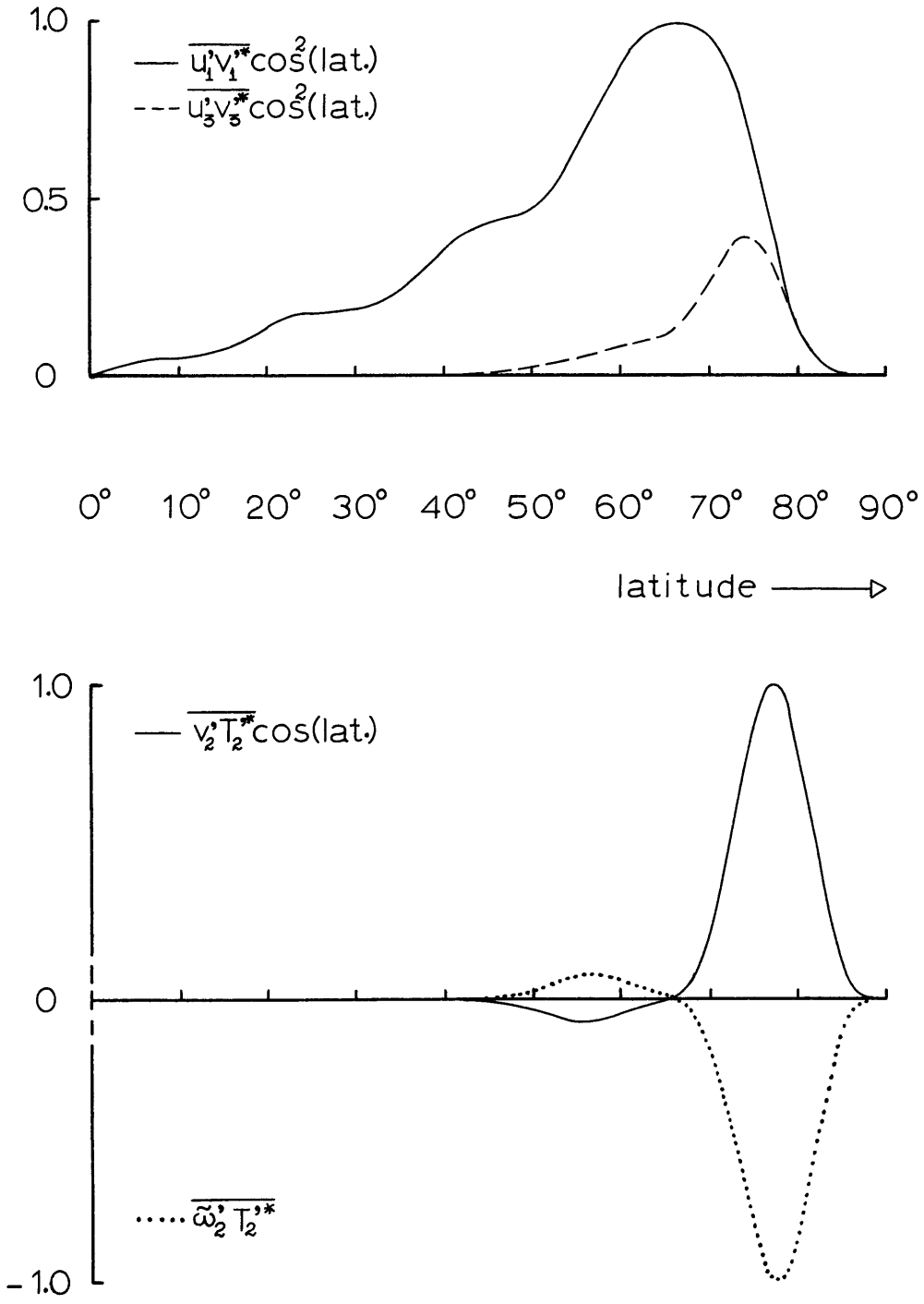


Fig. 28.b Angular momentum and heat transports corresponding to Fig. 28.a.

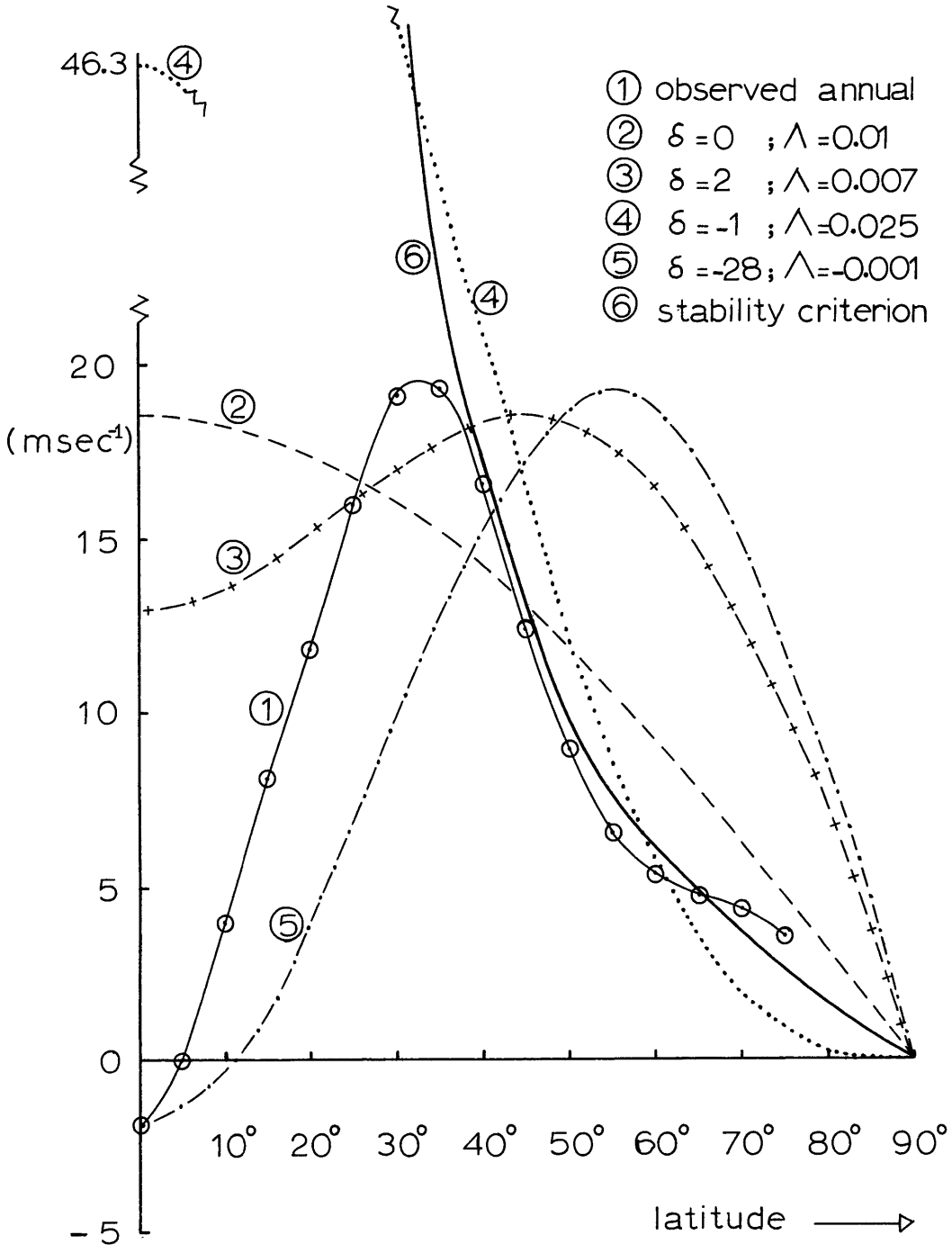


Fig. 29 Members of the family of shear profiles $\bar{U}_1 - \bar{U}_3 = 4\Omega a \Lambda \cos(\text{lat})(1 + \delta \sin^2(\text{lat}))$ used for the solutions far from neutral stability. The local baroclinic stability criterion $4\Omega a\, S \cos(\text{lat})/\sin^2(\text{lat})$ for S = 0.005 and the observed mean annual values of $\bar{U}$(200 mb) - $\bar{U}$(700 mb) (Oort and Rasmusson, 1971) are also shown.

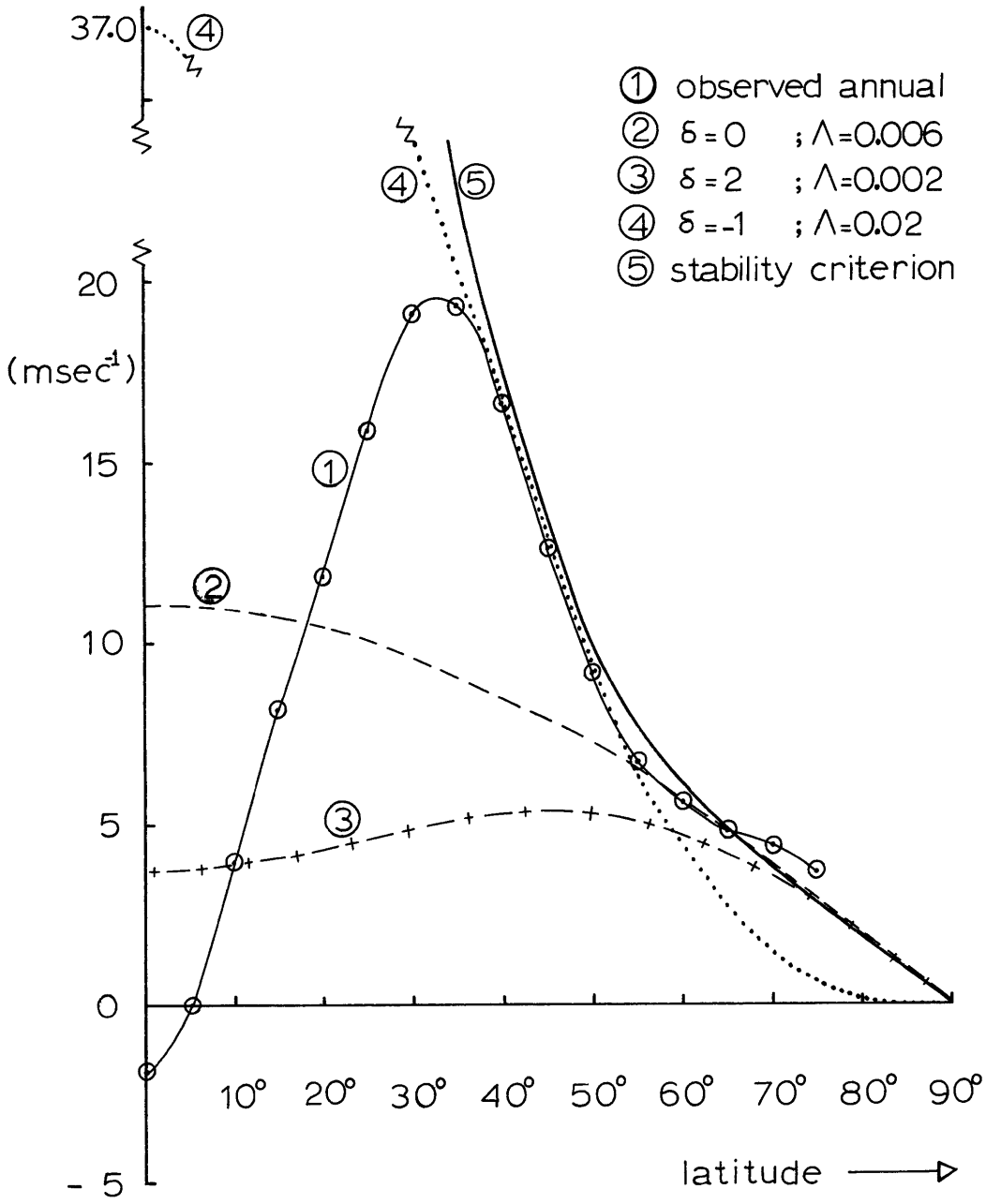


Fig. 30 Members of the family of shear profiles $\bar{U}_1 - \bar{U}_3 = 4\Omega a\Lambda\cos(\text{lat})(1 + \delta\sin^2(\text{lat}))$ used for the solutions near neutral stability. The local baroclinic stability criterion $4\Omega a\, S\cos(\text{lat})/\sin^2(\text{lat})$ for S = 0.005 and the observed mean annual values of $\bar{U}$(200 mb) - $\bar{U}$(700 mb) (Oort and Rasmusson, 1971) are also shown.

perhaps, to note that the mean annual shear for the atmosphere appears to be near neutral stability, according to the local stability criterion, from latitude 38°N up to 75°N (up to where the observations are available). It is also interesting to note that the local stability criterion seems to work quite well for the profiles used (see figure 30).

We will now discuss the numerical solutions displayed in figures 27,28 (profiles ②) and 31-35 (profiles ③ , ④ , and ⑤). The part a of each figure shows the amplitude of the geopotential eigenfunctions at the levels 1 and 3 and their respective phases. The part b shows the angular momentum transports and horizontal and vertical heat transports. For all the figures, the functions have been computed at every 2° of latitude.

6.4.1 The Geopotential Eigenfunctions ϕ_1' and ϕ_3'

The amplitude of the eigenfunctions ϕ_1' and ϕ_3' has two distinct behaviors depending on whether the basic zonal profile is near or far from neutral stability. In the latter case (part a of figures 27,31,33,35), the amplitudes are smooth functions of latitude, resembling the solutions found in Simmons (1974), with maxima in middle or high latitudes. In the former case (part a of figures 28, 32,34; near the instability threshold), the amplitudes oscillate rapidly between the equator and pole, in agreement with Stone's (1969) study. Especially in the upper layer, they penetrate further into low latitudes than do those for the more unstable profiles of $\overline{U}$. In almost all cases there seems to exist a strong correlation between the location

of the maximum of the amplitude of ϕ_1' and the latitude where the local instability is greatest (i.e., where $4\Omega a\Lambda \cos(\text{lat}) [1+\delta\sin^2(\text{lat}) - \frac{S}{\Lambda}\sin^{-2}(\text{lat})]$ is largest, for the family of profiles used). Table I summarizes these correlations. There is a noticeable discrepancy for the profile ④ in figure 30, which does not satisfy the local criterion for instability at any latitude. The eigenfunctions for this marginal case (shown in figure 34.a) for the levels 1 and 3 peak at two latitudes completely separated from each other (30°N and 69°N).

In all β-plane analyses, the amplitudes peak near where the vertical shear of the zonal velocity is a maximum. The simple baroclinic criterion in this case is a constant (because cos(lat.) and $\sin^2$(lat.) are evaluated at the coordinate origin). For a symmetric $\overline{U}$ profile, on the β-plane, the (constant) criterion is therefore automatically exceeded most at the location of maximum vertical shear of the zonal wind. The inclusion of curvature (e.g., the complete variability of f) in our spherical analysis makes a clear distinction between the location of maximum shear and the location of maximum excess of shear over the local criterion, allowing for the proper physical conclusion to be drawn.

6.4.2 Angular Momentum Flux

The momentum transport by the baroclinic eddies in the β-plane analysis is always against the latitudinal gradient of the basic zonal profile, changing sign where the profile is a maximum. It is then concluded that the baroclinic eddies, although not explaining the formation of jets, are able to maintain a pre-existing jet structure of the basic

	Profile no.	Figure no.	Growth rate ν	excess of shear over local criterion		$\lvert\phi_1'\rvert$	$\lvert\phi_3'\rvert$	$\overline{u_1'v_1'^*}(1-\mu^2)$		$\overline{u_3'v_3'^*}(1-\mu^2)$		$\overline{v_2'T_2'^*}(1-\mu^2)^{1/2}$		$\overline{\tilde{\omega}_2'T_2'^*}$	
				zero	peak	peak	peak	peak	max. flux conv.	peak	max. flux conv.	zero	peak	zero	peak
far	② S=.005	27	.0084	46°	62°	57°	60°	51°	62°	57°	65°	45°	60°	46°	61°
	③ S=.005	31	.018	40°	61°	60°	65°	53°	64°	60°	68°	—	63°	—	64°
	④ S=.005	33	.013	32° (58°)	41°	44°	44°	33° (54°)	44°	35° (52°)	43°	28°	44°	29°	43°
	⑤ S=.005	35	.022	42°	63°	66°	70°	60°	68°	65°	72°	no	67°	—	68°
	⑤ S=.00125	36	.014	42°	63°	64°	67°	61°	67°	64°	68°	no	65°	no	66°
near	② S=.005	28	.00071	66°	77°	76°	77°	67°	76°	74°	78°	66°	77°	66°	77°
	③ S=.005	32	.00035	72°	79°	73°	78°	70°	76°	76°	81°	70°	77°	70°	77°
	④ S=.005	34	.00041	—	below curve	30°	69°	22° (43°)	31°	21° (64°)	28°	(12°) 22° (43°)	29°	(12°) 22° (43°)	29°
	③ S=.00125	37	.00026	72°	79°	76°	78°	71°	77°	76°	80°	70°	78°	70°	78°

TABLE I Location of important features of the most unstable solutions.

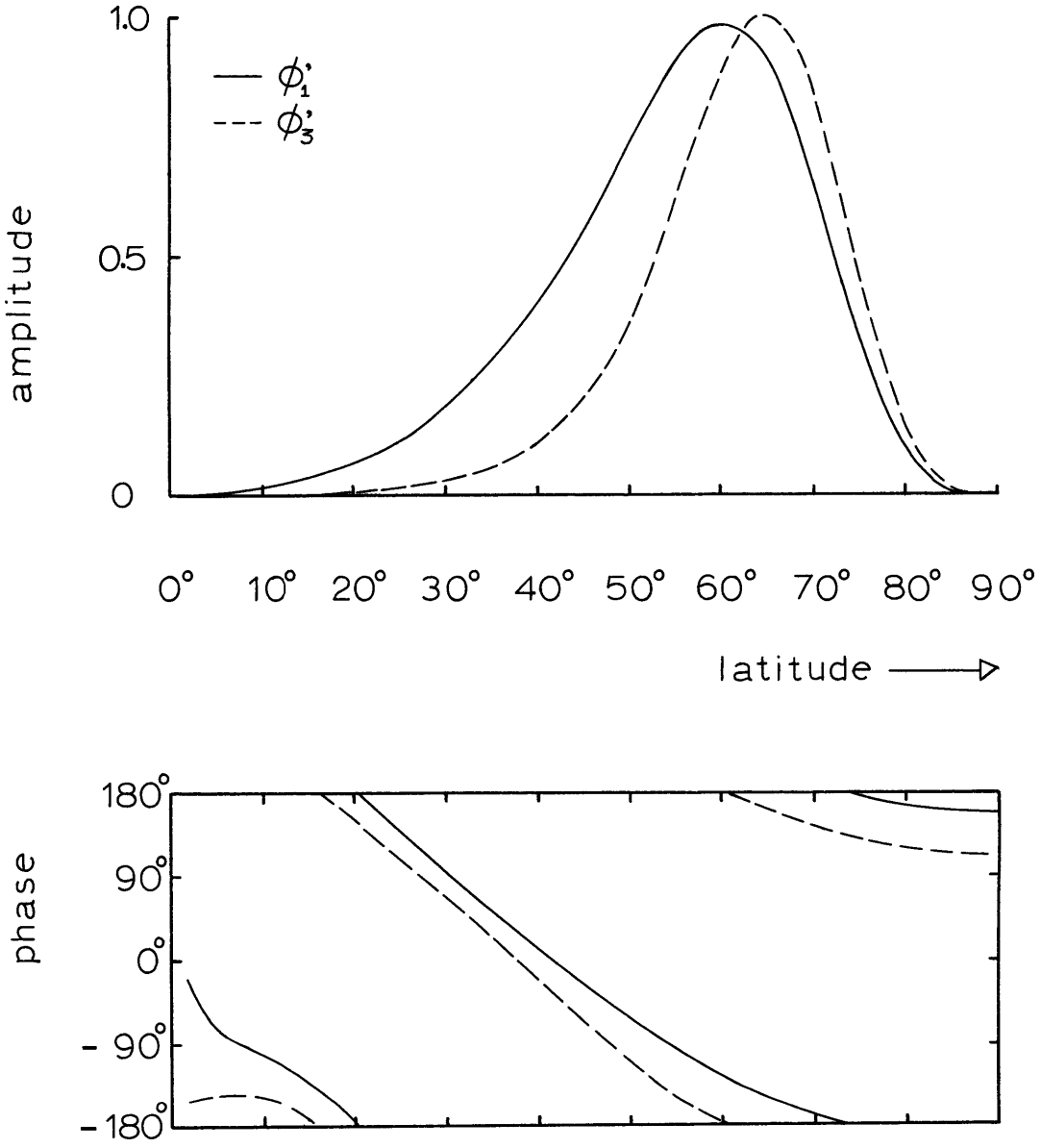
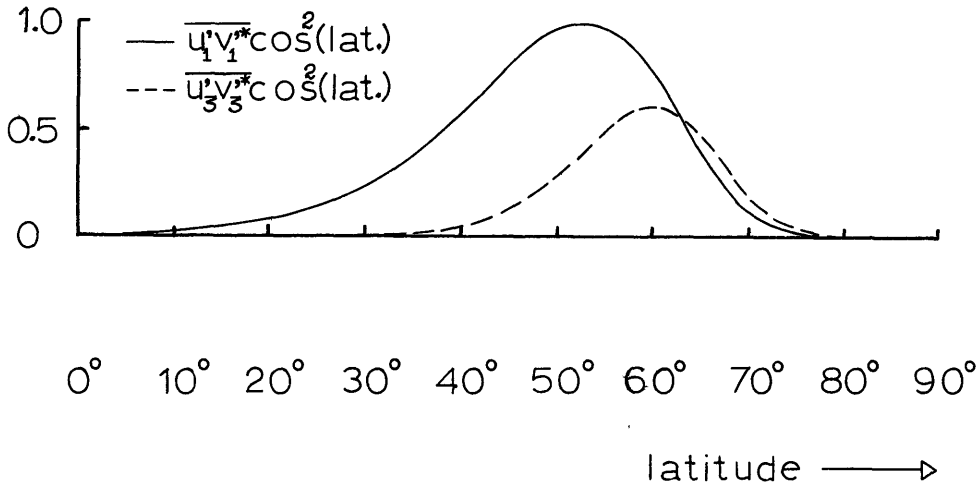


Fig. 31.a Eigenfunctions ϕ_1' and ϕ_3' for the most unstable mode for the profile ③ (Fig. 29), using the set of equations $\gamma = 0$. Numerical values of the parameters are; S = 0.005; $\omega = \Lambda = 0.007$; $\delta = 2$. This mode has $\sigma = 0.009452 + i\ 0.01809$; s = 4; m = 4; SYM = 0.



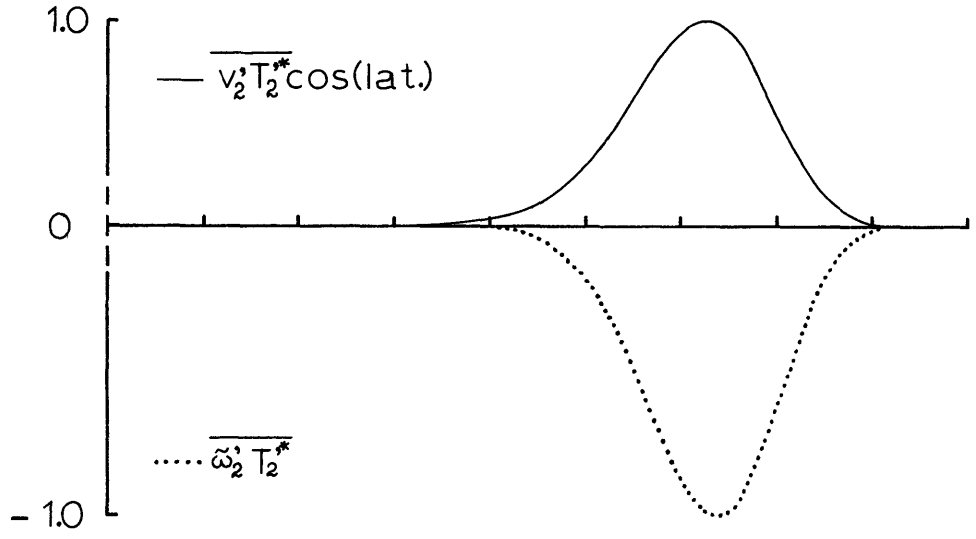


Fig. 31.b Angular momentum and heat transports corresponding to Fig. 31.a.

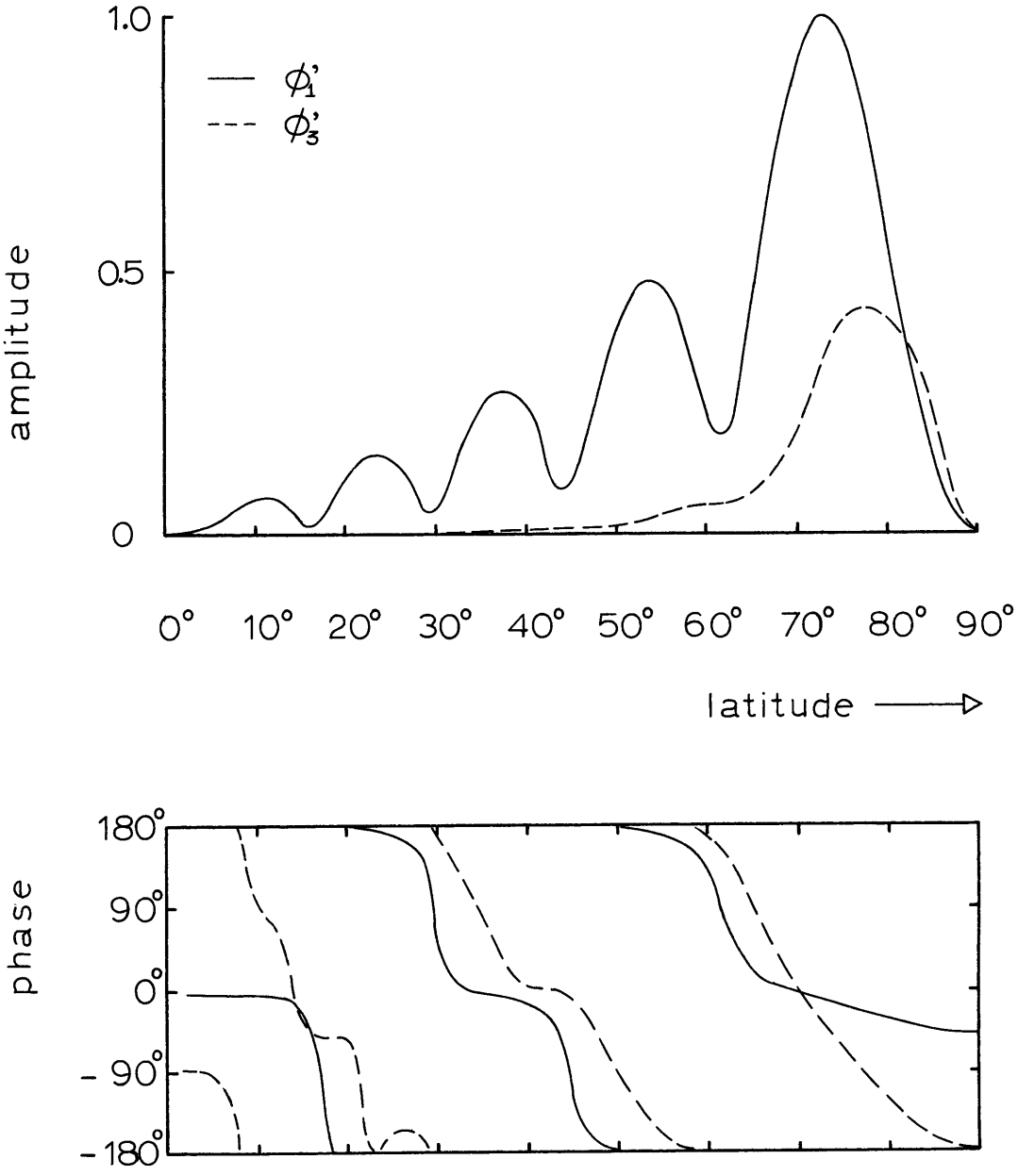
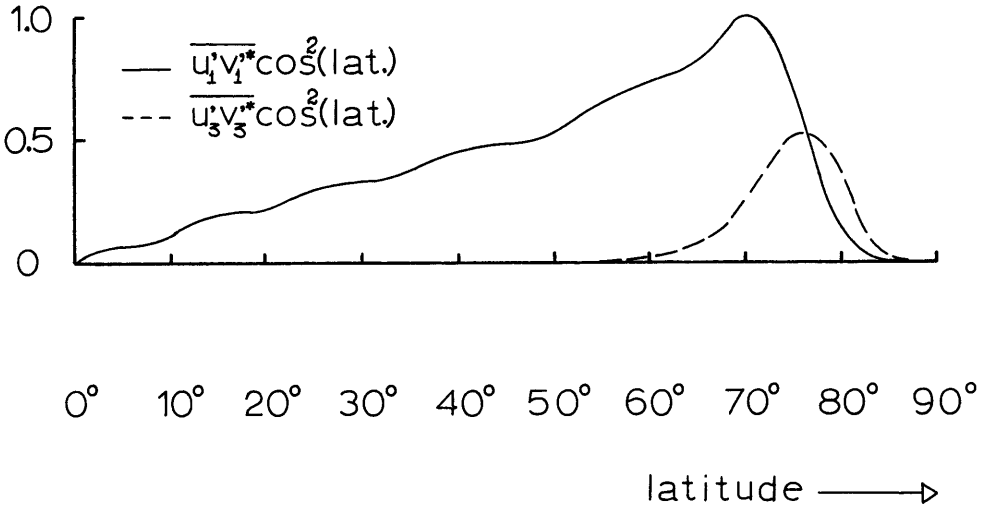


Fig. 32.a Eigenfunctions ϕ_1' and ϕ_3' for the most unstable mode for the profile ③ (Fig. 30), using the set of equations $\Upsilon = 0$. Numerical values of the parameters are: S = 0.005; $\omega = \Lambda = 0.002$; $\delta = 2$. This mode has $\sigma = -0.003585 + i\ 0.0003503$; s = 2; m = 5; SYM = 0.



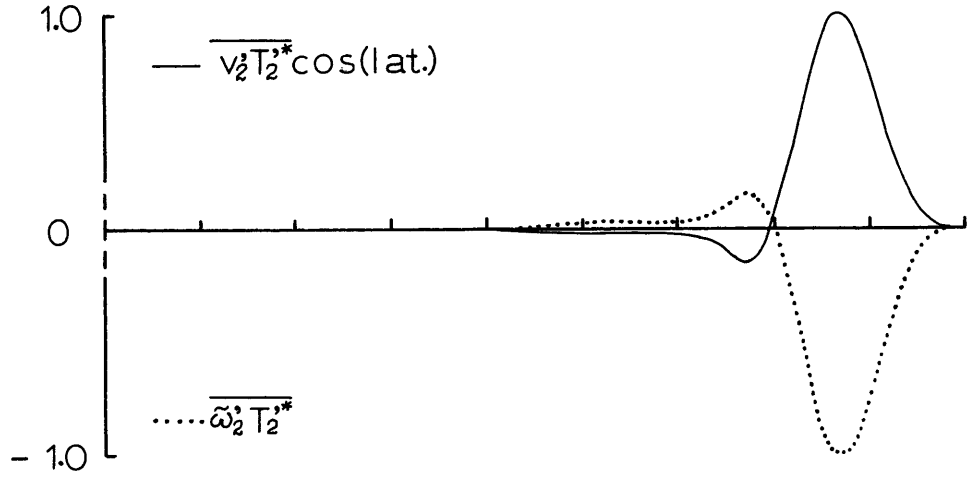


Fig. 32.b Angular momentum and heat transports corresponding to Fig. 32.a.

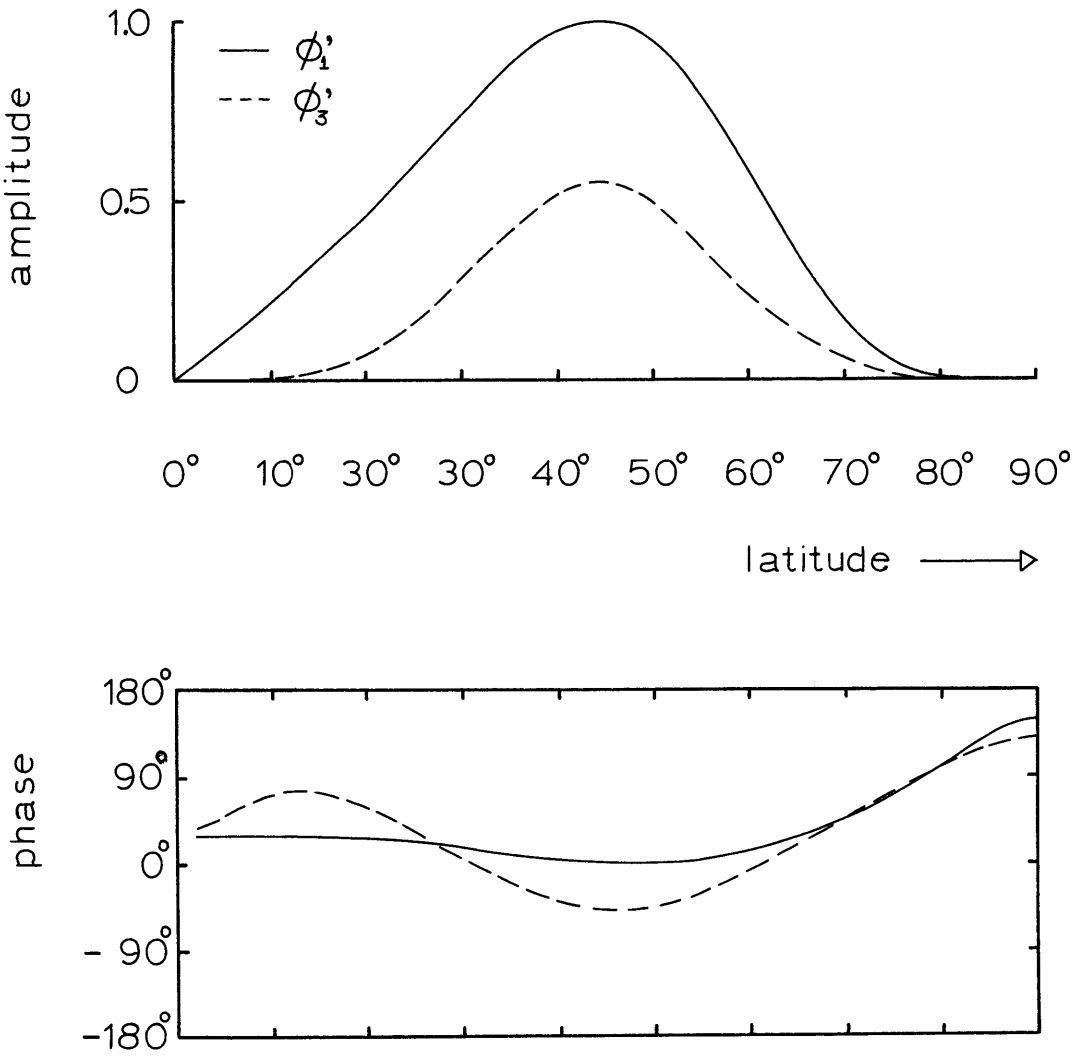
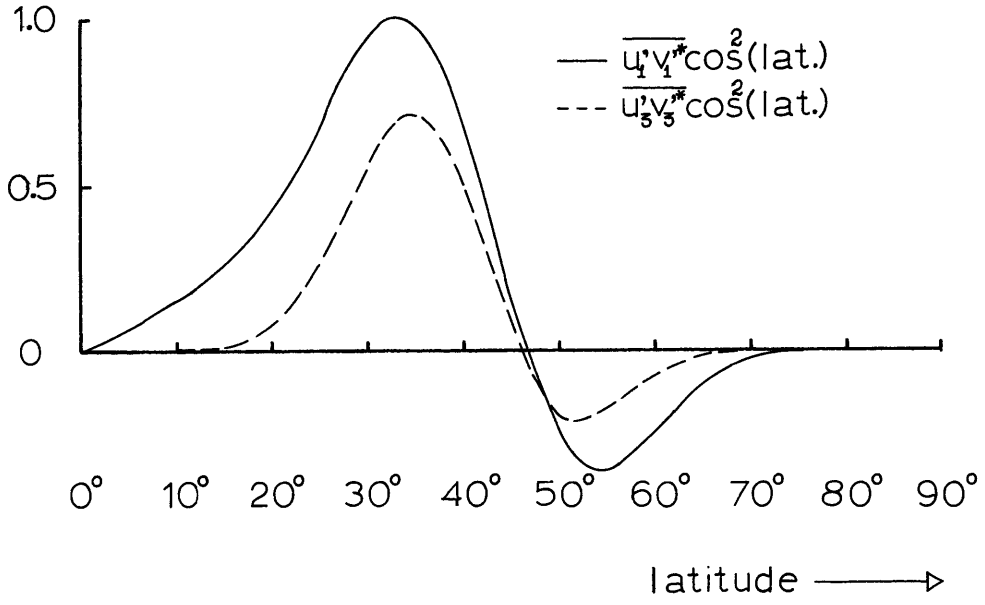


Fig. 33.a Same as Fig. 31.a, but for the profile ④ (Fig. 29);
$S = 0.005$; $\omega = \Lambda = 0.025$; $\delta = -1$.
$\sigma = -0.1210 + i\ 0.01267$; $s = 5$; $m = 2$; SYM = 0.



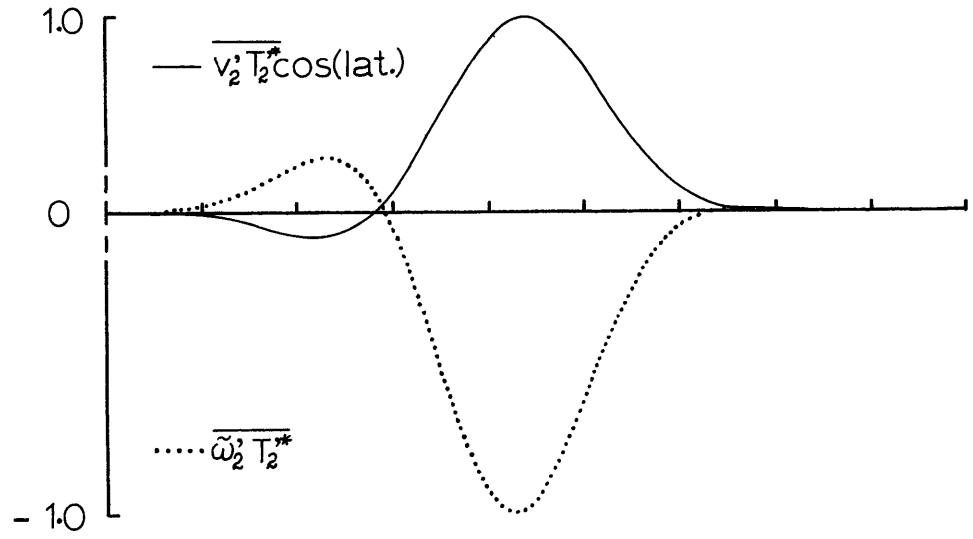


Fig. 33.b Angular momentum and heat transports corresponding to Fig. 33.a.

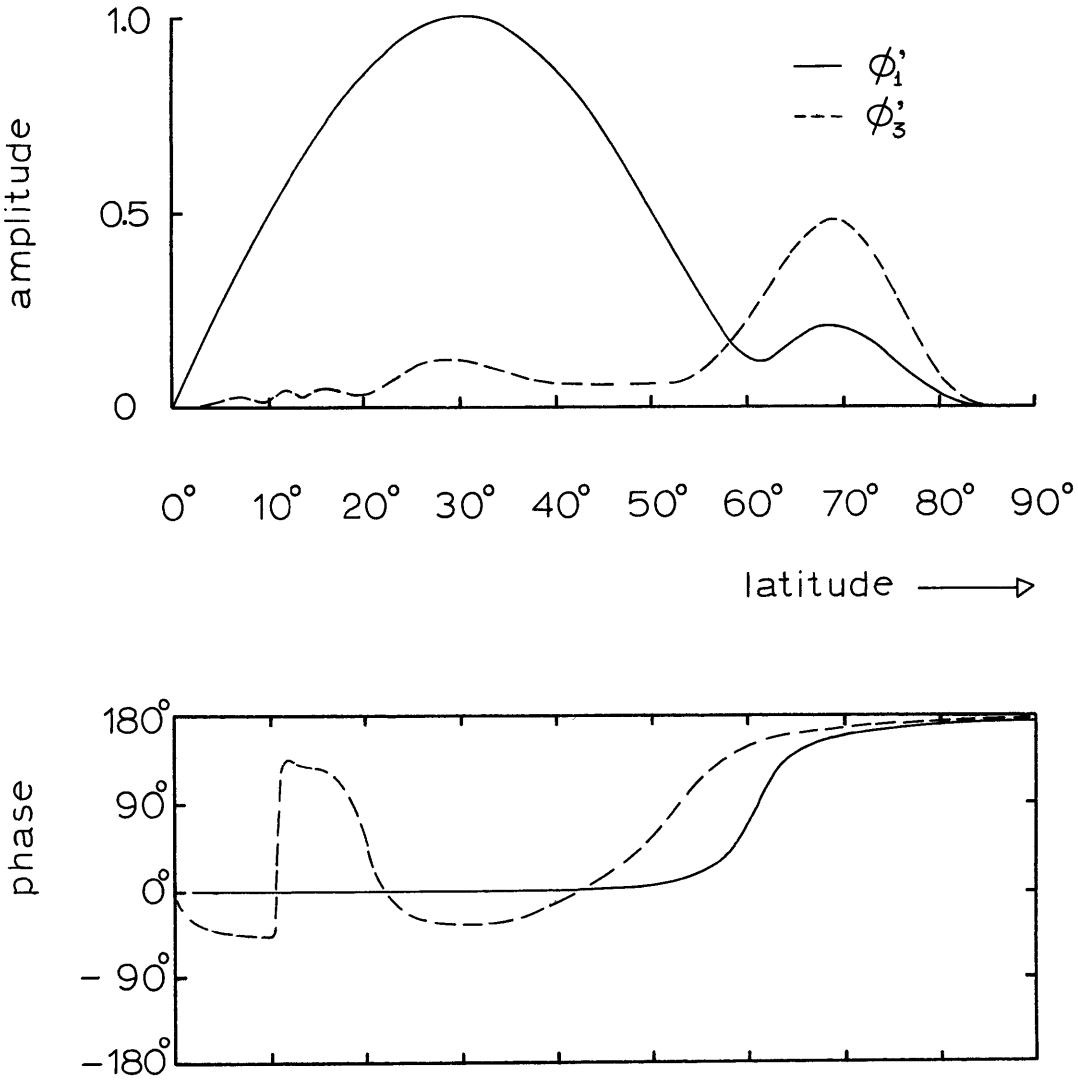


Fig. 34.a Same as Fig. 32.a, but for the profile ④ (Fig. 30);
S = 0.005; $\omega = \Lambda = 0.02$; $\delta = -1$.
$\sigma = -0.1087 + i\ 0.0004115$; s = 5; m = 2; SYM = 0.

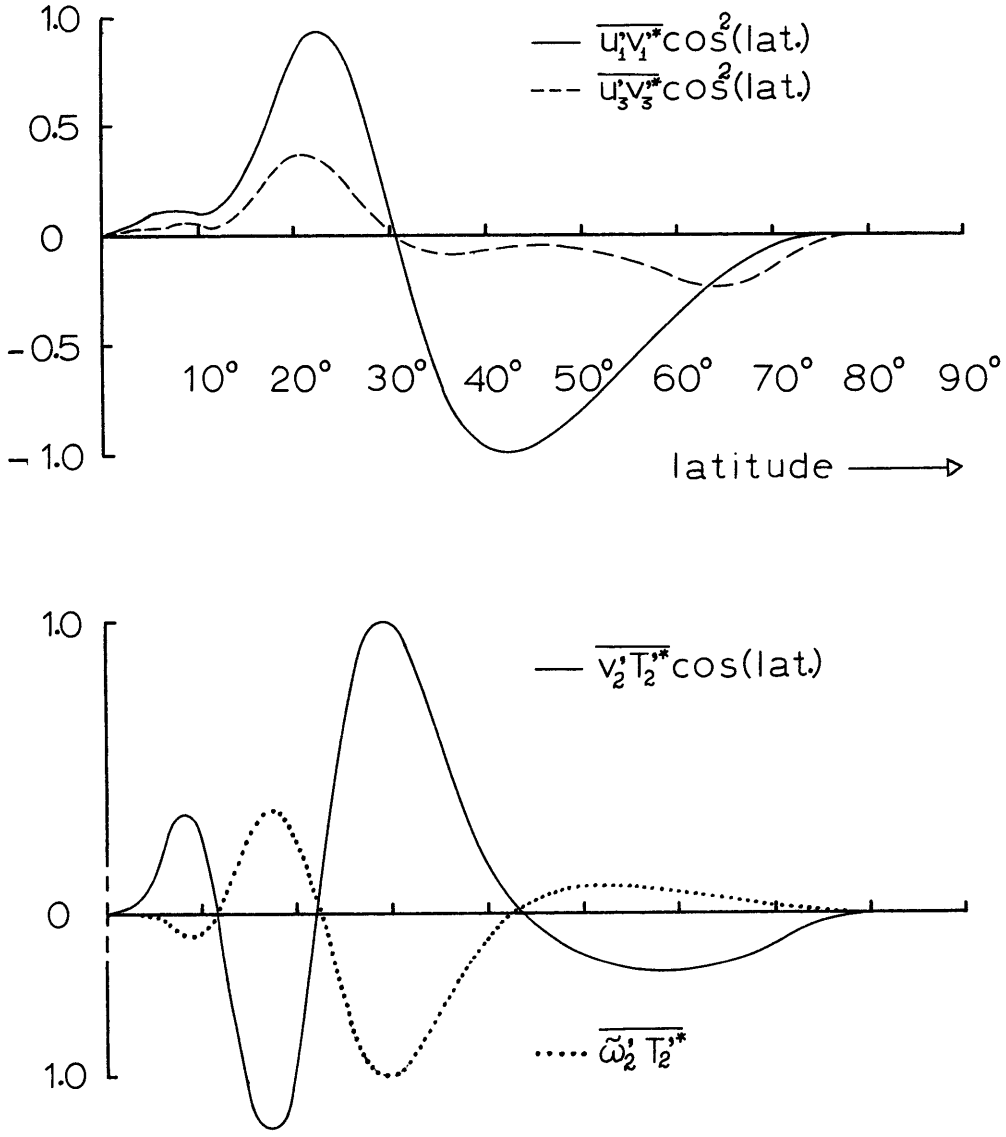


Fig. 34.b Angular momentum and heat transports corresponding to Fig. 34.a.

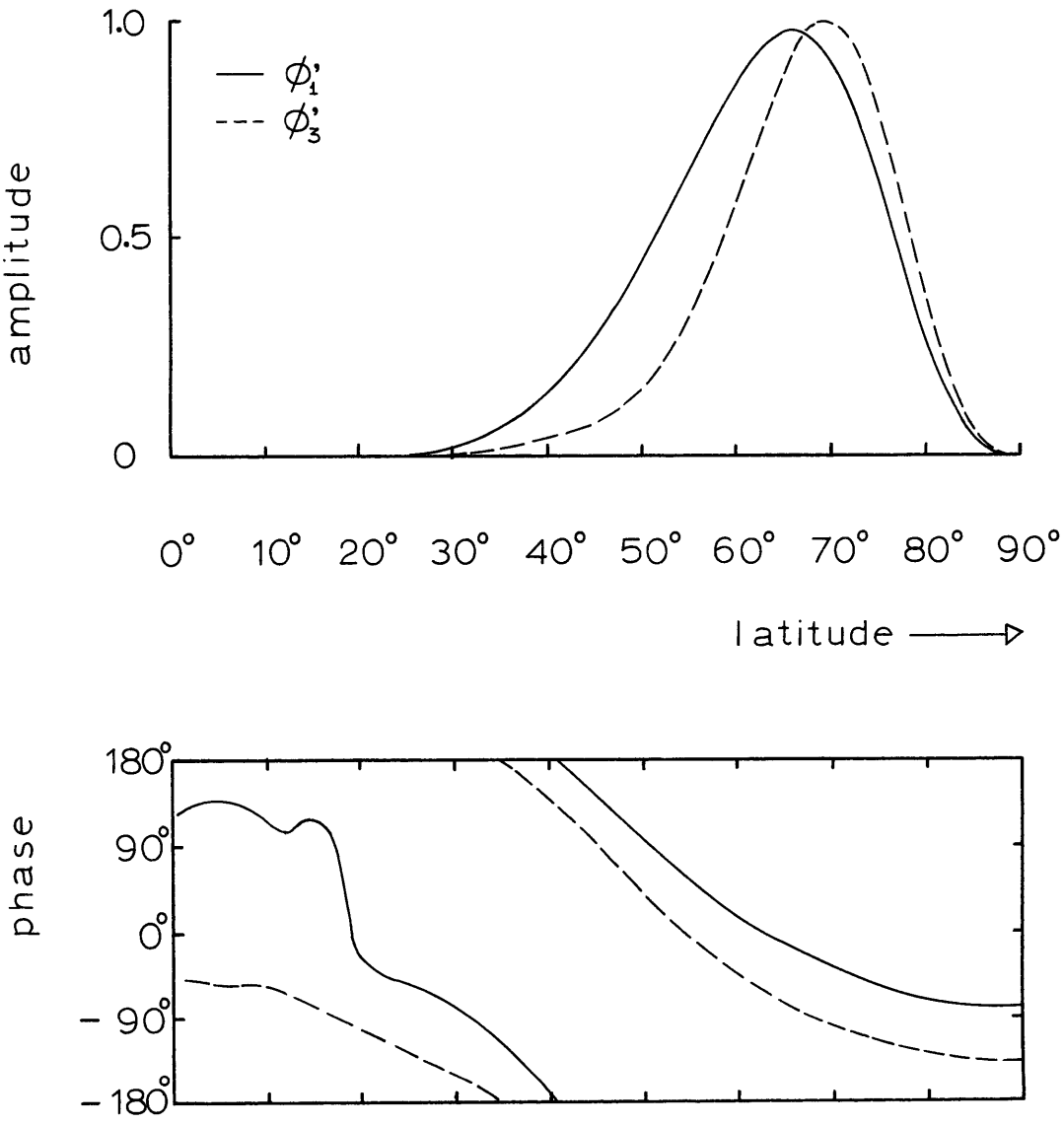
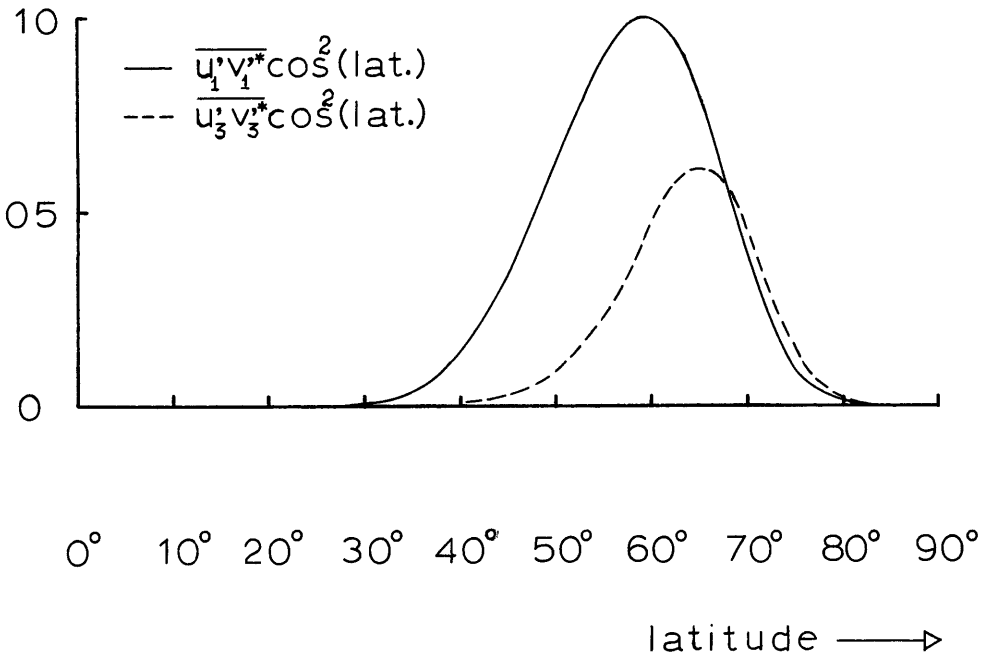


Fig. 35.a Same as Fig. 31.a, but for the profile ⑤ (Fig. 29);
S = 0.005; $\omega = \Lambda = -0.001$; $\delta = -28$.
$\sigma = 0.04293 + i\ 0.02188$; s = 3; m = 4; SYM = 1.



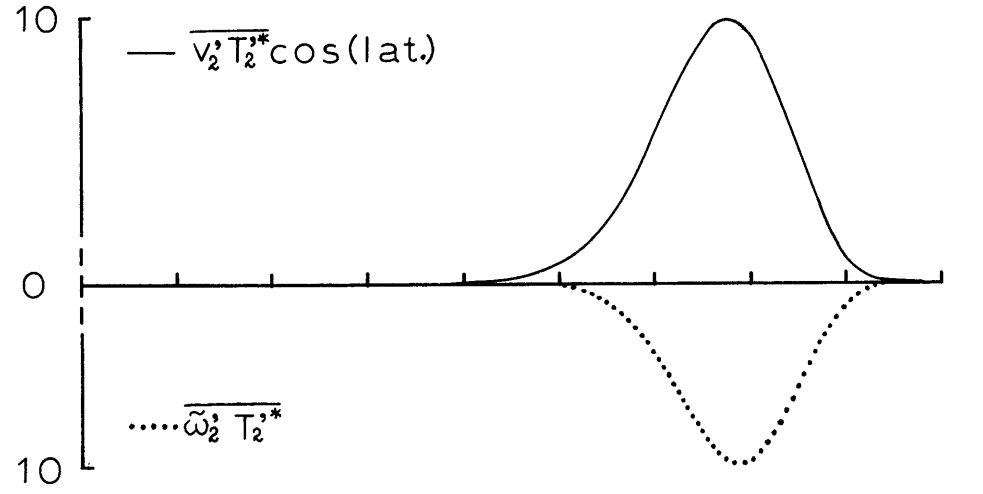


Fig. 35.b Angular momentum and heat transports corresponding to Fig. 35.a.

zonal flow (Pedlosky, 1964.b; Stone, 1969; Simmons, 1974).

The curvature effects show a quite different conclusion. The angular momentum transports are polewards for all the profiles (see figures 27.b, 28.b, 32.b - 35.b), with exception of profile ④ (figures 29 and 30) for which there is a reversal of sign (see figures 33.b, 34.b). For all of them, angular momentum is transported away from where the zonal velocity is a maximum to higher latitudes. For the profile ④ ($\bar{U} \propto \cos^3(\text{lat.})$) there exists a tendency for jet formation at approximately 45°N (figure 33.b) and 30°N for the solutions far from neutral stability and near neutral stability, respectively.

Here again there is a strong correlation between the location of maximum convergence of angular momentum flux and the latitude where the instability is a maximum. Table I shows the specific locations for the profiles studied.

6.4.3 Horizontal and Vertical Heat Transports

The latitudinal distributions of horizontal and vertical eddy heat transports look much alike; i.e., upward (downward) heat transport coinciding with poleward (equatorward) horizontal eddy heat transport, with peaks at the same latitude. One could then be tempted to extend the conclusion found in Stone (1974) even to cases not so close to near neutral stability (see his equation 2.19). For all the cases near neutral stability there is a reversal of sign of heat transports, located equatorward of the maximum heat transport (see figures 28.b, 32.b). Figure 34.b shows an exception for the profile ④ (figure 30),

which is always below the local stability curve. This sign reversal does not seem to occur for the solutions far from neutral stability (see figures 31.b, 35.b), with exception of figure 33.b (profile ④ in figure 29). The location of this sign reversal appears well correlated with the latitude where the local criterion for stability curve intercepts the curves of basic zonal wind profiles (figure 30). This fact is summarized in Table I, and seems to reinforce the conclusion reached by Stone (1974) that "... to a first approximation the heat flux is equatorward in regions where the local criterion for stability is satisfied, and poleward in regions where it is not."

The locations of maximum poleward heat transport are well correlated with the place where the baroclinic instability of the basic state is largest (see Table I). These locations are even better correlated with the locations of maximum convergence of angular momentum (see again Table I). This fact should be taken into account in any study which aims at a correct parameterization of heat transports by the baroclinic eddies. Curvature effects are very important in this respect (i.e. in locating the transport maxima), and could cure the defect in Stone's (1974) parameterization of the meridional variation of eddy heat fluxes by baroclinic waves (as he suggested in his concluding remarks).

6.4.4 Meridional Scale of Baroclinic Waves

Here we shall consider the question concerning the scale of the most unstable baroclinic wave on a globe. Stone (1969) addressed this question with an analysis (on a β-plane) for unstable waves near

the baroclinic stability threshold, concluding that the waves have their own internal meridional scale, given by the radius of deformation. His definition of the mean meridional scale is the mean separation of the zeros in the real part of the complex streamfunction in the upper layer, between the equator and pole. In figures 27.a, 28.a, and 31.a - 37.a, these number of zeros plus 1 are given by m (e.g., m=3 in figure 27.a).

In a recent numerical study, Simmons (1974) found that there are also some solutions (far from neutral stability) for which the scales are not the radius of deformation. Guided by his numerical solutions, he obtained an analytic formulation for a parabolic profile, valid for baroclinic waves far from neutral stability. These have meridional scales given by the geometric mean of the radius of deformation and the distance from the equator to pole. The amplitudes of the streamfunctions have a Gaussian behavior with latitude, centered at the position where the zonal profile is a maximum.

In an attempt to verify the existence of these two scales, when curvature effects are included, we have derived solutions (figures 36 and 37) for two additional cases, in which the radius of deformation is just half the value used in two of the solutions discussed earlier (figures 35 and 32). To accomplish this, we decreased S by a factor of 4, but kept the ratio S/Λ constant (i.e., the latitudinal shape of $4\Omega a\Lambda \cos(\text{lat}) [1+\delta \sin^2(\text{lat}) - (S/\Lambda)\sin^{-2}(\text{lat})]$ is the same in each comparison). Figure 35.a shows s=3 and m=4, with maximum value of $|\phi_1'|$ located at 66° of latitude. Its counterpart (figure 36.a) shows s=7 and m=10, with maximum value of $|\phi_1'|$ at 64° of

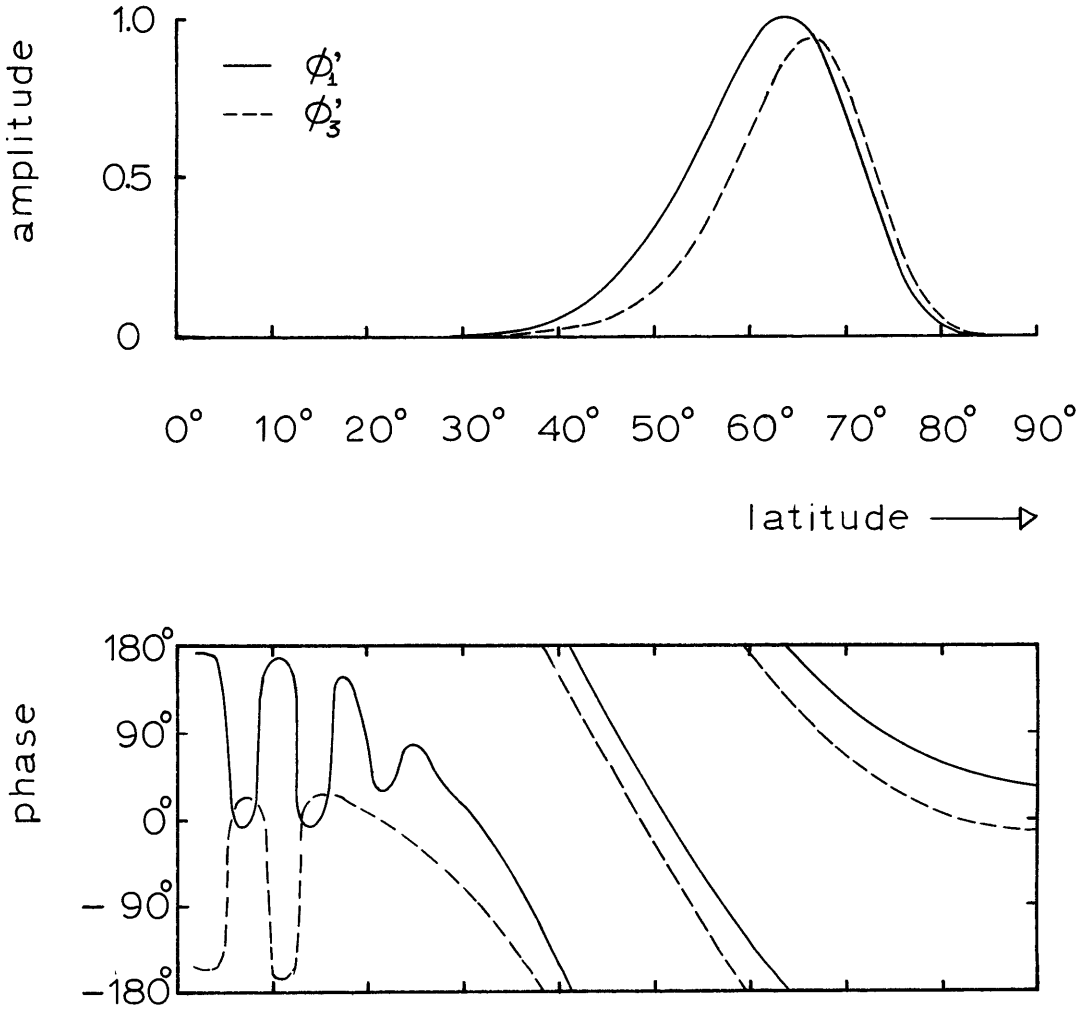
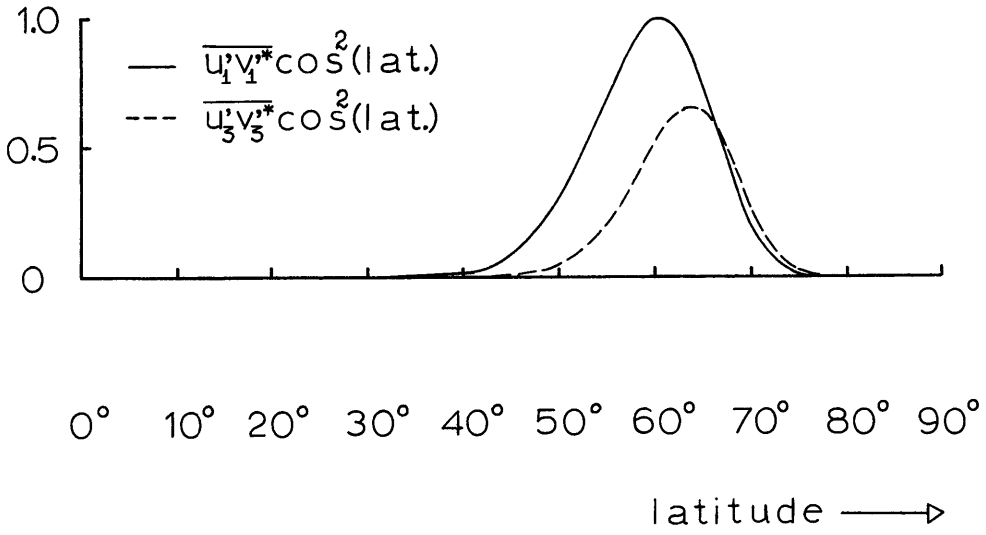


Fig. 36.a Same as Fig. 31.a, but for the profile ⑤ (Fig. 29 with shear coordinates decreased by a factor of 4);
S = 0.00125; $\omega = \Lambda = -0.00025$; $\delta = -28$.
$\sigma = 0.02617 + i\ 0.01362$; s = 7; m = 10; SYM = 0.



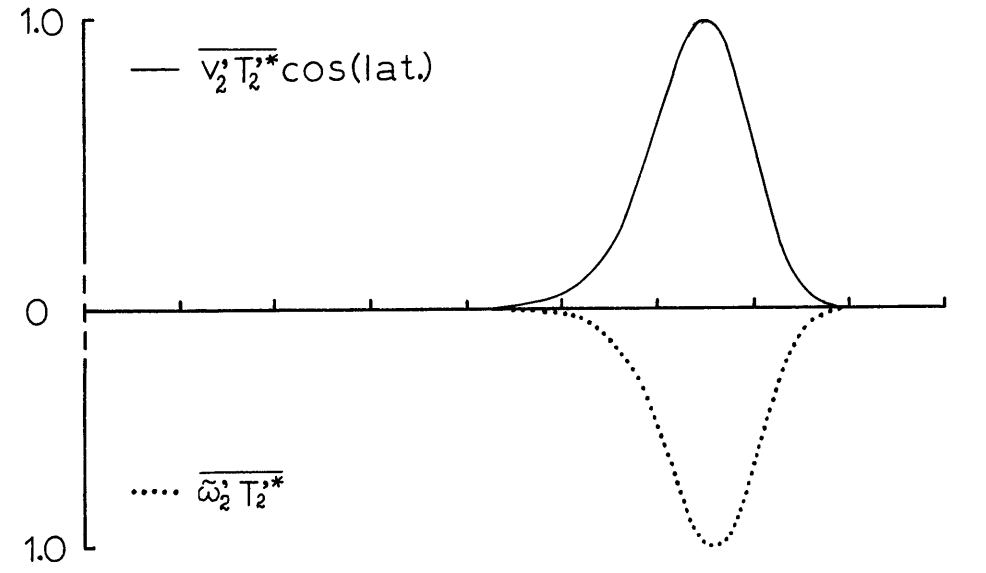


Fig. 36.b Angular momentum and heat transports corresponding to Fig. 36.a.

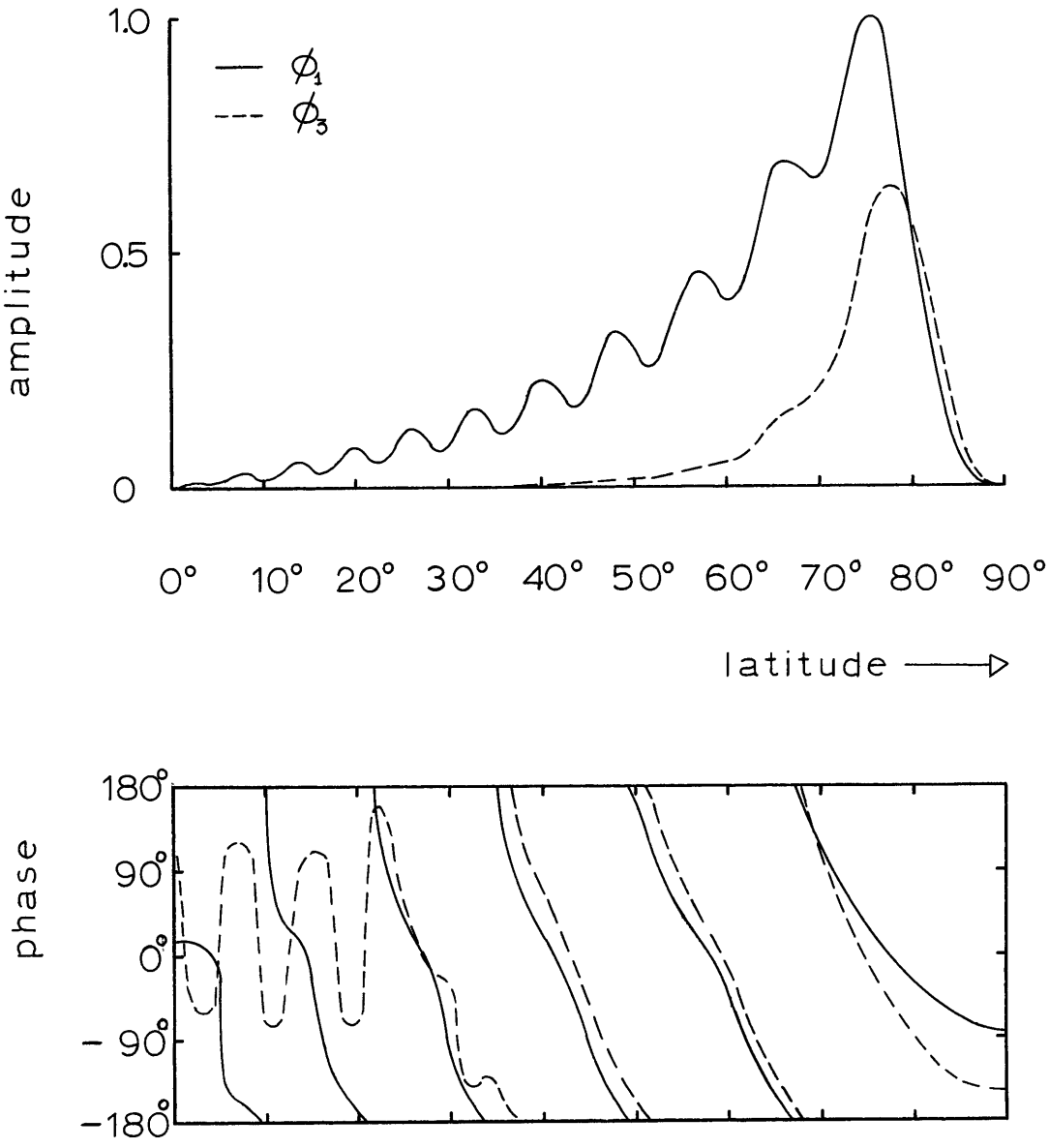


Fig. 37.a Same as Fig. 32.a, but for the profile ③ (Fig. 30 with shear coordinate decreased by a factor of 4).
S = 0.00125; $\omega = \Lambda = 0.0005$; $\delta = 2$.
$\sigma = -0.16 + i\ 0.00026$; s = 4; m = 11; SYM = 1.

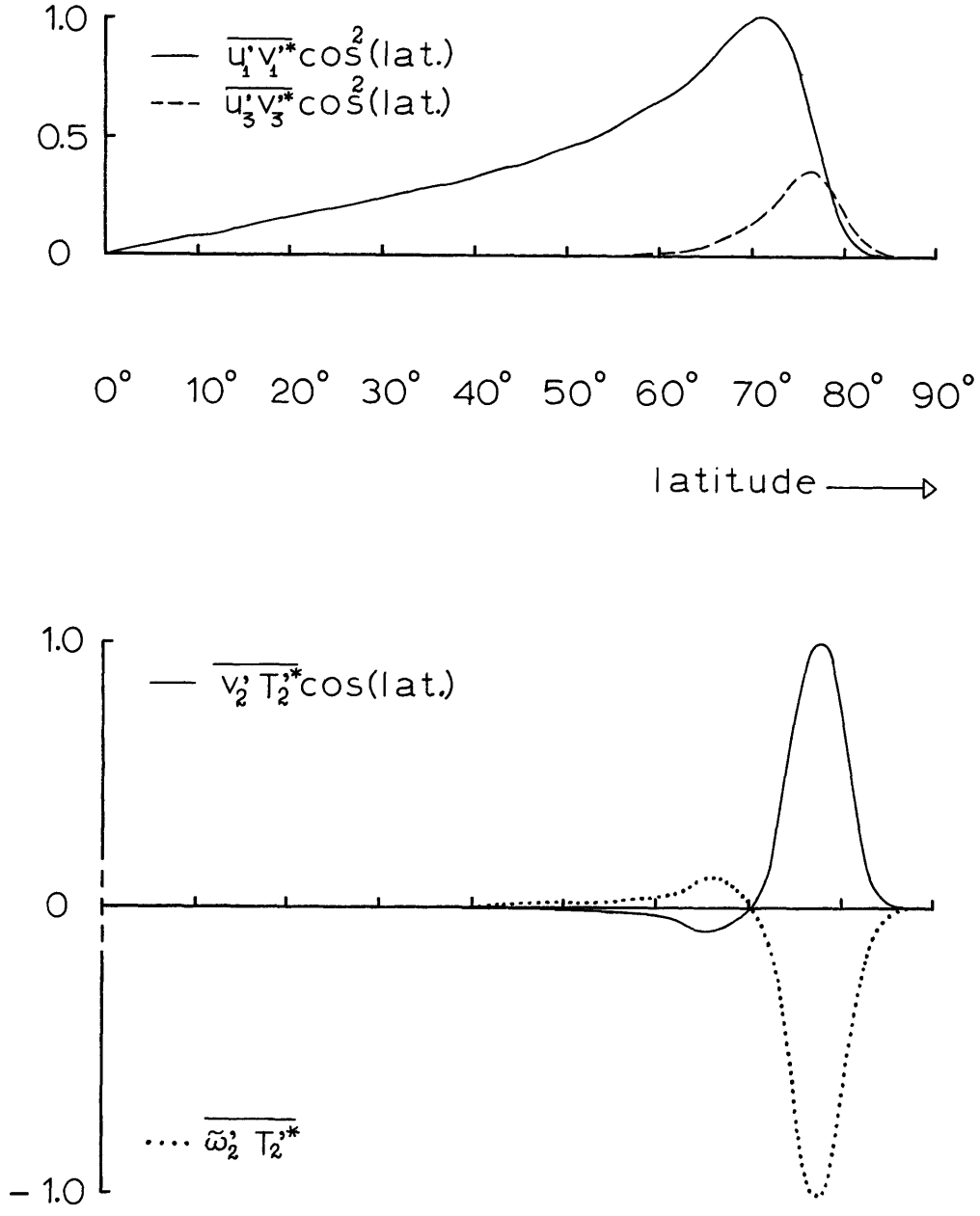


Fig. 37.b Angular momentum and heat transports corresponding to Fig. 37.a.

latitude. The width, where the amplitude of ϕ_1' is half its maximum value, decreases by a factor of 1.36, when the two solutions are compared. This pair of solutions is far from neutral stability.

For the other pair, which is near neutral stability, figure 32.a shows s=2 and m=5, with maximum value of $|\phi_1'|$ at 73° of latitude, while figure 37.a shows s=4 and m=11, with a shift in the maximum of $|\phi_1'|$ to 76° of latitude. In this case (and also for the case far from neutral stability), the value of s and m are roughly doubled.

The local meridional scale near the maximum amplitude of ϕ_1' is also of interest. In figure 32.a the only zero in $Re(\phi_1')$ near the amplitude peak is at 61°. This gives a scale of 29° of latitude from 61° to 90°(pole). Its counterpart (figure 37.a) has two zeros in $Re(\phi_1')$ near the amplitude peak, one at 62° and the other at 71°. The latter gives a scale of 19° of latitude, while the former gives a scale of 9° of latitude. The local meridional scale for these solutions (near neutral stability) does not decrease by a factor of 2 (compare 29° with 19°), unless one takes the mean scale for the former case ((19°+9°) ÷ 2 = 14°).

For the pair of solutions far from neutral stability, figure 35.a shows the only zero in $Re(\phi_1')$ near the amplitude peak is at 51°, implying a local scale of 39° of latitude. Figure 36.a shows two zeros in $Re(\phi_1')$ near the amplitude peak. One is at 57° and the other at 73°, with a local meridional scale of 16° of latitude. The local scale in this case has decreased by a factor greater than 2. It is worthwhile to note that in Simmons' (1974) Gaussian solution,

the maximum amplitude of the stream function coincides with the minimum in the phase (a parabolic variation with latitude). In our solutions (see figures 35.a and 36.a), the location of minimum phase is at the pole, while the amplitude peaks are at 66° and 64° of latitude. This displacement is caused by the variability of the Coriolis parameter, an effect not included in Simmons' solution. As a result, the large amplitudes occur in regions where the wave variations are rapid, not slow.

If one accepts the definition of mean meridional scale as that implied by m, the scale is roughly proportional to the radius of deformation (in both cases). Nevertheless, for the solutions far from neutral stability, the half amplitude width seems to vary roughly like the square root of the radius of deformation.

Our results are not completely conclusive, but they show that curvature affects the meridional scale of the baroclinic eddies. Therefore, we shall conclude with the remark that more work needs to be done for a clear understanding of curvature effects on the mean and local meridional scales of the most unstable baroclinic wave.

7. MODIFIED BALANCE EQUATIONS

Our study of the linearized balance equations has shown a significant discrepancy between the symmetric equatorial Rossby modes as described by the balance equations and the same modes (type 2) as described by the Laplace tidal equation (LTE) (section 3.3.2). A closer examination of this problem reveals that a very good description of these modes can be obtained by keeping the α -term (α=1) in the original equation of balance (equation 2.8 or 3.3). The system of equations (2.7)-(2.10) with α =1 is also energetically consistent and will be denominated "modified balance equations". Charney's (1962) scale analysis has shown that the magnitude of this α-term depends on the parameter $E = R_o^{-2}R_i^{-1}$, where R_o is the Rossby number and R_i a Richardson number. For $E = O(1)$ (typical of synoptic-scale atmospheric motions), the α -term appear as a first order term in an expansion in powers of R_o ; it is therefore smaller than the other important terms if the horizontal scale is small compared to the earth's radius.

7.1 Discussion of the Results

Figure 38 shows the eigenvalues for s=1. The inclusion of the α=1 term allows for eastward moving waves with $\varepsilon > 0$, which were not present in the balance equations. The integral expression (4.2) shows that this is true only for those modes with $\int_{-1}^{+1}|Q|^2 d\mu > \int_{-1}^{+1}|P|^2 d\mu$, i.e., modes with very significant divergence compared to their vorticity, over the whole globe. The modes for $\varepsilon > 0$ have

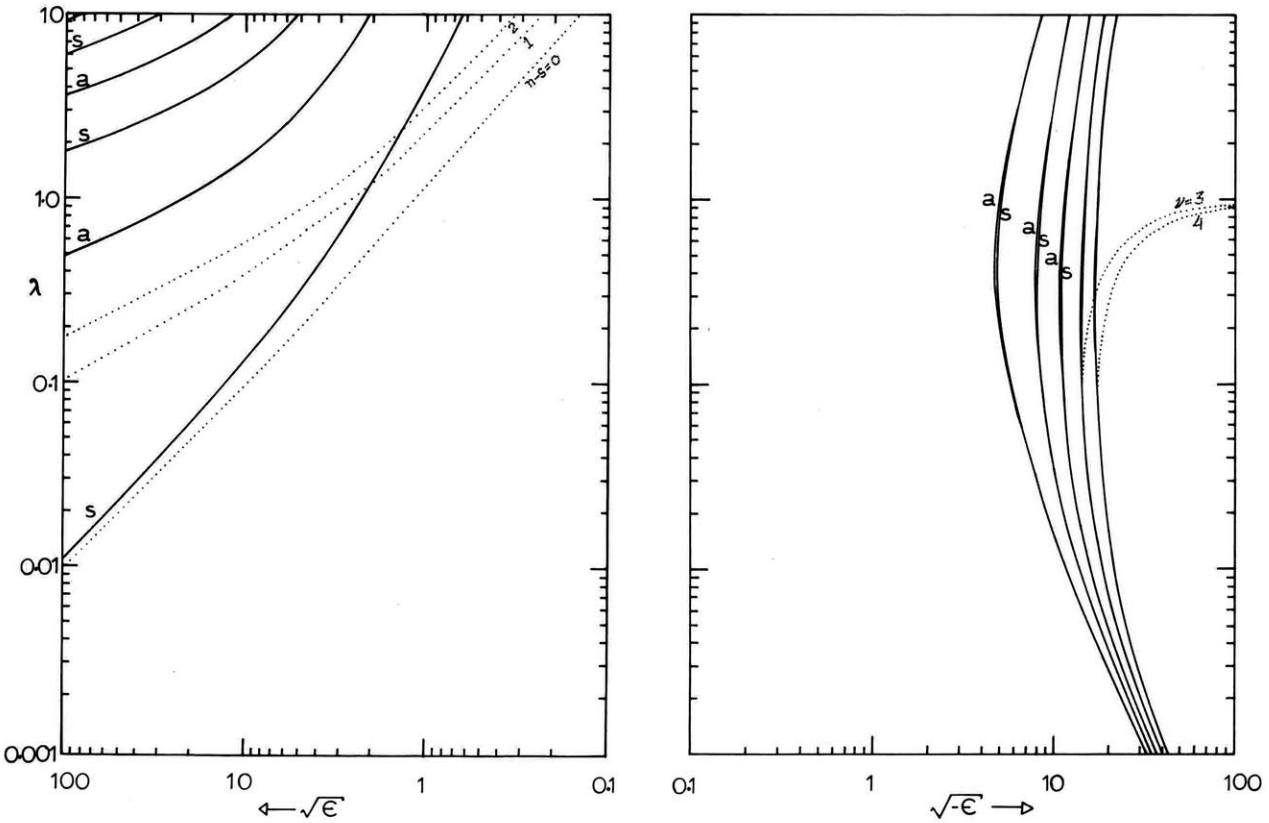


Fig. 38 Eigenvalues for the "modified balance equations" for the longitudinal wave number s = 1. The figure shows high frequency eastward propagating waves for ϵ positive. The equatorial Kelvin mode agrees well with Longuet-Higgins' results (dotted lines) at large ϵ . For negative values of ϵ and low frequencies, the "Burger" modes agree well with Longuet-Higgins' type 6. At large frequencies, however, they bend towards higher values of $-\epsilon$, but still do not accumulate at $\lambda = 1$. (Compare with Figs. 4 and 8).

have frequencies much higher than the corresponding ones for the LTE, with exception of the "Kelvin mode", where the agreement is better at large ε. As $\varepsilon \to +0$ the modes numerically approach the asymptote $\lambda\varepsilon = \frac{n^2(n+1)^2}{s}$.

For $\varepsilon < 0$, the limiting solutions $\lambda \sim \frac{s}{(-\varepsilon)}$ (equation 4.13) as $\varepsilon \to -\infty$ are also solutions to the modified balance equations, with a better pairing (described by 4.13) between symmetric and antisymmetric modes as compared to figure 8. As λ is increased, the modes bend toward higher values of $(-\varepsilon)$, instead of continuing straight upward as they do for the balance equations (see figure 8). However they still do not accumulate at $\lambda=1$.

Figure 39 is the counterpart of figure 9 for the modified balance equations for s=-1. The symmetric Rossby modes now also agree very well with Longuet-Higgins' results (compare also with figure 5), but the "mixed Rossby-gravity" mode still has too large a frequency as ε is increased. The solutions $\lambda \to \infty$ for finite $\varepsilon < 0$ of the balance equations (section 4.2.7), corresponding to the modes continuing straight upwards in figures 6 and 9, are changed so as to bend back toward small values of $-\varepsilon$, as λ increases. They are numerically asymptotic to $\lambda\varepsilon = \frac{n^2(n+1)^2}{s}$ (see section 7.3), which is the value of $\lambda\varepsilon$ that makes the coefficient of A_n^s vanish in expression A.10. [This occurs for $s < 0$ and $\varepsilon < 0$ and also for $s > 0$ and $\varepsilon > 0$.]

For s=0, the eigenvalues of the modified balance equations are the same as those of the balance equations (figure 7). This is explained by (4.2).

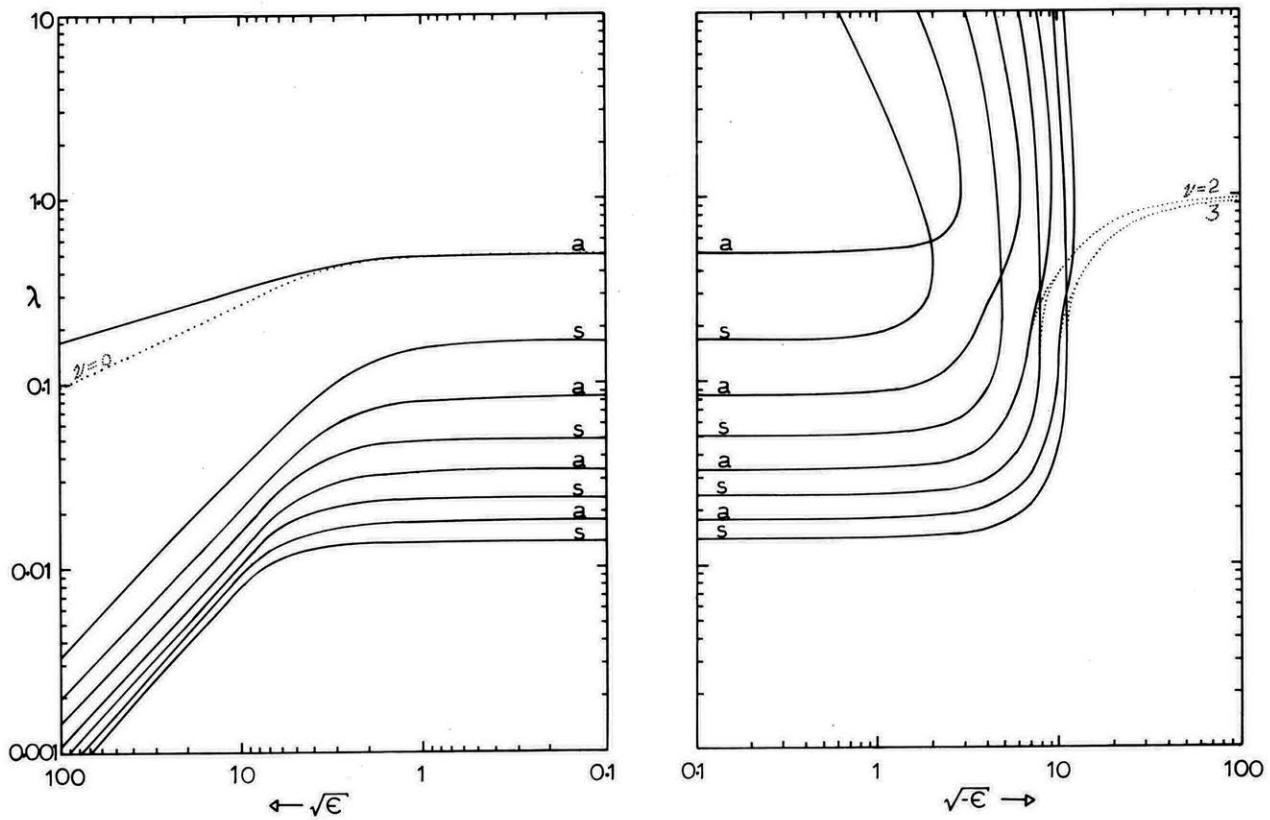


Fig. 39 Eigenvalues for the "modified balance equations" for the longitudinal wave number s = -1. All the equatorial Rossby modes agree well with Longuet-Higgins' type 2. The westward moving part of the mixed Rossby-Gravity mode has too high a frequency when compared with Longuet-Higgins' results (dotted lines). For negative values of ϵ, the modes bend back towards small values of $-\epsilon$, asymptotically to $\lambda \sim \frac{n^2(n+1)^2}{s\epsilon}$.

Figure 40 shows the excellent agreement between the total meridional velocities $[(1-\mu^2)^{1/2}\frac{dQ}{d\mu} + \frac{s}{(1-\mu^2)^{1/2}} P]$ in the first two "Rossby equatorial modes" as described by the modified balance equations and the corresponding asymptotic expressions (3.7) from Longuet-Higgins' study. [Compare with figure 23.]

7.2 Kelvin Wave Solution

The Kelvin wave solution of the LTE for large ϵ can be approximately described by the modified balance equations, as shown by our computations (see figure 38). Figure 41 shows U_T, $\epsilon^{1/2}R$, and V_T at a large value of ϵ from our calculations for this mode. The balance between U_T and $\epsilon^{1/2}R$ is approximate, with error typical of $O(\epsilon^{-1/2})$. An expansion in powers of $\epsilon^{-1/2}$, for large ϵ elucidates the approximation.

Let us return to equations (3.2)-(3.4) with $\alpha'=0$ and $\alpha=1$ and define $V = (1-\mu^2)\frac{dQ}{d\mu} + sP$ and $U = -\{(1-\mu^2)\frac{dP}{d\mu} + sQ\}$ These equations become:

$$\lambda\left(\frac{dU}{d\mu} + \frac{s}{1-\mu^2}V\right) + \frac{d}{d\mu}\mu V + \frac{s}{1-\mu^2}\mu U = 0 \tag{7.1}$$

$$\frac{d}{d\mu}\mu U + \frac{s}{1-\mu^2}\mu V + \left\{\frac{d}{d\mu}(1-\mu^2)\frac{d}{d\mu} - \frac{s^2}{1-\mu^2}\right\}R = 0 \tag{7.2}$$

$$\frac{dV}{d\mu} + \frac{s}{1-\mu^2}U - \lambda\epsilon R = 0 \tag{7.3}$$

Since the numerical solution appears equatorially trapped, we change the coordinate to $\mu = \epsilon^{-1/4}\eta$ ($\eta=O(1)$) and expand the

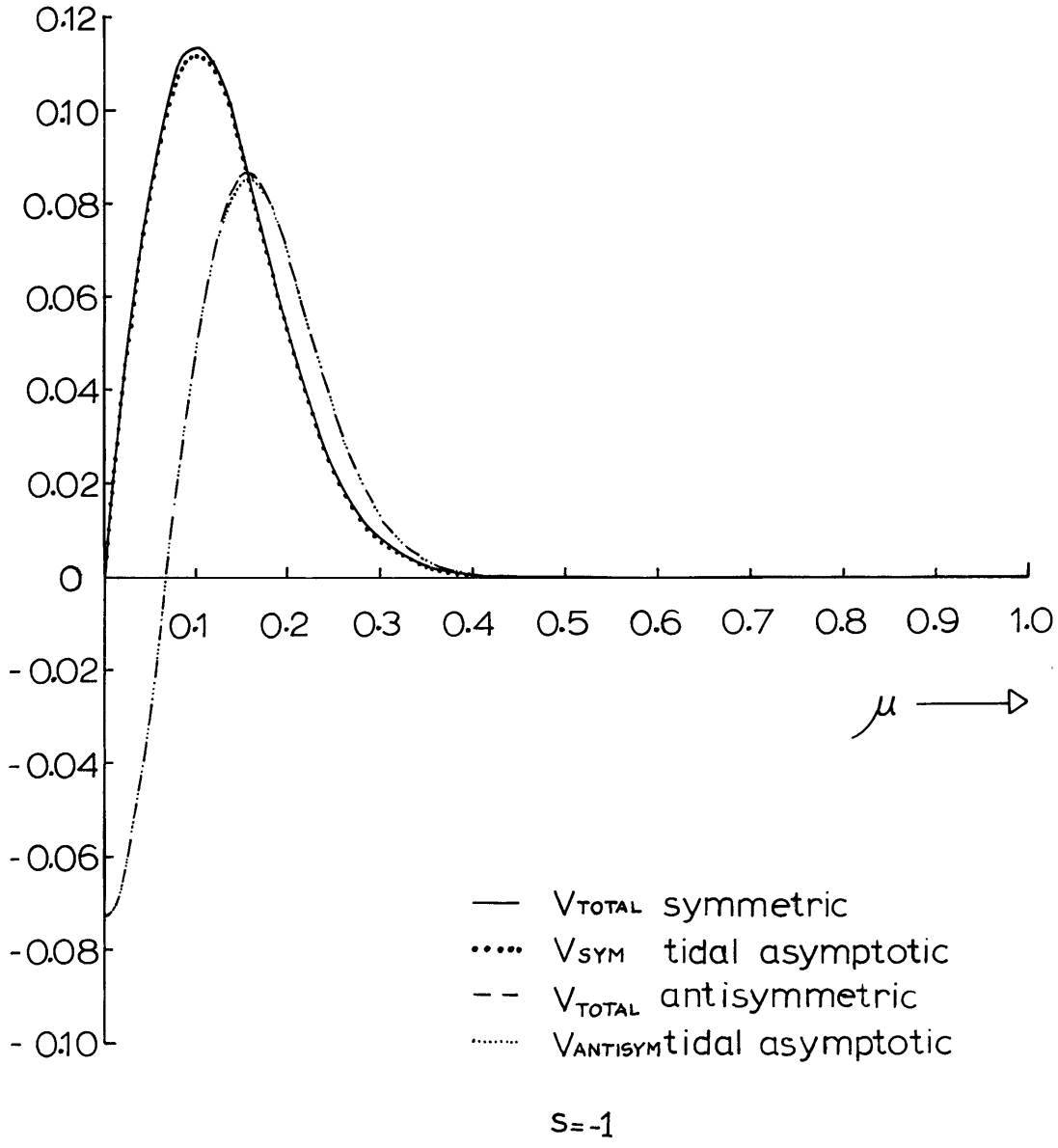


Fig. 40 Comparison of the total meridional (V_{TOTAL}) velocity of the "modified balance equations" with the asymptotic solutions of type 2 for $s = -1$ described by Longuet-Higgins. The agreement between the V_{TOTAL} Symmetric for $\epsilon = .956 \times 10^{-4}$ and the V_{TOTAL} Antisymmetric for $\epsilon = 1.03 \times 10^{-4}$ with their respective asymptotic solutions of type 2 ($\nu = 1$, and $\nu = 2$) is very good. (Compare with Fig. 23).

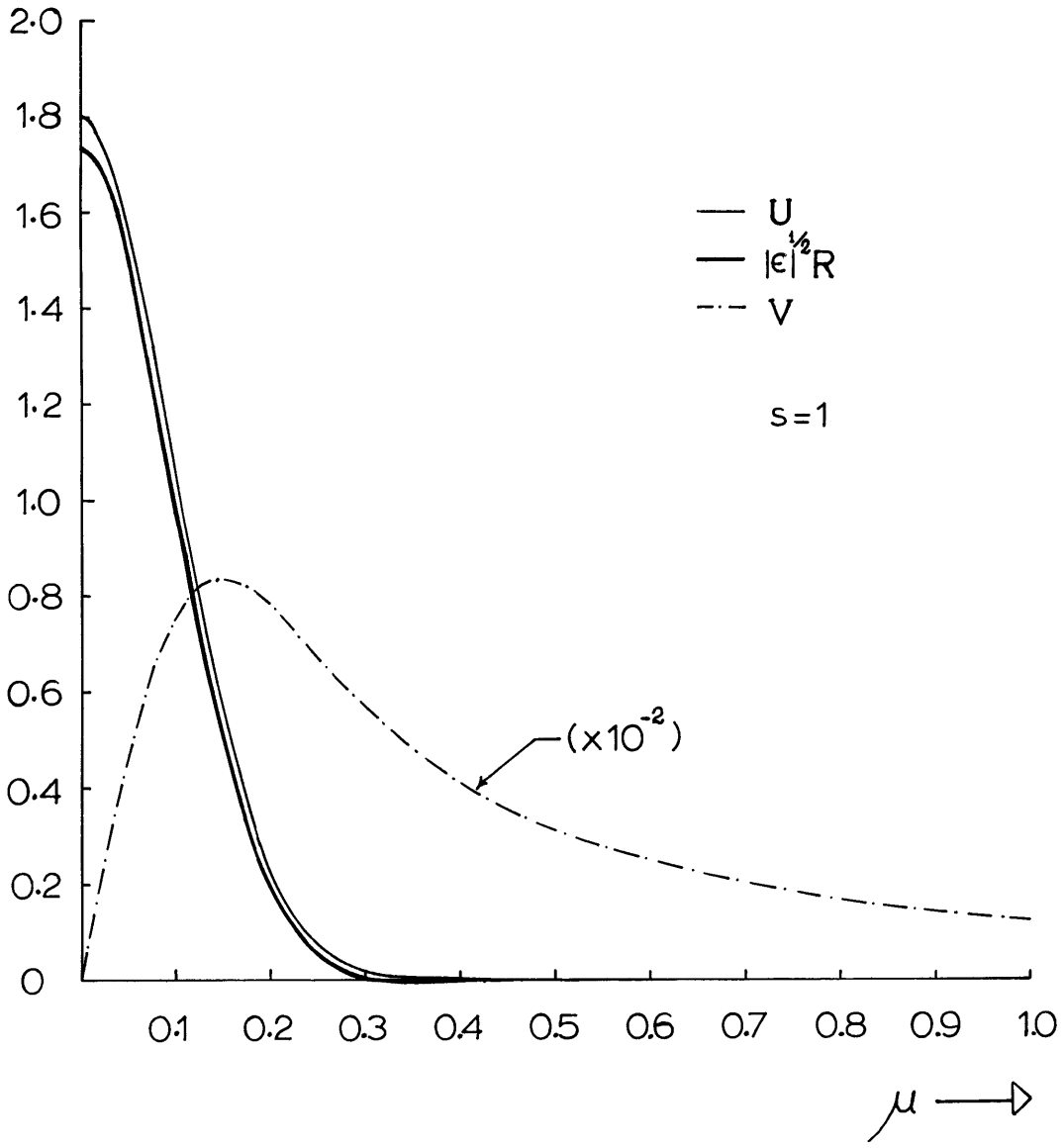


Fig. 41 Eigenfunctions $|\epsilon|^{1/2}R$ and total zonal and meridional velocities for the equatorial Kelvin mode as described by the "modified balance equations" for $\epsilon = 1.01 \times 10^{-4}$, $\lambda = 1.09 \times 10^{-2}$, and $s = 1$.

variables as follows:

$$\begin{aligned} \lambda &= \epsilon^{-1/2} s\,(\lambda_0 + \epsilon^{-1/2}\lambda_1 + \cdots) \qquad ; \; s \neq 0 \\ U &= \quad (U_0 + \epsilon^{-1/2} U_1 + \cdots) \\ R &= \epsilon^{-1/2}(R_0 + \epsilon^{-1/2} R_1 + \cdots) \\ V &= \epsilon^{-1/4} s(\,0 + \epsilon^{-1/2} V_1 + \cdots) \end{aligned} \tag{7.4}$$

The zeroth order solution is

$$\begin{aligned} \lambda_0 &= 1 \\ U_0 &= R_0 \propto e^{-\frac{1}{2}\eta^2} \end{aligned} \tag{7.5}$$

This zeroth order result is the same for the LTE (see 3.8). The first order equations can be combined to give the following equation for V_1:

$$\frac{d^2}{d\eta^2}\left(\frac{d}{d\eta} - \eta\right) V_1 = \frac{d^2}{d\eta^2}(2\lambda_1 - \eta^2)\, e^{-\frac{1}{2}\eta^2} + s^2\, e^{-\frac{1}{2}\eta^2} \tag{7.6}$$

If a similar expansion is made using the LTE instead, one also obtains (7.6) but without the last term in the right hand side. This term forces V_1 to have significant amplitude away from equatorial regions, which cannot be described by the asymptotic relation (3.8) for υ .

7.3 Asymptotic solutions as $\varepsilon \to \pm 0$

In addition to Hough's waves of the second class (Appendix E), there are other solutions to the modified balance equations as $\varepsilon \to +0$ (eastward moving waves) and as $\varepsilon \to -0$ (westward moving waves). Our computations of the eigenvalues (figure 39 and 38) have revealed the existence of asymptotic solutions $\lambda\varepsilon \sim \frac{n^2(n+1)^2}{s}$, which makes the

coefficient of A_n^s in A.10 vanish. To study this possibility we take equations (3.2)-(3.4) with $\alpha=1$ and $\alpha'=0$ and make the following expansion

$$\begin{aligned} \lambda &= \epsilon^{-1}\left(\lambda_0 + \epsilon\lambda_1 + \cdots\right) \\ P &= \left(P_0 + \epsilon P_1 + \cdots\right) \\ Q &= \left(Q_0 + \epsilon Q_1 + \cdots\right) \\ R &= \left(R_0 + \epsilon R_1 + \cdots\right) \end{aligned} \tag{7.7}$$

Collecting the zeroth order term ($\epsilon \to +0$), we obtain

$$\lambda_0 \mathcal{L}(P_0) = 0 \tag{7.8}$$

$$\mu \mathcal{L}(P_0) + (1-\mu^2)\frac{dP_0}{d\mu} + sQ_0 = \mathcal{L}(R_0) \tag{7.9}$$

$$\mathcal{L}(Q_0) = \lambda_0 R_0 \tag{7.10}$$

Equation (7.8) with the boundary conditions at the poles gives

$$P_0 \equiv 0 \tag{7.11}$$

Combining equations (7.9) and (7.10) results

$$\left(\mathcal{L} - \sqrt{s\lambda_0}\right)\left(\mathcal{L} + \sqrt{s\lambda_0}\right) Q_0 = 0 \tag{7.12}$$

$$\left(\mathcal{L} - \sqrt{s\lambda_0}\right)\left(\mathcal{L} + \sqrt{s\lambda_0}\right) R_0 = 0 \tag{7.13}$$

which have the solutions

$$R_o = P_n^{|s|}(\mu)$$

$$Q_o = -\frac{n(n+1)}{s} P_n^{|s|}(\mu) \qquad (7.14)$$

$$\lambda_o = \frac{n^2(n+1)^2}{s} \quad , \; s>0$$

These physically unrealistic solutions have very high frequency ($\lambda \sim \varepsilon^{-1}$), even when compared to the frequency of the first class waves (section 3.3.1). (Note that the solutions (7.14) also applies to $\varepsilon \to -0$, but for negatives values of s). Large λ of course makes it unrealistic to neglect the α' term in (3.3).

In closing this chapter, we shall compare the balance equations with the modified balance equation with respect to their numerical practicability using a numerical model.

Suppose we want to integrate (2.7)-(2.10) numerically with the forcing ($\vec{F}$) and heating (q) given and with the proper boundary conditions. Given Ψ_o (or ϕ_o) at t=0 we then calculate ϕ_o (or Ψ_o) from (2.8) if α =0 [the ellipticity condition must be satisfied; see Houghton (1968)]. With Ψ_o and ϕ_o known, equations (2.7), (2.9) and (2.10) contain four unknowns $\frac{\partial \Psi}{\partial t}$, $\dot{\chi}$, $\dot{Z}$, $\frac{\partial \phi}{\partial t}$ at t=0. The fourth equation relating $\frac{\partial \Psi}{\partial t}$ and $\frac{\partial \phi}{\partial t}$ is obtained by taking the time derivative of (2.8). Once $\frac{\partial \Psi}{\partial t}$ and $\frac{\partial \phi}{\partial t}$ are calculated, $\Psi_{\Delta t}$ and $\phi_{\Delta t}$ are obtained at t=Δt (say by a forward time extrapolation). [Charney (1962) has integrated these equations through an iterative scheme for a homogeneous incompressible ocean.]

This procedure is of no use in the case α=1. Now ϕ_o (or Ψ_o) cannot be calculated from Ψ_o (or ϕ_o) by means of (2.8), and

the initial condition is incomplete. A way to integrate the modified balance equations could be to have Ψ_o and ϕ_o both given at t=0 and use (2.8) to solve for χ_o. Then (2.10) is used to calculate $\dot{Z}_o$ which (together with χ_o) is used to compute $\frac{\partial \Psi}{\partial t}$ and $\frac{\partial \phi}{\partial t}$ from (2.7) and (2.9), respectively. One could try to get around this difficulty in an iterative manner. Suppose Ψ_o is given at t=0; one can solve the equations with α=0 as explained above, to get $\frac{\partial \Psi}{\partial t}$, $\frac{\partial \phi}{\partial t}$, χ , and $\dot{Z}$ at t=0. Now that χ is known, we can go back to (2.8) with α=1 and evaluate a new value for ϕ_o from Ψ_o and χ . Equation (2.9) is then used to get a new estimate of $\frac{\partial \phi}{\partial t}$ at t=0. An iteration could then be performed. After each convergence, the equations are integrated to the next time step, when a new iteration is performed. An alternative is to obtain $\phi_{\Delta t}$ and $\Psi_{\Delta t}$ at t=Δt, and from this time on, one could solve (2.8) for χ and march in time. It is possible that one runs into a problem of truncation error. If ϕ and χ are a well balanced field, χ is a small quantity and may be "contaminated" by truncation errors.

If ϕ_o is given instead of Ψ_o at t=0, one goes into the same procedure as outlined above, but in addition, a new estimate of $\frac{\partial \phi}{\partial t}$ at t=0 has to be calculated using (2.7).

The main virtue of the balance equations, i.e., that they are able to describe motions without gravity waves, is no longer true for the modified balance equations. Since the latter ones admit high frequency free mode solutions, these modes might require the use of shorter time steps. Therefore, if one does not devise an efficient method to get rid of these high frequency modes, it will seem hardly

acceptable to use these equations in numerical models for practical purposes.

APPENDIX A

Expansion in Surface Spherical Harmonics

The method used to solve the set of equations (3.2)-(3.4) is to expand $P(\mu)$ and $Q(\mu)$ in series of surface spherical harmonics. In doing so we use the convention $s \geq 0$, with λ possibly being negative, for computational convenience. The results are readily converted to the other convention of non-negative λ, with both positive and negative s. Then,

$$P(\mu) = \sum_{n=s}^{\infty} B_n^s \; \mathcal{P}_n^s(\mu)$$
$$Q(\mu) = \sum_{n=s}^{\infty} A_n^s \; \mathcal{P}_n^s(\mu) \qquad \text{(A.1)}$$

where $\mathcal{P}_n^s(\mu)$ is the associated Legendre 'polynomial' of degree n and order s with the following properties:

$$\left\{ \frac{d}{d\mu}(1-\mu^2)\frac{d}{d\mu} - \frac{s^2}{1-\mu^2} \right\} \mathcal{P}_n^s(\mu) = -n(n+1)\,\mathcal{P}_n^s(\mu) \qquad \text{(A.2)}$$

$$\int_{-1}^{1} \mathcal{P}_n^s(\mu)\,\mathcal{P}_m^s(\mu)\,d\mu = \delta_{nm}\,\frac{(n+s)!}{(n+\frac{1}{2})(n-s)!} \qquad \text{(A.3)}$$

$$(2n+1)\mu\,\mathcal{P}_n^s(\mu) = (n-s+1)\,\mathcal{P}_{n+1}^s(\mu) + (n+s)\,\mathcal{P}_{n-1}^s(\mu) \quad ; \; (0 \leq s \leq n-1) \qquad \text{(A.4)}$$

$$(1-\mu^2)\frac{d}{d\mu}\mathcal{P}_n^s(\mu) = -(n-s+1)\mathcal{P}_{n+1}^s(\mu) + (n+1)\,\mu\,\mathcal{P}_n^s(\mu) \quad ; \; (0 \leq s \leq n) \qquad \text{(A.5)}$$

Equation (3.4) with (A.1) and (A.2) gives:

$$R(\mu) = -(\lambda\epsilon)^{-1} \sum_{n=s}^{\infty} n(n+1)\, A_n^s\, P_n^s(\mu) \tag{A.6}$$

The series (A.1) and (A.6) when put into (3.2) and (3.3) gives:

$$\sum_{n=s}^{\infty} \left\{ \lambda n(n+1) B_n^s P_n^s - n(n+1) A_n^s \mu P_n^s + A_n^s (1-\mu^2) \frac{d}{d\mu} P_n^s + s B_n^s P_n^s \right\} = 0 \tag{A.7}$$

$$\sum_{n=s}^{\infty} \left\{ n(n+1) B_n^s P_n^s - B_n^s (1-\mu^2) \frac{d}{d\mu} P_n^s + \frac{n^2(n+1)^2}{\lambda\epsilon} A_n^s P_n^s - \alpha \left[s A_n^s P_n^s \right] \right\} = \tag{A.8}$$

$$= \alpha' \sum_{n=s}^{\infty} \left\{ \lambda n(n+1) A_n^s P_n^s \right\}$$

The properties (A.3)-(A.5) are used in (A.7) and (A.8), which then become (only the $\alpha'=0$ case is considered):

$$\left\{ \lambda n(n+1) + s \right\} B_n^s - \left\{ \frac{n(n+2)(n+s+1)}{2n+3} \right\} A_{n+1}^s - \left\{ \frac{(n-1)(n+1)(n-s)}{2n-1} \right\} A_{n-1}^s = 0 \tag{A.9}$$

$$\left\{ \frac{n^2(n+1)^2}{\lambda\epsilon} - \alpha[s] \right\} A_n^s = -\left\{ \frac{n(n+2)(n+s+1)}{2n+3} \right\} B_{n+1}^s - \left\{ \frac{(n-1)(n+1)(n-s)}{2n-1} \right\} B_{n-1}^s \tag{A.10}$$

We now substitute A_n^s from (A.10) ($n^2(n+1)^2 \neq \lambda\epsilon\alpha[s]$) into (A.9) to get:

$$d_{n-2} B_{n-2}^s + (a_n + g_n + b_n - \lambda) B_n^s + c_{n+2} B_{n+2}^s = 0 \tag{A.11}$$

where:

$$\begin{aligned} d_n &= e_{n+1} \left\{ \frac{n(n-s+1)(n-s+2)}{(2n+1)(2n+3)(n+1)(n+2)^2} \right\} \\ a_n &= e_{n+1} \left\{ \frac{n(n-s+1)(n+s+1)}{(2n+1)(2n+3)(n+1)^3} \right\} \\ g_n &= e_{n-1} \left\{ \frac{(n+1)(n-s)(n+s)}{(2n-1)(2n+1)\, n^3} \right\} \end{aligned} \tag{A.12}$$

$$b_n = -\frac{s}{n(n+1)}$$

$$c_n = e_{n-1}\left\{\frac{(n+1)(n+s-1)(n+s)}{(n-1)^2 n(2n-1)(2n+1)}\right\} \qquad \text{(A.12) cont.}$$

$$e_n = \lambda\epsilon\left\{\alpha\left[\frac{s\lambda\epsilon}{n^2(n+1)^2}\right]-1\right\}^{-1} \quad ; \quad (\alpha = 0 \text{ or } 1)$$

$(g_1 = b_n = 0$ for $s=0$; $g_n = 0$ when $n=s$, $s=1,2,\ldots)$

There are two separate systems of equations described by (A.11), which can be put in matrix form as follows:

$$\begin{bmatrix} [a_s+g_s+b_s-\lambda] & [\ c_{s+2}\ ] & 0 & \cdots & \\ [\ d_s\ ] & [a_{s+2}+g_{s+2}+b_{s+2}-\lambda] & [\ c_{s+4}\ ] & 0 & \cdots \\ 0 & [\ d_{s+2}\ ] & [a_{s+4}+g_{s+4}+b_{s+4}-\lambda] & [& \\ \vdots & 0 & [\ d_{s+4}\ ] & [& \\ & \vdots & 0 & \ddots & \\ & & \vdots & & \end{bmatrix} \begin{bmatrix} B_s^s \\ B_{s+2}^s \\ B_{s+4}^s \\ \vdots \end{bmatrix} = \begin{bmatrix} 0 \\ 0 \\ 0 \\ \vdots \end{bmatrix} \qquad \text{(A.13)}$$

$$\begin{bmatrix} [a_{s+1}+g_{s+1}+b_{s+1}-\lambda] & [\ c_{s+3}\ ] & 0 & \cdots & \\ [\ d_{s+1}\ ] & [a_{s+3}+g_{s+3}+b_{s+3}-\lambda] & [\ c_{s+5}\ ] & 0 & \cdots \\ 0 & [\ d_{s+3}\ ] & [a_{s+5}+g_{s+5}+b_{s+5}-\lambda] & [& \\ \vdots & 0 & [\ d_{s+5}\ ] & [& \\ & \vdots & 0 & \ddots & \\ & & \vdots & & \end{bmatrix} \begin{bmatrix} B_{s+1}^s \\ B_{s+3}^s \\ B_{s+5}^s \\ \vdots \end{bmatrix} = \begin{bmatrix} 0 \\ 0 \\ 0 \\ \vdots \end{bmatrix} \qquad \text{(A.14)}$$

System A.13 (A.14) with n-s an even (odd) number correspond to motions for which P is an even (odd) function of μ, whereas Q and R are odd (even) functions of μ. These two tridiagonal systems may be solved by fixing values of s and of the product $\lambda\varepsilon$ ($n^2(n+1)^2 \neq \lambda\varepsilon\alpha[s]$ if $\alpha=1$) and treating a simple eigenvalue problem for λ. In practice we have to truncate the infinite tridiagonal matrices and take the first NxN elements. The size of N is dictated by the convergence of the eigenvalues which we are interested in. Our computations (with double precision arithmetic) for N=40, when verified against those with N=50 have shown excellent agreement: the values of λ for N=40 and N=50 agree to 10 places for $|\lambda| \geqslant 10^{-3}$ and $|\varepsilon| \leqslant 10^{4}$. Slower convergence occurs when the frequency is smaller than 0.001 for large positive ε (equatorial Rossby waves, section 4.2.5) and for large negative ε (section 4.2.4).

Once we obtain the eigenvectors B_n^s from (A.13) and (A.14) we calculate the corresponding A_n^s from (A.10). The values of A_n^s and B_n^s are normalized in the following way, consistent with the normalization used by Longuet-Higgins (1968). Let $\mathcal{E}$ be the total energy (solenoidal kinetic + potential):

$$\mathcal{E} = \int_{-1}^{+1} \int_{0}^{2\pi} \left(\frac{1}{2} \nabla\psi \cdot \nabla\psi + \frac{1}{2c^2} \phi^2 \right) a^2 d\mu d\varphi \qquad \text{(A.15)}$$

Since $\{\Psi,\phi\} = \mathrm{Re}\ \{(P(\mu),\ 2\Omega R(\mu))\ e^{i(s\varphi-\sigma t)}\}$, we have:

$$\frac{1}{2} \nabla\psi \cdot \nabla\psi = \frac{1}{4a^2} \left\{ (1-\mu^2) \left| \frac{dP}{d\mu} \right|^2 + s^2 \frac{|P|^2}{1-\mu^2} \right\}$$

$$\frac{1}{2c^2}\phi^2 = \frac{1}{4a^2}\left(\frac{4\Omega^2a^2}{c^2}\right)|R|^2 \qquad ; \quad \frac{4\Omega^2a^2}{c^2} = \epsilon$$

Then $$\mathcal{E} = \frac{\pi}{2}\left\{\int_{-1}^{+1}(1-\mu^2)\left|\frac{dP}{d\mu}\right|^2 d\mu + s^2\int_{-1}^{+1}\frac{|P|^2}{1-\mu^2}d\mu + \epsilon\int_{-1}^{+1}|R|^2 d\mu\right\}$$

The choice $\mathcal{E} = \frac{\pi}{2}$ implies that

$$s^2 I_2 + I_3 + |\epsilon| I_4 = 1 \tag{A.16}$$

where I_2, I_3, and I_4 are the integrals defined in (4.3), and the absolute value of ϵ is taken for the $\epsilon < 0$ modes (Longuet-Higgins). When (A.1) and (A.6) are used in (A.16) the normalized A_n^s and B_n^s ensure that

$$\sum_{n=s}^{\infty}\frac{(n+s)!\,n(n+1)}{(n+\frac{1}{2})(n-s)!}\left\{\frac{|\epsilon|\,n(n+1)}{(\lambda\epsilon)^2}\left(A_n^s\right)^2 + \left(B_n^s\right)^2\right\} = 1 \tag{A.17}$$

A similar relation is imposed for the truncated matrices used in computation (Appendix B).

The eigenfunctions are all defined in terms of the normalized A_n^s and B_n^s. Truncated series of spherical harmonics are used to compute $P(\mu)$, $Q(\mu)$, and $R(\mu)$ using (A.1) and (A.6). Other variables are then derived from $P(\mu)$, $Q(\mu)$, and $R(\mu)$:

Meridional velocity V

$$(1-\mu^2)^{1/2}V = (1-\mu^2)\frac{dQ}{d\mu} + sP = \sum_{n=s}^{N}\left\{sB_n^s + \frac{(n+2)(n+s+1)}{2n+3}A_{n+1}^s - \frac{(n-1)(n-s)}{2n-1}A_{n-1}^s\right\}P_n^s \tag{A.18}$$

Zonal velocity U

$$(1-\mu^2)^{1/2} U = -(1-\mu^2)\frac{dP}{d\mu} - sQ = -\sum_{n=s}^{N}\left\{s A_n^s + \frac{(n+2)(n+s+1)}{2n+3} B_{n+1}^s - \frac{(n-1)(n-s)}{2n-1} B_{n-1}^s\right\} P_n^s \quad \text{(A.19)}$$

Geopotential

$$R(\mu) = -(\lambda\epsilon)^{-1} \sum_{n=s}^{N} n(n+1) A_n^s P_n^s(\mu) \quad \text{(A.20)}$$

The rotational parts of V and U in (A.18) and (A.19) are obtained by omitting the A terms in the respective series. It is these which form the major displays in figures 11-22.

APPENDIX B

Integral Theorem for Truncated Matrix

Since the two systems described in Appendix A have to be truncated for actual computations of the eigenfunctions, it is desirable that the truncated systems retain the properties of the continuous ones. An "integral" theorem for the truncated matrix will be derived in order to give a rationale for terminating the spherical harmonics series on the basis of energy conservation. Let us rewrite (A.9) and (A.10)

$$(\lambda \gamma_n + s) B_n^s = a_n^s A_n^s + b_{n-1}^s A_{n-1}^s \tag{B.1}$$

$$\left(\frac{\gamma_n^2}{\lambda\epsilon} - \alpha[s]\right) A_n^s = -a_{n+1}^s B_{n+1}^s - b_{n-1}^s B_{n-1}^s \tag{B.2}$$

where $\gamma_n = n(n+1)$

$$a_n^s = \frac{(n-1)(n+1)(n+s)}{2n+1}$$

$$b_n^s = \frac{n(n+2)(n-s+1)}{2n+1}$$

Using the normalization factor for the associated Legendre polynomials we define

$$(\mathcal{A}_n^s , \mathcal{B}_n^s) = \left\{\frac{2}{2n+1}\frac{(n+s)!}{(n-s)!}\right\}^{1/2} (A_n^s , B_n^s) \tag{B.3}$$

The relations (B.1) and (B.2) then become

$$(\lambda \gamma_n + s)\, \mathbb{B}_n^s = c_n^s \mathbb{A}_{n+1}^s + c_{n-1}^s \mathbb{A}_{n-1}^s \tag{B.4}$$

$$\left(\frac{\gamma_n^2}{\lambda\epsilon} - \alpha(s)\right) \mathbb{A}_n^s = -c_n^s \mathbb{B}_{n+1}^s - c_{n-1}^s \mathbb{B}_{n-1}^s \tag{B.5}$$

where $c_n^s = n(n+2)\left\{\frac{(n-s+1)(n+s+1)}{(2n+1)(2n+3)}\right\}^{1/2}$; $c_{s-1}^s = 0$.

After multiplying (B.4) by $\mathbb{B}_n^s$ and (B.5) by $\mathbb{A}_n^s$ we add them to get

$$\sum_{n=s}^{N} \left\{ \lambda \left[\gamma_n \mathbb{B}_n^{s\,2} + \epsilon \left(\frac{\gamma_n}{\lambda\epsilon}\right)^2 \mathbb{A}_n^{s\,2} \right] + s\mathbb{B}_n^s - \alpha\left[s\mathbb{A}_n^{s\,2}\right] \right\} = c_N^s \left(\mathbb{A}_{N+1}^s \mathbb{B}_N^s - \mathbb{A}_N^s \mathbb{B}_{N+1}^s \right) \tag{B.6}$$

This relation with $N \to \infty$ is exactly the same as (4.1) integrated from pole to pole. The right hand side of (B.6) represents a flux which presumably vanishes as $N \to \infty$. Since (B.6) is like an energy conservation statement, we require that the right hand side vanish. This is easily accomplished by setting either g or a equal to zero in the last diagonal element of A.13) or (A.14) respectively. An "integral" theorem for the truncated matrix follows from (B.6)

$$\lambda = - \frac{s\left\{\sum_{n=s}^{N} \mathbb{B}_n^{s\,2}\right\} - \alpha\left[s \sum_{n=s} \mathbb{A}_n^{s\,2}\right]}{\sum_{n=s}^{N} \left\{ \gamma_n \mathbb{B}_n^{s\,2} + \epsilon \left(\frac{\gamma_n}{\lambda\epsilon}\right)^2 \mathbb{A}_n^{s\,2} \right\}} \tag{B.7}$$

The denominator of (B.7) is the sum of potential plus rotational kinetic energy. With ϵ replaced by $|\epsilon|$, and $\mathbb{A}_n^s$, $\mathbb{B}_n^s$ replaced by the corresponding A_n^s, B_n^s from (B.3), the denominator of (B.7) defines the numerical equivalent of (A.17) used to normalize the eigenfunctions.

APPENDIX C

Asymptotic Solutions as $\varepsilon \to -\infty$

Our numerical computations have suggested a possible asymptotic behavior $\lambda \sim (-\varepsilon)^{-1}$ for large negative ε. In order to explore this possibility we rewrite (3.2)-(3.4) using the colatitude θ as independent variable:

$$-\lambda L(P) + \cos\theta\, L(Q) - \sin^3\theta \frac{dQ}{d\theta} + \sin^2\theta\, sP = 0 \qquad (C.1)$$

$$\cos\theta\, L(P) - \sin^3\theta \frac{dP}{d\theta} - L(R) + \alpha\left[\sin^2\theta\, sQ\right] = \alpha'\left[\lambda L(Q)\right] \qquad (C.2)$$

$$L(Q) + \lambda(-\epsilon)\sin^2\theta\, R = 0 \qquad (C.3)$$

where $L(\,) = (\sin^2\theta \frac{d^2}{d\theta^2} + \sin\theta\cos\theta \frac{d}{d\theta} - s^2)(\,)$. The solutions are expected to be concentrated around the poles. Let $\omega = (-\varepsilon)^{1/4}\theta$ be the stretched coordinate (or $\omega = (-\varepsilon)^{1/4}(\pi-\theta)$ for the South pole), $\omega = 0(1)$.

The operator $L(\,)$ then becomes

$$L(\,) = L_0(\,) - (-\epsilon)^{-\frac{1}{2}}\tfrac{1}{3}\omega^2 L_1(\,) + (-\epsilon)^{-1}\tfrac{2}{45}\omega^4 L_2(\,) - (-\epsilon)^{-\frac{3}{2}}\tfrac{4}{315}\omega^6 L_3(\,) + \cdots \qquad (C.4)$$

where $L_0(\,) = \omega^2\frac{d^2}{d\omega^2} + \omega\frac{d}{d\omega} - s^2 = \left(\omega\frac{d}{d\omega}\right)^2 - s^2$

$$L_j(\,) = L_0(\,) + j\omega\frac{d}{d\omega} + s^2 \quad ; \; j = 1,2,3,\cdots$$

We now explore the consequences of the following expansion:

$$\begin{aligned}
\lambda &= s(-\epsilon)^{-1}\left[\lambda_0 + (-\epsilon)^{-\frac{1}{2}}\lambda_1 + (-\epsilon)^{-1}\lambda_2 + \cdots\right] \\
P &= \left[P_0 + (-\epsilon)^{-\frac{1}{2}}P_1 + (-\epsilon)^{-1}P_2 + \cdots\right] \\
Q &= (-\epsilon)^{-\frac{1}{2}}\left[Q_0 + (-\epsilon)^{-\frac{1}{2}}Q_1 + (-\epsilon)^{-1}Q_2 + \cdots\right] \\
R &= \left[R_0 + (-\epsilon)^{-\frac{1}{2}}R_1 + (-\epsilon)^{-1}R_2 + \cdots\right]
\end{aligned} \tag{C.5}$$

Ordering in increasing powers of $(-\epsilon)^{-1/2}$, we obtain:

$$\begin{aligned}
&\left\{L_0(Q_0) + s\omega^2 P_0\right\} + (-\epsilon)^{-\frac{1}{2}}\left\{-s\lambda_0 L_0(P_0) + L_0(Q_1) - \tfrac{1}{3}\omega^2 L_1(Q_0) - \right. \\
&-\tfrac{1}{2}\omega^2 L_0(Q_0) - \tfrac{1}{3}s\omega^4 P_0 + s\omega^2 P_1 - \left.\omega^3\frac{dQ_0}{d\omega}\right\} + (-\epsilon)^{-1}\left\{-\lambda_0 s L_0(P_1) + \right. \\
&+\tfrac{1}{3}s\lambda_0\omega^2 L_1(P_0) - s\lambda_1 L_0(P_0) + L_0(Q_2) - \tfrac{1}{2}\omega^2 L_0(Q_1) + \tfrac{1}{24}\omega^4 L_0(Q_0) - \\
&-\tfrac{1}{3}\omega^2 L_1(Q_1) + \tfrac{2}{45}\omega^4 L_2(Q_0) + \tfrac{1}{6}\omega^4 L_1(Q_0) + s\omega^2 P_2 - \tfrac{1}{3}s\omega^4 P_1 + \\
&+\tfrac{2}{45}s\omega^6 P_0 - \omega^3\frac{dQ_1}{d\omega} + \tfrac{1}{2}\omega^5\left.\frac{dQ_0}{d\omega}\right\} + \cdots\cdots\cdots = 0
\end{aligned} \tag{C.6}$$

$$\begin{aligned}
&\left\{L_0(P_0) - L_0(R_0)\right\} + (-\epsilon)^{-\frac{1}{2}}\left\{L_0(P_1) - \tfrac{1}{2}\omega^2 L_0(P_0) - \tfrac{1}{3}\omega^2 L_1(P_0) - \omega^3\frac{dP_0}{d\omega} - \right. \\
&-L_0(R_1) + \left.\tfrac{1}{3}\omega^2 L_1(R_0)\right\} + (-\epsilon)^{-1}\left\{L_0(P_2) - \tfrac{1}{2}\omega^2 L_0(P_1) + \tfrac{1}{24}\omega^4 L_0(P_0) + \right. \\
&+\tfrac{1}{6}\omega^4 L_1(P_0) - \tfrac{1}{3}\omega^2 L_1(P_1) + \tfrac{2}{45}\omega^4 L_2(P_0) + \omega^5\frac{dP_0}{d\omega} - \omega^3\frac{dP_1}{d\omega} - L_0(R_2) + \\
&+\tfrac{1}{3}\omega^2 L_1(R_1) + \tfrac{2}{45}\omega^4 L_2(R_0) + \alpha[sQ_0]\left.\right\} + \\
&+(-\epsilon)^{-\frac{3}{2}}\left\{-\alpha'\left[sL_0(Q_0)\right] + \cdots\right\} + \cdots\cdots = 0
\end{aligned} \tag{C.7}$$

$$\left\{ L_o(Q_o) + s\lambda_o \omega^2 R_o \right\} + (-\epsilon)^{-\frac{1}{2}} \left\{ L_o(Q_1) - \tfrac{1}{3}\omega^2 L_1(Q_o) + \right.$$

$$+ s\lambda_o \omega^2 R_1 - \tfrac{1}{3} s\lambda_o \omega^4 R_o + s\lambda_1 \omega^2 R_o \Big\} + (-\epsilon)^{-1} \Big\{ L_o(Q_2) -$$

$$- \tfrac{1}{3}\omega^2 L_1(Q_1) + \tfrac{2}{45}\omega^4 L_2(Q_o) + s\lambda_o \omega^2 R_2 - \tfrac{1}{3} s\lambda_o \omega^4 R_1 +$$

$$+ \left(\tfrac{2}{45} s\lambda_o \omega^6 R_o + s\lambda_1 \omega^2 R_1 - \tfrac{1}{3} s\lambda_1 \omega^4 R_o + s\lambda_2 \omega^2 R_o \right\} + \ldots = 0 \qquad \text{(C.8)}$$

Expression (C.7) shows that the α term and the α' term do not appear until the second or third order in $(-\epsilon)^{-1/2}$, respectively. Therefore, the motions characterized by the expansion (C.5) are not affected by the α term and α' term in zeroth and in first order in $(-\epsilon)^{-1/2}$.

Zeroth order solution

$$L_o(Q_o) + s\omega^2 P_o = 0 \qquad \text{(C.9)}$$

$$L_o(P_o) - L_o(R_o) = 0 \qquad \text{(C.10)}$$

$$L_o(Q_o) + s\lambda_o \omega^2 R_o = 0 \qquad \text{(C.11)}$$

(C.9) and (C.11) give

$$s\omega^2 (P_o - \lambda_o R_o) = 0$$

For $s \neq 0$ we have

$$P_o = \lambda_o R_o \qquad \text{(C.12)}$$

When the operator L_o is applied to (C.12) and the result compared to

(C.10) we obtain

$$\lambda_o = 1 \tag{C.13}$$

$$P_o = R_o \tag{C.14}$$

$$L_o(Q_o) + s\omega^2 P_o = 0 \tag{C.15}$$

The functional form of the solutions to (C.14)-(C.15) are not obtainable from the zeroth order equations alone. We may conclude then that the kind of motions which we are looking for as a result of the expansion (C.5) cannot be described by a conventional β-plane approximation around the pole, in which the Coriolis parameter would be a constant because cosine of latitude = 0.

First order terms

Now we take the first order terms in $(-\varepsilon)^{-1/2}$ from (C.6)-(C.8) and use the results (C.13)-(C.15):

$$L_o(Q_1) + s\omega^2 P_1 = s L_o(P_o) - \tfrac{1}{6} s\omega^4 P_o + \tfrac{1}{3}\omega^2 L_1(Q_o) + \omega^3 \frac{dQ_o}{d\omega} \tag{C.16}$$

$$L_o(P_1 - R_1) = \tfrac{1}{2}\omega^2 L_o(P_o) + \omega^3 \frac{dP_o}{d\omega} \tag{C.17}$$

$$L_o(Q_1) + s\omega^2 R_1 = \tfrac{1}{3}\omega^2 L_1(Q_o) - s\lambda_1 \omega^2 P_o + \tfrac{1}{3} s\omega^4 P_o \tag{C.18}$$

Let us subtract (C.18) from (C.16):

$$s\omega^2 (P_1 - R_1) = s L_o(P_o) - \tfrac{1}{2} s\omega^4 P_o + s\lambda_1 \omega^2 P_o + \omega^3 \frac{dQ_o}{d\omega} \tag{C.19}$$

This equation is now divided out by $s\omega^2$ and the operator L_o is applied

$$L_o(P_1 - R_1) = L_o\left\{\frac{1}{\omega^2} L_o(P_o) - \frac{1}{2}\omega^2 P_o + \lambda_1 P_o\right\} + \frac{1}{s} L_o\left(\omega \frac{dQ_o}{d\omega}\right) \qquad (C.20)$$

We compare (C.20) to (C.17) and make use of the following relations:

$$\omega^2 L_o(P_o) = L_o(\omega^2 P_o) - 4\omega^2\left(\omega \frac{dP_o}{d\omega} + P_o\right)$$

$$L_o\left(\omega \frac{dQ_o}{d\omega}\right) = \omega \frac{d}{d\omega}\left(L_o(Q_o)\right) = -s\omega \frac{d}{d\omega}(\omega^2 P_o)$$

to obtain:

$$L_o\left\{\frac{1}{\omega^2} L_o(P_o) - \omega^2 P_o + \lambda_1 P_o\right\} = 0 \qquad (C.21)$$

The integration of (C.21) gives

$$\left\{\frac{d^2}{d\omega^2} + \frac{1}{\omega}\frac{d}{d\omega} - \frac{s^2}{\omega^2} - \omega^2 + \lambda_1\right\} P_o = A\omega^s + B\omega^{-s} \qquad (C.22)$$

A and B are integration constants, which we take as zero for finiteness as $\omega \to 0$ and $\omega \to \infty$.

Equation (C.22) may be written as

$$\left\{\frac{d^2}{d\omega^2} - \frac{1}{\omega}\frac{d}{d\omega} - \frac{(s^2-1)}{\omega^2} - \omega^2 + \lambda_1\right\}(\omega P_o) = 0$$

By letting $x = \omega^2$ we obtain

$$\left\{ \frac{d^2}{dx^2} - \frac{1}{4} + \frac{\left(\frac{\lambda_1}{4}\right)}{x} + \frac{\left(\frac{1-s^2}{4}\right)}{x^2} \right\} \left(x^{\frac{1}{2}} P_o \right) = 0 \qquad \text{(C.23)}$$

This equation is recognized as Whittaker's equation, which also appears in the study of Schrodinger's equation for the hydrogen-like atom (Jeffreys & Jeffreys, p.616).

The only solution finite as $\omega \to 0$ and $\omega \to \infty$ is

$$x^{1/2} P_o \propto e^{-\frac{1}{2}x} x^{m+\frac{1}{2}} L_\nu^{(2m)}(x)$$

where $L_\nu^{(2m)}(X)$ is the generalized Laguerre polynomial

$$\nu = k - m - \frac{1}{2} \quad ; \quad \nu = 0,1,2,3,\ldots$$

$$k = \frac{\lambda 1}{4}$$

$$4m^2 - 1 = (s^2 - 1) \quad \therefore \quad 2m = |s|$$

The final solution, in terms of the variable ω is

$$P_o = R_o \propto e^{-\frac{1}{2}\omega^2} \omega^s L_\nu^{(s)}(\omega^2) \qquad \text{(C.24)}$$

$$L_o(Q_o) = s\,\omega^2 P_o \qquad \text{(C.25)}$$

And for the frequency

$$\lambda = \frac{s}{(-\epsilon)} \left\{ 1 + \frac{2(s+2\nu+1)}{(-\epsilon)^{1/2}} + \cdots \right\} \quad ; \; s > 0 \qquad \text{(C.26)}$$

These solutions correspond to very slow eastward propagating waves with energy concentrated around the poles. The non-divergent and geostrophic character of these motions is expressed by (C.24)-(C.25) with the streamfunction equal to the geopotential in zeroth order and small velocity potential.

The same asymptotic formula (C.26) would be obtained for an expansion about the south pole. Each value of ν in (C.26) then corresponds to <u>two</u> solutions, each with eigenfunctions concentrated at one of the poles. Symmetric and antisymmetric modes in this context are obtained from the sum and difference of these eigenfunctions, but (C.26), because it assigns the same frequency to each of these two combinations, does not show the separation in frequency between symmetric and antisymmetric modes appearing on figure 8.

APPENDIX D

Asymptotic Solutions as $\varepsilon \to +\infty$

In this appendix we study the asymptotic behavior of the "equatorial Rossby waves" as $\varepsilon \to \infty$. The solutions are expected to be concentrated about the equator. We then take the stretched coordinate $\eta = \varepsilon^{1/4}\mu$ and make the expansion (4.16). When put into (3.2)-(3.4), this leads to:

$$\left\{-\lambda_0 \frac{d^2P_0}{d\eta^2} + \eta \frac{d^2Q_0}{d\eta^2} + \frac{dQ_0}{d\eta} + sP_0\right\} + (\epsilon)^{-\frac{1}{2}}\left\{-\lambda_0 \frac{d^2P_1}{d\eta^2} - \lambda_1 \frac{d^2P_0}{d\eta^2} + \right.$$
$$+ \lambda_0\left(\frac{d}{d\eta}\eta^2\frac{d}{d\eta} + s^2\right)P_0 - \eta\left(\frac{d}{d\eta}\eta^2\frac{d}{d\eta} + s^2\right)Q_0 + \eta\frac{d^2Q_1}{d\eta^2} + \frac{dQ_1}{d\eta} -$$
$$\left. - \eta^2\frac{dQ_0}{d\eta} + sP_1\right\} + \cdots\cdots\cdots = 0 \qquad \text{(D.1)}$$

$$\left\{\eta\frac{d^2P_0}{d\eta^2} + \frac{dP_0}{d\eta} - \frac{d^2R_0}{d\eta^2}\right\} + (\epsilon)^{-\frac{1}{2}}\left\{\eta\frac{d^2P_1}{d\eta^2} - \eta\left(\frac{d}{d\eta}\eta^2\frac{d}{d\eta} + s^2\right)P_0 + \right.$$
$$+ \frac{dP_1}{d\eta} - \eta^2\frac{dP_0}{d\eta} - \frac{d^2R_1}{d\eta^2} + \left(\frac{d}{d\eta}\eta^2\frac{d}{d\eta} + s^2\right)R_0 + \alpha[sQ_0] -$$
$$\left. - \alpha'\left[\lambda_0\frac{d^2}{d\eta^2}Q_0\right]\right\} + \cdots\cdots\cdots = 0 \qquad \text{(D.2)}$$

$$\left\{\frac{d^2Q_0}{d\eta^2} - \lambda_0 R_0\right\} + (\epsilon)^{-\frac{1}{2}}\left\{\frac{d^2Q_1}{d\eta^2} - \left(\frac{d}{d\eta}\eta^2\frac{d}{d\eta} + s^2\right)Q_0 - \lambda_0 R_1 - \right.$$
$$\left. - \lambda_1 R_0\right\} + \cdots\cdots\cdots = 0 \qquad \text{(D.3)}$$

Zeroth order solution

Let us take the zeroth order terms from (D.1)-(D.3)

$$-\lambda_0\frac{d^2P_0}{d\eta^2} + \frac{d}{d\eta}\eta\frac{dQ_0}{d\eta} + sP_0 = 0 \qquad \text{(D.4)}$$

$$\frac{d}{d\eta}\eta\frac{dP_o}{d\eta} - \frac{d^2R_o}{d\eta^2} = 0 \qquad \text{(D.5)}$$

$$\frac{d^2Q_o}{d\eta^2} - \lambda_o R_o = 0 \qquad \text{(D.6)}$$

Equation (D.5) is integrated to give

$$\eta\frac{dP_o}{d\eta} - \frac{dR_o}{d\eta} = A \qquad \text{(A is an integration constant)}$$

This equation multiplied by s and added to (D.4) gives

$$\frac{d}{d\eta}\left\{-\lambda_o\frac{dP_o}{d\eta}\right\} + \frac{d}{d\eta}\left\{\eta\left(\frac{dQ_o}{d\eta} + sP_o\right)\right\} - \frac{d}{d\eta}\left\{sR_o\right\} = As$$

After integrating this equation, we rewrite (D.4)-(D.6) as follows:

$$\lambda_o\left(-\frac{dP_o}{d\eta}\right) + \eta\left(\frac{dQ_o}{d\eta} + sP_o\right) - sR_o = As\eta + C \qquad \text{(D.7)}$$

$$-\eta\left(-\frac{dP_o}{d\eta}\right) - \frac{dR_o}{d\eta} = A \qquad \text{(D.8)}$$

$$\frac{d}{d\eta}\left(\frac{dQ_o}{d\eta} + sP_o\right) + s\left(-\frac{dP_o}{d\eta}\right) - \lambda_o R_o = 0 \qquad \text{(D.9)}$$

where C is another integration constant. Let us define:

$$U_o = -\frac{dP_o}{d\eta} \quad \text{and} \quad V_o = \frac{dQ_o}{d\eta} + sP_o$$

Equations (D.7)-(D.9) gain the new form:

$$\lambda_o U_o + \eta V_o - sR_o = sA\eta + C \tag{D.10}$$

$$-\eta U_o - \frac{dR_o}{d\eta} = A \tag{D.11}$$

$$sU_o + \frac{dV_o}{d\eta} - \lambda_o R_o = 0 \tag{D.12}$$

Further discussion is in section 4.2.5.

APPENDIX E

Asymptotic Solutions as $\epsilon \to 0$

The asymptotic behavior as $\epsilon \to 0$ can be obtained in zeroth order directly from the matrix systems (4.10) and (4.11). For higher order corrections to these solutions, the following expansion is used:

$$\begin{aligned} \lambda &= \lambda_0 + \epsilon \lambda_1 + \epsilon^2 \lambda_2 + \cdots \\ P &= P_0 + \epsilon P_1 + \epsilon^2 P_2 + \cdots \\ Q &= Q_0 + \epsilon Q_1 + \epsilon^2 Q_2 + \cdots \\ R &= R_0 + \epsilon R_1 + \epsilon^2 R_2 + \cdots \end{aligned} \tag{E.1}$$

When this expansion is put into (3.2)-(3.4) we get in zeroth order

$$-\lambda_0 \mathcal{L}(P_0) + \mu \mathcal{L}(Q_0) + (1-\mu^2)\frac{dQ_0}{d\mu} + s P_0 = 0 \tag{E.2}$$

$$\mu \mathcal{L}(P_0) + (1-\mu^2)\frac{dP_0}{d\mu} - \mathcal{L}(R_0) + \alpha[sQ_0] - \alpha'[\lambda_0 \mathcal{L}(Q_0)] = 0 \tag{E.3}$$

$$\mathcal{L}(Q_0) = 0 \tag{E.4}$$

$Q_0 = 0$ is the solution which satisfies (E.4) and the boundary conditions at the poles. This result when substituted into (E.2) and (E.3) gives

$$P_0 = P_n^{|s|}(\mu) \tag{E.5}$$

$$-\frac{s}{\lambda_0} = n(n+1) \quad ; \quad (s<0 \quad ; \quad n-|s| = 0,1,2,\cdots) \tag{E.6}$$

$$R_0 = \frac{(n+1)(n+s)}{n(2n+1)} P_{n-1}^{|s|}(\mu) + \frac{n(n-s+1)}{(n+1)(2n+1)} P_{n+1}^{|s|}(\mu) \qquad (E.7)$$

Let us now take the <u>first order</u> terms in ε:

$$\frac{s}{n(n+1)} \left[\mathcal{L} + n(n+1) \right] P_1 + \mu \mathcal{L}(Q_1) + (1-\mu^2) \frac{dQ_1}{d\mu} = \lambda_1 \mathcal{L}(P_0) \qquad (E.8)$$

$$\mu \mathcal{L}(P_1) + (1-\mu^2) \frac{dP_1}{d\mu} - \mathcal{L}(R_1) + \alpha [s Q_1] - \alpha' [\lambda_0 \mathcal{L}(Q_1)] = 0 \qquad (E.9)$$

$$\mathcal{L}(Q_1) = \lambda_0 R_0 \qquad (E.10)$$

(E.10) is solved for Q_1. When substituted into (E.8) one obtains $[\mathcal{L} + n(n+1)]\, P_1$ equal to a linear combination of P_{n-2}^s, P_n^s, and P_{n+2}^s. The coefficient of P_n^s must vanish in order to make P_1 determinate. This determines λ_1:

$$\lambda_1 = -\frac{\lambda_0}{n(n+1)} \left\{ \frac{(n+1)^2 (n-s)(n+s)}{n^2 (2n-1)(2n+1)} + \frac{n^2 (n-s+1)(n+s+1)}{(n+1)^2 (2n+1)(2n+3)} \right\} \qquad (E.11)$$

In first order in ε, the only dependence on α and α' terms appears in $R_1(\mu)$.

Combining (E.6) and (E.11) we get an approximate formula for the eigenfrequencies

$$\lambda = \frac{-s}{n(n+1) + \epsilon \left\{ \frac{(n+1)^2 (n-s)(n+s)}{n^2 (2n-1)(2n+1)} + \frac{n^2 (n-s+1)(n+s+1)}{(n+1)^2 (2n+1)(2n+3)} \right\}} \qquad \text{(E.12)}$$

This formula corresponds to Hough's (1898) formula specialized for the "waves of the second class" for small ε, and correct up to $0(\varepsilon)$. (E.12) also holds for small but negative ε. Since the α and the α' terms do not enter in (E.12), we conclude that the "second class" Rossby waves have their frequency correctly described (up to first order in ε) by using the balance equations (or the "modified" balance equations).

APPENDIX F

F.1 Numerical Solution of the Matrix Equation $\underset{\sim}{A}\dot{Y} = \underset{\sim}{B}Y$ for $\delta = 0$

The solution of the system of equations (6.23)–(6.26) is obtained through the truncated expansion (6.30), resulting in the set of algebraic equations (6.31)–(6.34), where

$$
\begin{aligned}
a_n &= \frac{(n-1)(n-s)}{n(2n-1)} \\
b_n &= \frac{(n+2)(n+s+1)}{(n+1)(2n+3)} \\
c_n &= s\Lambda\left(\frac{n-s}{2n-1}\right) \\
d_n &= s\Lambda\left(\frac{n+s+1}{2n+3}\right) \\
e_n &= -s\left(\frac{1+2\omega}{n(n+1)}\right) \\
f_n &= s\Lambda\left(1-\frac{2}{n(n+1)}\right) \\
w_n &= \frac{1+2\gamma\omega}{n(n+1)S} \\
r_n &= \frac{2\gamma\Lambda}{n(n+1)S} \\
A_n &= \gamma\Lambda(n+2)a_n \\
B_n &= \gamma\Lambda(n-1)b_n \\
C_n &= (1+2\gamma\omega)a_n \\
D_n &= (1+2\gamma\omega)b_n
\end{aligned}
\qquad \text{(F.1)}
$$

Eliminate T_n^s between (6.33) and (6.34) to get

$$w_n(a_n\dot{\Theta}_{n-1}^s + b_n\dot{\Theta}_{n+1}^s) + \Gamma_n(a_n\dot{\psi}_{n-1}^s + b_n\dot{\psi}_{n+1}^s) = -w_n(c_n\psi_{n-1}^s + d_n\psi_{n+1}^s) - X_n^s \qquad (F.2)$$

We now use (F.2) to eliminate X_{n-1}^s and X_{n+1}^s from (6.32) and (6.31) which result in the following two equations.

$$\begin{aligned} &C_n w_{n-1} a_{n-1}\dot{\Theta}_{n-2}^s + C_n\Gamma_{n-1}a_{n-1}\dot{\psi}_{n-2}^s + (1 + C_n w_{n-1} b_{n-1} + D_n w_{n+1} a_{n+1})\dot{\Theta}_n^s \\ &+ (C_n\Gamma_{n-1}b_{n-1} + D_n\Gamma_{n+1}a_{n+1})\dot{\psi}_n^s + D_n w_{n+1} b_{n+1}\dot{\Theta}_{n+2}^s + D_n\Gamma_{n+1}b_{n+1}\dot{\psi}_{n+2}^s = \\ &= -w_{n-1}c_{n-1}\psi_{n-2}^s + e_n\Theta_n^s + (f_n - C_n w_{n-1} d_{n-1} - D_n w_{n+1} c_{n+1})\psi_n^s - \\ &- D_n w_{n+1} d_{n+1}\psi_{n+2}^s \end{aligned} \qquad (F.3)$$

$$\begin{aligned} &A_n w_{n-1} a_{n-1}\dot{\Theta}_{n-2}^s + A_n\Gamma_{n-1}a_{n-1}\dot{\psi}_{n-2}^s + (A_n w_{n-1} b_{n-1} - B_n w_{n+1} a_{n+1})\dot{\Theta}_n^s \\ &+ (1 + A_n\Gamma_{n-1}b_{n-1} - B_n\Gamma_{n+1}a_{n+1})\dot{\psi}_n^s - B_n w_{n+1} b_{n+1}\dot{\Theta}_{n+2}^s - B_n\Gamma_{n+1}b_{n+1}\dot{\psi}_{n+2}^s = \\ &- w_{n-1}c_{n-1}\psi_{n-2}^s + f_n\Theta_n^s + (e_n - A_n w_{n-1} d_{n-1} + B_n w_{n+1} c_{n+1})\psi_n^s - \\ &+ B_n w_{n+1} d_{n+1}\psi_{n+2}^s \end{aligned} \qquad (F.4)$$

The system of equations (F.3)-(F.4) separates out into two symmetries. One for n=s,s+2,s+4,...,(N-1) and the other for n=s+1,s+3,...,N.

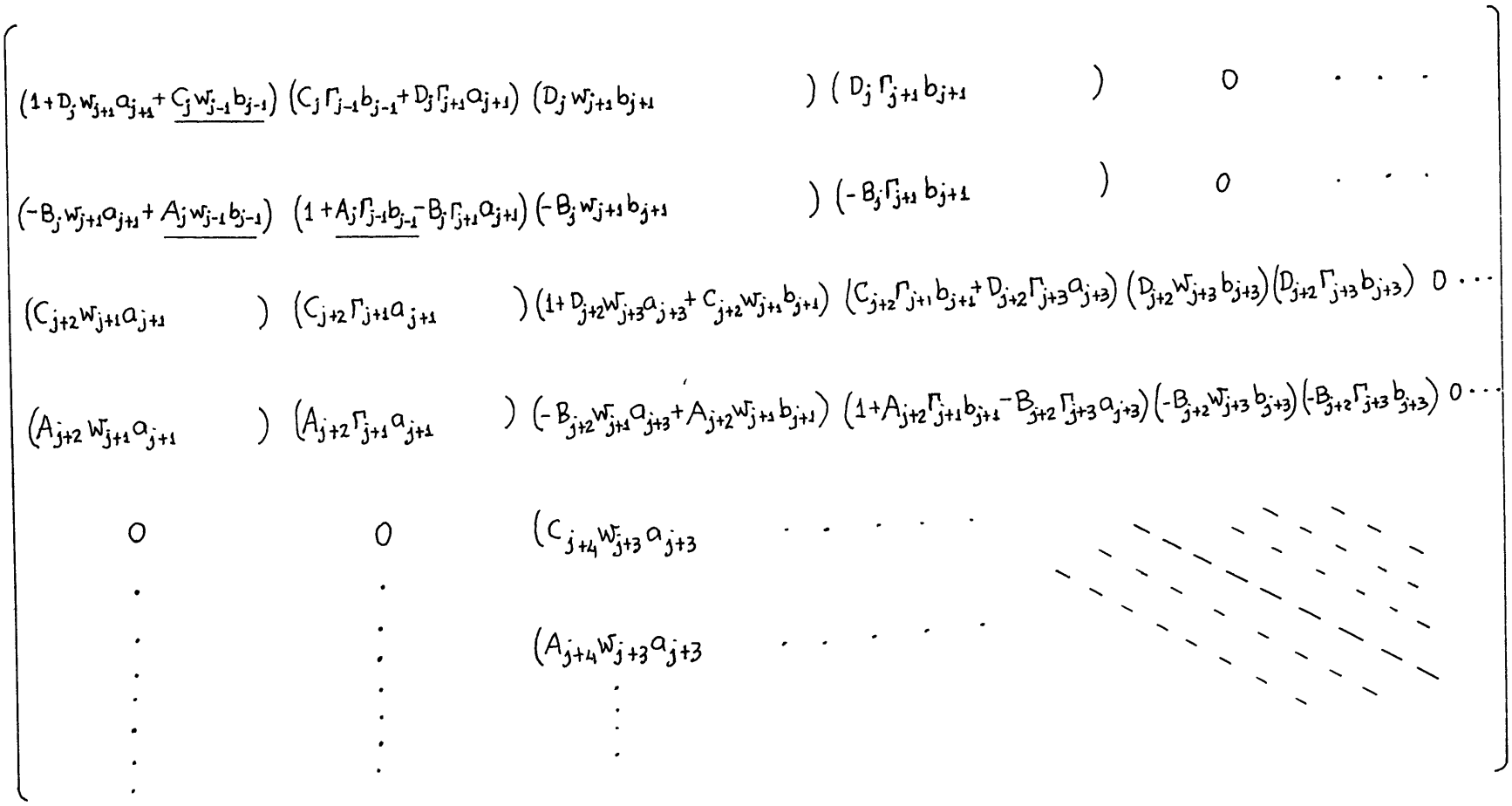
Let us write (F.3)-(F.4) in matrix form

$$\underset{\sim}{A}\,\dot{\underset{\sim}{Y}} = \underset{\sim}{B}\,\underset{\sim}{Y} \qquad (F.5)$$

where the matrices $\underset{\sim}{Y}$, $\underset{\sim}{A}$, and $\underset{\sim}{B}$ are

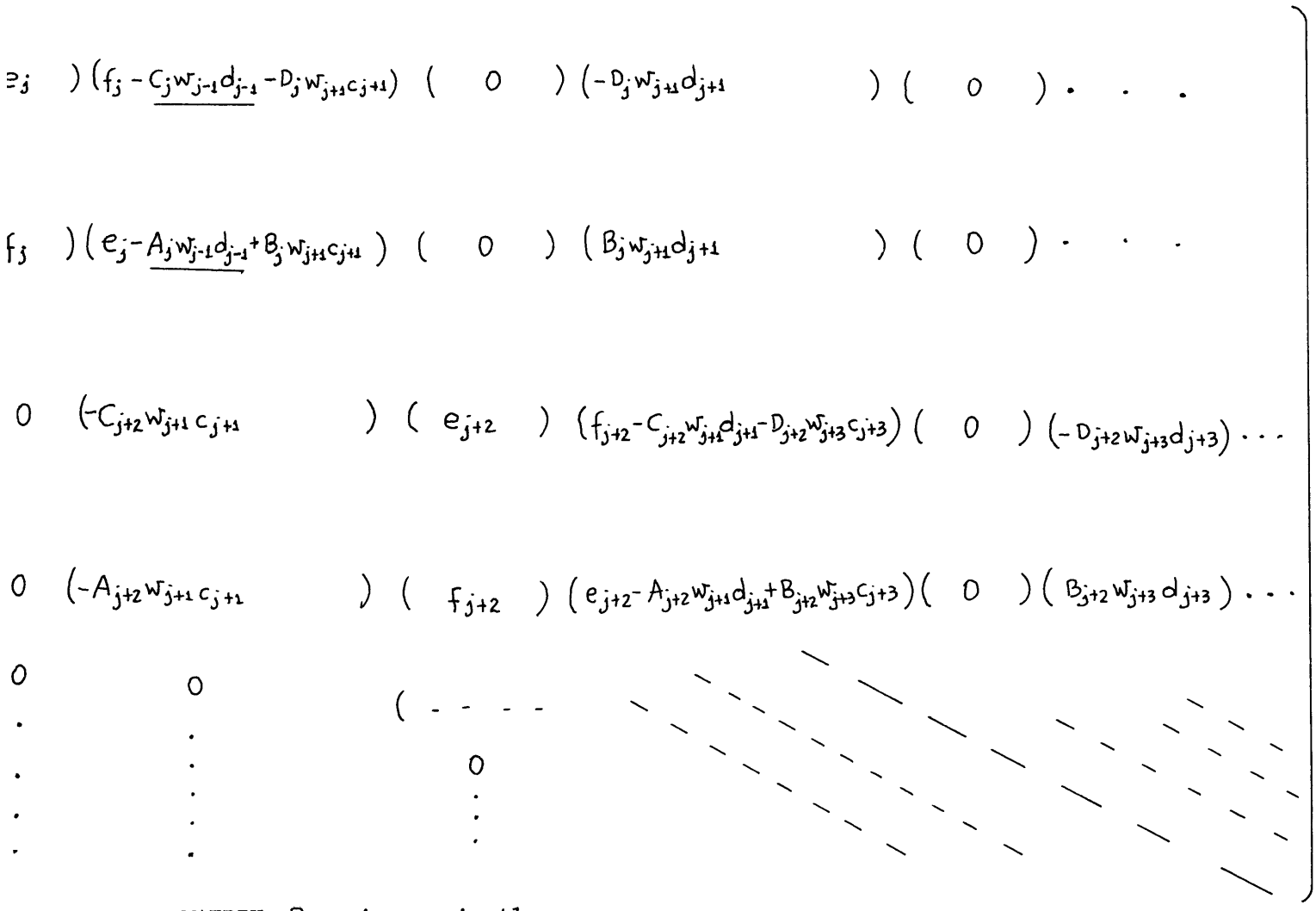
$$\underset{\sim}{Y} = \begin{pmatrix} \Theta_j^s \\ \Psi_j^s \\ \Theta_{j+2}^s \\ \Psi_{j+2}^s \\ \vdots \\ \Theta_R^s \\ \Psi_R^s \\ \vdots \end{pmatrix}$$

$j=s \quad or \quad j=s+1$



MATRIX $\underset{\sim}{A}$ j=s or j=s+1

Banded matrix with bandwidth 7. The underlined terms are equal to zero when j=s.



MATRIX $\underset{\sim}{B}$ j=s or j=s+1

Banded matrix with bandwidth 6. The underlined terms are equal to zero when j=s.

Equation (F.5) is multiplied by the inverse of matrix $\underset{\sim}{A}$ to give

$$\dot{\underset{\sim}{Y}} = \underset{\sim}{C}\,\underset{\sim}{Y} \quad ; \quad \underset{\sim}{C} = \underset{\sim}{A}^{-1}\underset{\sim}{B}$$

when we put $\underset{\sim}{Y}(t') = e^{-i\sigma t'}\underset{\sim}{\mathcal{Y}}$ in (F.6) we get

$$\left(\underset{\sim}{C} - \sigma \underset{\sim}{I}\right)\underset{\sim}{\mathcal{Y}} = 0$$

which is an ordinary eigenvalue-eigenfunction problem for σ if ω, Λ, s, and S are given. $\underset{\sim}{I}$ is the unity matrix and σ is in general complex: $\sigma = \lambda + i\nu$, where ν is the exponential growth rate of the solution.

In order to solve (F.7) it is necessary to truncate the matrix $\underset{\sim}{C}$, the size of which is changed in order to obtain a good accuracy of the eigenvalue being sought. For most of the calculations we have used 30x30 elements of $\underset{\sim}{C}$. The convergence of the desired eigenvalues was verified by comparison with those of 36x36 and 42x42 matrices with agreement of 10^{-9}. The convergence of the most unstable root near neutral stability is slower because the solutions oscillate more between $\mu = 0$ and $\mu = 1$ than for the unstable modes far from neutral stability. For these cases the accuracy was better than 10^{-6}.

Once the eigenvectors containing Θ_n^s and Ψ_n^s are obtained, we may compute the following variables.

T_n^s are computed using (6.34) and X_n^s are then obtained from (6.33). Momentum and heat transports are computed after we know the velocities:

$$U1_n^s = -\frac{1}{a(1-\mu^2)^{1/2}}\left[s X_n^s - \frac{(n-1)(n-s)}{2n-1}\left(\Psi_{n-1}^s + \Theta_{n-1}^s\right) + \frac{(n+2)(n+s+1)}{2n+3}\left(\Psi_{n+1}^s + \Theta_{n+1}^s\right)\right]$$

$$U3_n^s = -\frac{1}{a(1-\mu^2)^{1/2}}\left[-s X_n^s - \frac{(n-1)(n-s)}{2n-1}\left(\Psi_{n-1}^s - \Theta_{n-1}^s\right) + \frac{(n+2)(n+s+1)}{2n+3}\left(\Psi_{n+1}^s - \Theta_{n+1}^s\right)\right]$$

$$V1_n^s = \frac{i}{a(1-\mu^2)^{1/2}}\left[s\left(\Psi_n^s + \Theta_n^s\right) - \frac{(n-1)(n-s)}{2n-1} X_{n-1}^s + \frac{(n+2)(n+s+1)}{2n+3} X_{n+1}^s \right]$$

$$V3_n^s = \frac{i}{a(1-\mu^2)^{1/2}}\left[s\left(\Psi_n^s - \Theta_n^s\right) + \frac{(n-1)(n-s)}{2n-1} X_{n-1}^s - \frac{(n+2)(n+s+1)}{2n+3} X_{n+1}^s \right]$$

$$V2_n^s = \frac{i s}{a(1-\mu^2)^{1/2}} \Psi_n^s$$

$$\tilde{\omega}2_n^s = i \frac{\Delta p\, n(n+1)}{a^2} X_n^s$$

(F.8)

The longitudinally average transports are computed using:

$$\overline{u_1' v_1'} = \frac{1}{2} Re\left(\overline{U1'\, V1'^*}\right)$$

$$\overline{u_3' v_3'} = \frac{1}{2} Re\left(\overline{U3'\, V3'^*}\right)$$

$$\overline{v_2' T_2'} = \frac{1}{2} Re\left(\overline{V2'\, T2'^*}\right)$$

$$\overline{\omega_2' T_2'} = \frac{1}{2} Re\left(\overline{\tilde{\omega}2'\, T2'^*}\right)$$

(F.9)

where the asterisks mean complex conjugate.

In figures 26.a and 27.a we present the latitudinal dependence of the amplitude and phase of the geopotential functions ϕ_1' and ϕ_3', and in figures 26.b and 27.b we present the respective

momentum ($\overline{u_1' v_1'}^*(1-\mu^2)$ and $\overline{u_3' v_3'}^*(1-\mu^2)$) and heat ($\overline{v_2' T_2'}^*\sqrt{1-\mu^2}$ and $\overline{\omega_2' T_2'}^*$) transports.

F.2 Energetics of the Model with $\delta = 0$

Let us multiply (6.23)-(6.25) with $\delta = 0$ by Ψ, Θ, and $\frac{2\tau}{S}$, respectively. We then add the resulting first two equations and apply the operators

$$\overline{(\ )} \equiv \frac{1}{2\pi}\int_0^{2\pi}(\ )\,d\varphi \quad \text{and} \quad \langle(\ )\rangle \equiv \frac{1}{2}\int_{-1}^{+1}(\ )\,d\mu$$

after using equation (6.26) multiplied by χ to obtain

$$\frac{\partial}{\partial t'}\left\langle \overline{\frac{(D\Psi)^2+(D\Theta)^2}{2}} \right\rangle = -2\gamma\Lambda\left\langle \overline{\mu D\chi\cdot D\Psi}\right\rangle - (1+2\gamma\omega)\left\langle \overline{\mu D\chi\cdot D\Theta}\right\rangle + \\ + \gamma\Lambda\left\langle (1-\mu^2)\,\overline{\frac{\partial\Psi}{\partial\mu}\,\mathcal{L}\chi}\right\rangle \qquad \text{(F.10)}$$

$$\frac{\partial}{\partial t'}\left\langle \overline{\frac{1}{2S}\tau^2}\right\rangle = 2\gamma\Lambda\left\langle \mu\,\overline{D\chi\cdot D\Psi}\right\rangle + (1+2\gamma\omega)\left\langle \mu\,\overline{D\chi\cdot D\Theta}\right\rangle + \\ + (1+2\gamma\omega)\frac{\Lambda}{S}\left\langle \mu\,\overline{\frac{\partial\Psi}{\partial\varphi}\tau}\right\rangle \qquad \text{(F.11)}$$

By adding (F.10) and (F.11) we get

$$\frac{\partial}{\partial t'}\langle\overline{E}\rangle = (1+2\gamma\omega)\frac{\Lambda}{S}\left\langle \mu\,\overline{\frac{\partial\Psi}{\partial\varphi}\tau}\right\rangle + \gamma\Lambda\left\langle (1-\mu^2)\,\overline{\frac{\partial\Psi}{\partial\mu}\,\mathcal{L}\chi}\right\rangle \qquad \text{(F.12)}$$

where $2\langle\overline{E}\rangle = \left\langle \overline{(D\Psi)^2+(D\Theta)^2+\frac{1}{S}\tau^2}\right\rangle$ and $D \equiv \alpha\nabla\cdot$

The total energy $\langle\overline{E}\rangle$ is the sum of the rotational kinetic plus available potential energy. The two terms on the right hand side of (F.12) can be identified and written as

$$\frac{\partial}{\partial t}\langle\overline{E}\rangle = -\frac{\Delta p}{8\Omega^2 S}\left\langle \left|\left(\nabla\frac{\partial\bar{\Phi}}{\partial p}\right)_2\right| \overline{v_2'\left(\frac{\phi_1'-\phi_3'}{4\Omega}\right)}\right\rangle + \gamma\frac{\alpha^2}{4\Omega}\left\langle\left(\frac{\partial\bar{U}}{\partial p}\right)_2\overline{u_2'\tilde{\omega}_2'}\right\rangle \quad \text{(F.13)}$$

The unstable modes have $\frac{\partial}{\partial t}\langle\overline{E}\rangle > 0$. For $\gamma = 0$, the change in $\langle\overline{E}\rangle$ with time depends on the integral with respect to μ of the horizontal heat transport by the baroclinic eddies weighted by the horizontal basic temperature gradient. For $\gamma = 1$ there is an additional vertical Reynolds stress term acting upon the vertical shear of the zonal basic flow that contributes to the increase (or decrease) of the perturbation total energy.

We can finally note that if $\Lambda = 0$ (i.e., no vertical shear) $\frac{\partial}{\partial t}\langle\overline{E}\rangle = 0$. [This means that the basic zonal wind profile $\overline{U} \propto \alpha(p)\cos(\text{lat})$ is stable with respect to barotropic disturbances.]

APPENDIX G

G.1 Numerical Solution of the Matrix Equation $\underset{\sim}{A}\dot{\underset{\sim}{Y}} = \underset{\sim}{B}\underset{\sim}{Y}$ for $\gamma = 0$

The coefficients appearing in equations (6.37)=(6.40) are:

$$a_n = s\left[-\frac{1+2\omega(1-\delta)}{n(n+1)} + \delta\omega\left(1-\frac{12}{n(n+1)}\right)\left(\frac{(n-s+1)(n+s+1)}{(2n+1)(2n+3)} + \frac{(n-s)(n+s)}{(2n-1)(2n+1)}\right)\right]$$

$$b_n = \delta\omega s\left(\frac{(n-2)(n-1)-12}{n(n+1)}\right)\left(\frac{(n-s-1)(n-s)}{(2n-3)(2n-1)}\right)$$

$$c_n = \delta\omega s\left(\frac{(n+2)(n+3)-12}{n(n+1)}\right)\left(\frac{(n+s+1)(n+s+2)}{(2n+3)(2n+5)}\right)$$

$$d_n = \Lambda s\left[1-\frac{2(1-\delta)}{n(n+1)} + \delta\left(1-\frac{12}{n(n+1)}\right)\left(\frac{(n-s+1)(n+s+1)}{(2n+1)(2n+3)} + \frac{(n-s)(n+s)}{(2n-1)(2n+1)}\right)\right]$$

$$e_n = \frac{\Lambda}{\omega} b_n$$

$$f_n = \frac{\Lambda}{\omega} c_n$$

$$g_n = \frac{(n-1)(n-s)}{n(2n-1)}$$

$$h_n = \frac{(n+2)(n+s+1)}{(n+1)(2n+3)}$$

$$i_n = \delta\omega s\left(\frac{(n-s+1)(n+s+1)}{(2n+1)(2n+3)} + \frac{(n-s)(n+s)}{(2n-1)(2n+1)}\right) \qquad (G.1)$$

$$j_n = \delta\omega s\left(\frac{(n-s-1)(n-s)}{(2n-3)(2n-1)}\right)$$

$$k_n = \delta\omega s\left(\frac{(n+s+1)(n+s+2)}{(2n+3)(2n+5)}\right)$$

$$\ell_n = -\delta\Lambda s\left(\frac{(n-s-2)(n-s-1)(n-s)}{(2n-5)(2n-3)(2n-1)}\right)$$

$$p_n = -\Lambda s\left[\frac{(n-s)}{(2n-1)} + \delta\left(\frac{(n-s)(n-s+1)(n+s+1)}{(2n-1)(2n+1)(2n+3)} + \frac{(n-s)^2(n+s)}{(2n-1)^2(2n+1)} + \frac{(n-s-1)(n-s)(n+s-1)}{(2n-3)(2n-1)^2}\right)\right]$$

$$q_n = -\Lambda s\left[\frac{(n+s+1)}{(2n+3)} + \delta\left(\frac{(n-s+2)(n+s+1)(n+s+2)}{(2n+3)^2(2n+5)} + \frac{(n-s+1)(n+s+1)^2}{(2n+1)(2n+3)^2} + \frac{(n-s)(n+s)(n+s+1)}{(2n-1)(2n+1)(2n+3)}\right)\right]$$

$$r_n = -\delta\Lambda s\left(\frac{(n+s+1)(n+s+2)(n+s+3)}{(2n+3)(2n+5)(2n+7)}\right)$$

$$s_n = -S\, n(n+1)$$

When T_n^s is eliminated between (6.39) and (6.40), we get:

$$g_n\dot{\Theta}^s_{n-1}+h_n\dot{\Theta}^s_{n+1} = j_n g_{n-2}\Theta^s_{n-3} + (j_n h_{n-2}+i_n g_n)\Theta^s_{n-1}+(k_n g_{n+2}+i_n h_n)\Theta^s_{n+1}$$
$$+ k_n h_{n+2}\Theta^s_{n+3} + l_n\psi^s_{n-3} + p_n\psi^s_{n-1} + q_n\psi^s_{n+1} + r_n\psi^s_{n+3} + s_n X^s_n \qquad (G.2)$$

This equation is used to substitute for X^s_{n-1} and X^s_{n+1} in (6.38) to give

$$-(t_n g_{n-1})\dot{\Theta}^s_{n-2} + (1-t_n h_{n-1}-u_n g_{n+1})\dot{\Theta}^s_n - (u_n h_{n+1})\dot{\Theta}^s_{n+2} = -(t_n j_{n+1} g_{n-3})\Theta^s_{n-4} +$$
$$+[b_n - t_n(j_{n-1}h_{n-3}+i_{n-1}g_{n-1}) - u_n(j_{n+1}g_{n-1})]\Theta^s_{n-2} + [a_n - t_n(k_{n-1}g_{n+1}+h_{n-1}i_{n-1}) -$$
$$-u_n(j_{n+1}h_{n-1}+i_{n+1}g_{n+1})]\Theta^s_n + [c_n - t_n(k_{n-1}h_{n+1}) - u_n(k_{n+1}g_{n+3}+i_{n+1}h_{n+1})]\Theta^s_{n+2} - \qquad (G.3)$$
$$-(u_n k_{n+1}h_{n+3})\Theta^s_{n+4} - (t_n l_{n-1})\psi^s_{n-4} + (e_n - t_n p_{n-1} - u_n l_{n+1})\psi^s_{n-2} +$$
$$+[d_n - t_n q_{n-1} - u_n p_{n+1}]\psi^s_n + [f_n - t_n r_{n-1} - u_n q_{n+1}]\psi^s_{n+2} - (u_n r_{n+1})\psi^s_{n+4}$$

where $$t_n = \frac{g_n}{s_{n-1}} = -\frac{n-s}{s\,n^2(2n-1)} \quad ; \ (t_s = 0 \ \text{for all } s)$$

$$u_n = \frac{h_n}{s_{n+1}} = -\frac{n+s+1}{s(n+1)^2(2n+3)}$$

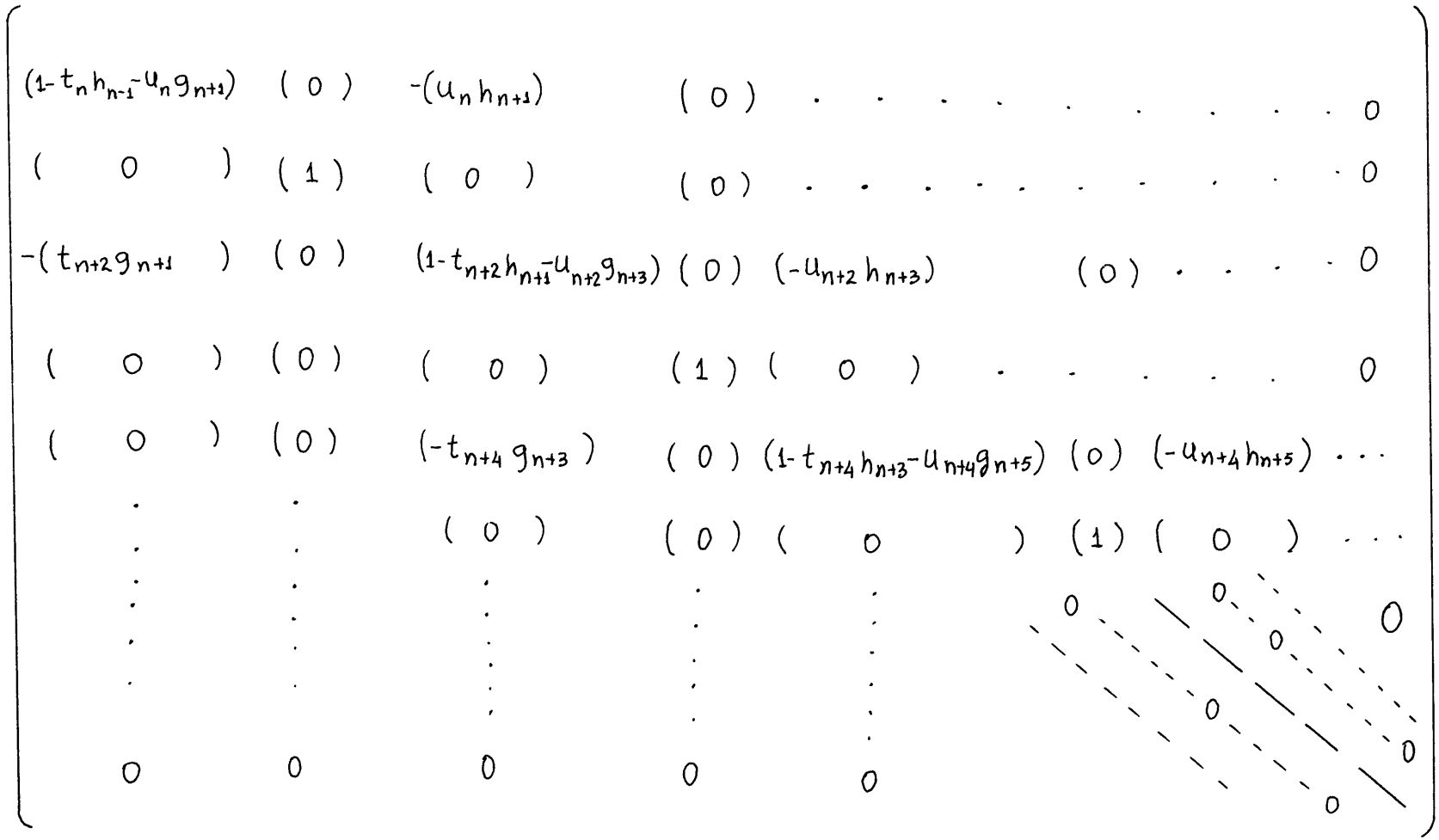
Equations (G.3) and (6.37) can be written in matrix form as follows

$$\underset{\sim}{A}\,\dot{\underset{\sim}{Y}} = \underset{\sim}{B}\,\underset{\sim}{Y} \qquad (G.4)$$

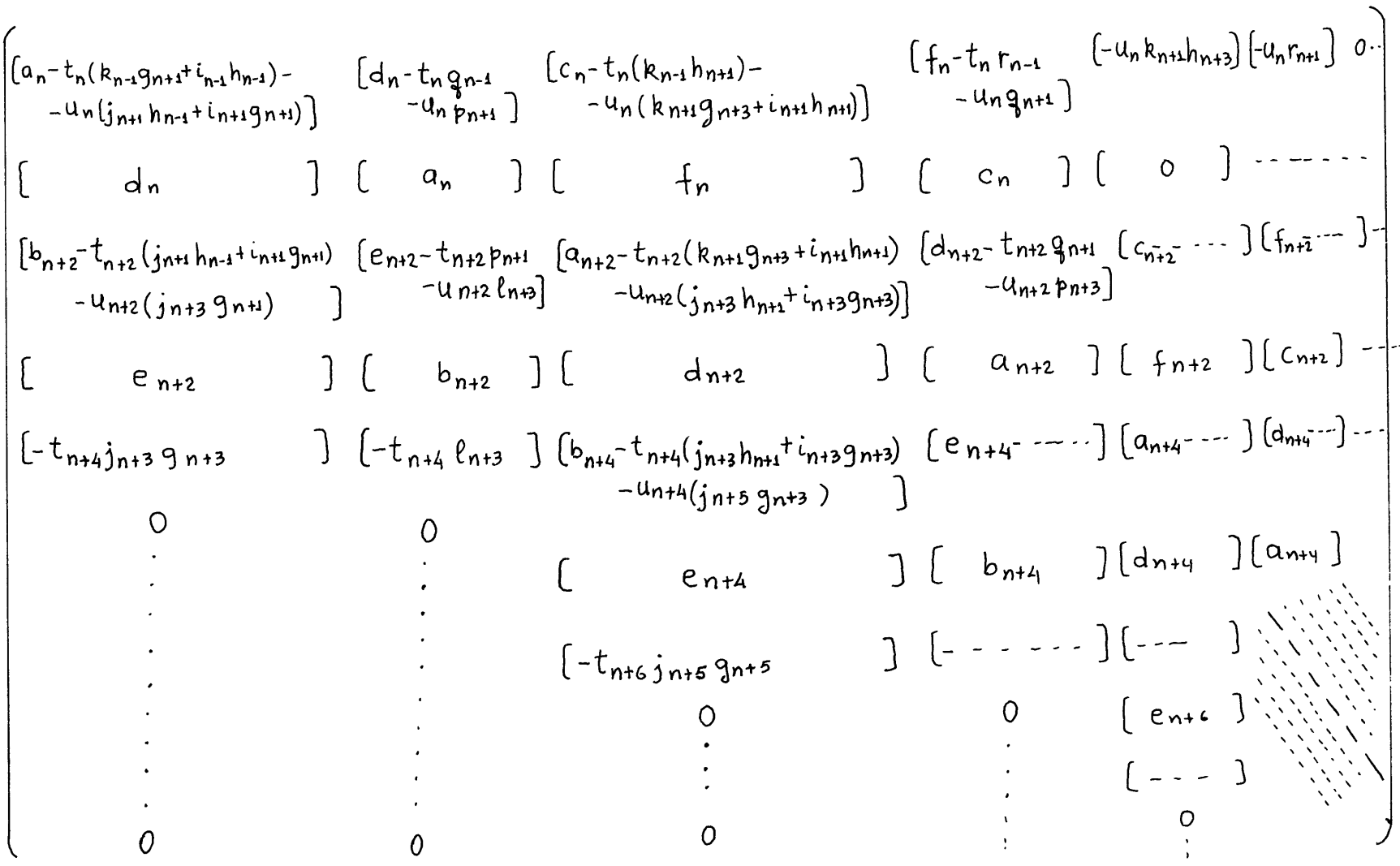
To solve (G.4), we follow the same procedure described in Appendix F (from equation (F.6) up to (F.9)). The convergence of the most unstable root was obtained by comparing its value for matrices of sizes 30x30, 36x36, and 42x42 (as mentioned in Appendix F.1). For the solutions far from neutral stability we have obtained agreement of 10^{-6}, while for the solutions near neutral stability the accuracy was better than 10^{-2}.

The matrices $\underset{\sim}{A}$ and $\underset{\sim}{B}$ appearing in (G.4) are now:

(see following two pages)



MATRIX $\underset{\sim}{A}$ (n=s or n+s+1)



MATRIX $\underset{\sim}{B}$ (n=s or n=s+1) Banded matrix with bandwidth 10.

G.2 Energetics of the Model with $\gamma = 0$

An energy equation for our model with $\gamma = 0$ is obtained in the same way as that derived in Appendix F.2. Let us multiply (6.23)-(6.26) by Ψ, Θ, $\frac{2\tau}{S}$, χ. After using the operators $\overline{(\ )} \equiv \frac{1}{2\pi}\int_0^{2\pi}(\ )d\varphi$ and $\langle(\ )\rangle \equiv \frac{1}{2}\int_{-1}^{+1}(\ )d\mu$, we combine the equations to obtain

$$\frac{\partial}{\partial t'}\left\langle\overline{\frac{(D\Psi)^2+(D\Theta)^2}{2}+\frac{1}{2S}\tau^2}\right\rangle = 2\omega\delta\left\langle\mu(1-\mu^2)\overline{\left(\frac{\partial\Psi}{\partial\varphi}\frac{\partial\Psi}{\partial\mu}+\frac{\partial\Theta}{\partial\varphi}\frac{\partial\Theta}{\partial\mu}\right)}\right\rangle + \tag{G.5}$$

$$+2\Lambda\delta\left\langle\mu(1-\mu^2)\overline{\left(\frac{\partial\Theta}{\partial\varphi}\frac{\partial\Psi}{\partial\mu}+\frac{\partial\Psi}{\partial\varphi}\frac{\partial\Theta}{\partial\mu}\right)}\right\rangle + \frac{\Lambda}{S}\left\langle\mu(1+\delta\mu^2)\overline{\left(\tau\frac{\partial\Psi}{\partial\varphi}\right)}\right\rangle$$

This equation with $\delta = 0$ is the same as (F.12) with $\gamma = 0$.

There is now a possibility for barotropic instability as well as for baroclinic instability. In order to derive a criterion for barotropic instability, we take (6.23) with $\gamma = 0$ and $\Lambda = 0$ (i.e., no vertical shear).

$$\frac{\partial}{\partial t'}\mathcal{L}\Psi = -\omega(1+\delta\mu^2)\frac{\partial}{\partial\varphi}\mathcal{L}\Psi - \left[1+2\omega(1-\delta+6\delta\mu^2)\right]\frac{\partial\Psi}{\partial\varphi} \tag{G.6}$$

When solutions of the form $\Psi(\varphi,\mu,t') = (R(\mu) + iI(\mu))\, e^{i(s\varphi-\sigma t')}$ is sought, (G.6) gives

$$\left[\sigma - s\omega(1+\delta\mu^2)\right]\frac{d}{d\mu}(1-\mu^2)\frac{d}{d\mu}(R+iI) - \left\{s^2\left(\frac{\sigma - s\omega(1+\delta\mu^2)}{1-\mu^2}\right) + \right.$$

$$\left. + s\frac{d}{d\mu}\left[\mu+2\omega\mu(1-\delta+2\delta\mu^2)\right]\right\}(R+iI) = 0$$

Since we are looking for unstable solutions, we may divide the last equation by $[\sigma - s\omega(1+\delta\mu^2)]$, with $\sigma = \lambda + i\nu$. The resulting equation is separated out into real and imaginary parts

$$\frac{d}{d\mu}(1-\mu^2)\frac{dR}{d\mu} - \left\{\frac{s^2}{1-\mu^2} + a(\mu)\frac{d}{d\mu}\left[\mu + 2\omega\mu(1-\delta+2\delta\mu^2)\right]\right\} R - \\ - b(\mu)\, I \frac{d}{d\mu}\left[\mu + 2\omega\mu(1-\delta+2\delta\mu^2)\right] = 0 \tag{G.7}$$

$$\frac{d}{d\mu}(1-\mu^2)\frac{dI}{d\mu} - \left\{\frac{s^2}{1-\mu^2} + a(\mu)\frac{d}{d\mu}\left[\mu + 2\omega\mu(1-\delta+2\delta\mu^2)\right]\right\} I + \\ + b(\mu)\, R \frac{d}{d\mu}\left[\mu + 2\omega\mu(1-\delta+2\delta\mu^2)\right] = 0 \tag{G.8}$$

where $a(\mu) = \dfrac{s[\lambda - s\omega(1+\delta\mu^2)]}{\nu^2 + [\lambda - s\omega(1+\delta\mu^2)]^2}$; $b(\mu) = \dfrac{s\nu}{\nu^2 + [\lambda - s\omega(1+\delta\mu^2)]^2}$

Equation (G.7) is multiplied by $I(\mu)$ and subtracted from (G.8) multiplied by $R(\mu)$, to give

$$\frac{d}{d\mu}\left[(1-\mu^2)\left(I\frac{dR}{d\mu} - R\frac{dI}{d\mu}\right)\right] = b(\mu)\,|\psi|^2 \frac{d}{d\mu}\left[\mu + 2\omega\mu(1-\delta+2\delta\mu^2)\right] \tag{G.9}$$

Integrating (G.9) from $\mu = -1$ up to $\mu = +1$, we get

$$\int_{-1}^{+1} b(\mu)\,|\psi|^2 \frac{d}{d\mu}\left[\mu + 2\omega\mu(1-\delta+2\delta\mu^2)\right] d\mu = 0 \tag{G.10}$$

We must then conclude that a necessary condition for barotropic instability is that $\frac{d}{d\mu}[\mu+2\omega\mu(1-\delta+2\delta\mu^2)]$ changes sign between $\mu = -1$ and $\mu = +1$. The same result is obtained in a β-plane analysis, i.e., that the derivative of the total vorticity has to change sign between the boundaries for instability. This criterion is in the same spirit as that proved by Lord Rayleigh (1880).

REFERENCES

Bolin, B., 1955: Numerical forecasting with the barotropic model. Tellus, 7, 27-49.

Bryan, K., 1959: A numerical investigation of certain features of the general circulation. Tellus, 11, 163-174.

Burger, A.P., 1958: Scale consideration of planetary motions of the atmosphere. Tellus, 10, 195-205.

Chapman, S. and R. S. Lindzen, 1970: Atmospheric Tides. Gordon and Breach Science Publishers, Inc.; New York, 200 pp.

Charney, J. G., 1955: The use of the primitive equations of motion in numerical prediction. Tellus, 7, 22-26.

Charney, J. G., 1962: Integration of the primitive and balance equations. Proc. International Symposium on N.W.P. (Tokyo, 1960). Met. Soc. Japan, 131-152.

Charney, J. G., 1973: Planetary Fluid Dynamics, a chapter of the book Dynamic Meteorology, editor P. Morel. D. Reidel Publishing Co., Boston, 622 pp.

Clark, J. H. E., 1970: A quasi-geostrophic model of the winter stratospheric circulation. Mon. Wea. Rev., 98, 443-461.

Cunnold, D., F. Alyea, N. Phillips and R. Prinn, 1974: A three-dimensional dynamical-chemical model of atmospheric ozone. J. Atmos. Sci. (to be published).

Dikii, L. A., 1965: The terrestrial atmosphere as an oscillating system. Izv. Akad. Nauk. SSSR, Atmos. and Oceanic Physics, 1, 7, 275-286.

Eliassen, A. and E. Palm, 1960: On the transfer of energy in stationary mountain waves. Geofys. Publik. 22, 1-23.

Flattery, T. W., 1967: Hough functions. Tech. Report No.21, Dept. Geophys. Sci., Univ. of Chicago, 175 pp.

Haurwitz, B., 1940: The motion of atmospheric disturbances on the spherical earth. J. Mar. Res., 3, 254-267.

Hough, S. S., 1898: On the application of harmonic analysis to the dynamical theory of tides. Part II: On the general integration of Laplace's dynamical equations. Phil. Trans. Roy. Soc., A 191, 139-185.

Houghton, D., 1968: Derivation of the elliptic condition for the balance equation in spherical coordinates. J. Atmos. Sci., 25, 927-928.

Jeffreys & Jeffreys, 1972: Methods of Mathematical Physics. Cambridge University Press, London, Third Edition, 718 pp.

Kato, S., 1966: Diurnal atmospheric oscillations. J. Geophys. Res., 71, 3201-3214.

Lamb, H., 1932: Hydrodynamics. Dover Publications, New York, Sixth Edition, 738 pp.

Lindzen, R. S., 1966: On the theory of the diurnal tide. Mon. Wea. Rev., 94, 295-301.

Lindzen, R. S., 1967: Planetary waves on Beta-Planes. Mon. Wea. Rev., 95, 441-451.

Lindzen, R. S., 1971: Atmospheric tides. A chapter in Lectures in Applied Mathematics, Vol. 14, Amer. Math. Soc., Providence, R.I.

Longuet-Higgins, M. S., 1968: The eigenfunctions of Laplace's tidal equations over a sphere. Phil. Trans. Roy. Soc. London, 262 A, No. 1132, 511-607.

Lord Rayleigh, 1880: On the stability or instability of certain fluid motions. Scientific Papers, Vol. I, 474-487. Dover Publications, Inc., New York, N.Y.

Lorenz, E. N., 1960: Energy and numerical weather prediction. Tellus, 12, 4, 364-373.

Maruyama, T., 1967: Large-scale disturbances in the equatorial lower stratosphere. J. Met. Soc. Japan, 46, 391-408.

Matsuno, T., 1966: Quasi-geostrophic motions in the equatorial area. J. Met. Soc. Japan, 44, 25-42.

Miyakoda, K., 1960: Numerical solution of the balance equation. Tech Report JMA No. 3. Japan Met. Agency, Tokyo.

Monin, A. S., 1952: Changes of pressure in a barotropic atmosphere. Izv. Akad. Nauk. SSSR, Ser. Geofiz., 4, 76-85.

Monin, A. S., 1958: Pressure variations in a baroclinic atmosphere. Izv. Akad. Nauk. SSSR, Ser. Geofiz., 4, 280-286.

Oort, A. H. and E. M. Rasmusson, 1971: Atmospheric circulation statistics. NOAA Prof. Paper 5, 323 pp.

Pedlosky, J., 1964,a: The stability of currents in the atmosphere and the ocean: Part I. J. Atmos. Sci., 21, 201-219.

Pedlosky, J., 1964,b: The stability of currents in the atmosphere and the ocean: Part II. J. Atmos. Sci., 21, 342-353.

Peng, L., 1965: A simple numerical experiment concerning the general circulation in the lower stratosphere. Pure and Applied Geophysics, 61, 191-218.

Phillips, N.A., 1954: Energy transformations and meridional circulations associated with simple baroclinic waves in a two-level, quasi-geostrophic model. Tellus, 6, 273-286.

Phillips, N. A., 1960: On the problem of initial data for the primitive equations. Tellus, 12, 121-126.

Phillips, N.A., 1963: Geostrophic motion. Rev. Geophys., 1, 123-176.

Phillips, N.A., 1973: Principles of large scale numerical weather prediction. A chapter in the book Dynamic Meteorology, editor P. Morel. D. Reidel Publishing Co., Boston, 622 pp.

Rossby, C. G., 1939: Relation between variations in the intensity of the zonal circulation of the atmosphere and the displacement of the semi-permanent centers of action. J. Mar. Res., 2, 38-55.

Simmons, A. J., 1974: The meridional scale of baroclinic waves. J. Atmos. Sci., 31, 1515-1525.

Stone, P. H., 1969: The meridional structure of baroclinic waves. J. Atmos. Sci., 26, 376-389.

Stone, P. H., 1974: The meridional variation of the eddy heat fluxes by baroclinic waves and their parameterization. J. Atmos. Sci., 31, 444-456.

Taylor, G. I., 1936: The oscillations of the atmosphere. Proc. Roy. Soc. A 156, 318-326.

Yanai, M. and T. Maruyama, 1966: Stratospheric wave disturbances propagating over the equatorial Pacific. J. Met. Soc. Japan, 44, 291-294.

Wallace, J. M. and V. E. Kousky, 1968: Observational evidence of Kelvin waves in the tropical atmosphere. J. Atmos. Sci., 25, 900-907.

Wallace, J. M., 1971: Spectral studies of tropospheric disturbances in the tropical western Pacific. Rev. Geophys. Space Phys., 9, 557-612.

BIOGRAPHICAL NOTE

The author was born on October 21, 1945 in Ituiutaba, Minas Gerais, Brazil. He attended secondary school at Colégio São José and Colégio Estadual de Uberlandia. He was awarded the Gold Medal in the entrance examinations for the Escola de Engenharia da U.F.M.G. in 1965, in competition among 2000 students. There, he was appointed as a Teaching Assistant in physics for three years. He was awarded the Degree of Engenheiro Eletricista with the Silver Medal in December 1969.

He joined the Instituto de Pesquisas Espaciais (INPE) at São José dos Campos, São Paulo, in January 1970, where he first became interested in atmospheric sciences. There he worked in a meteorological satellite project and initiated his graduate studies.

He started graduate studies at M.I.T. in June 1971 on an INPE Fellowship and a NASA International Fellowship. He attended the Colloquium in Dynamics of the Tropical Atmosphere at NCAR in the summer of 1972. The author is married to Lilia Sampaio Moura and their son Alexandre was born three months prior to the completion of this thesis.

The author will return to INPE, where he hopes to work with others towards the continuing development of meteorological studies in Brazil.